Original Article

CAMBRIDGE
UNIVERSITY PRESS

Integrated geochemical and thermobarometric approach to ascertain provenance and pressure–temperature conditions from detrital Himalayan garnets (Siwalik Group, Surai Khola, Nepal)

Elizabeth J. Catlos[1] [iD], Llewnosuke D. Priimak[1], Rasoul B. Sorkhabi[2],
Hector Garza[1] [iD], Pitambar Gautam[3] [iD] and Priyanka Periwal[4]

[1]Department of Earth and Planetary Sciences, Jackson School of Geosciences, The University of Texas at Austin, Austin, TX, USA; [2]Energy & Geoscience Institute, The University of Utah, Salt Lake City, UT, USA; [3]The Hokkaido University Museum, Hokkaido University, Sapporo, Hokkaido, Japan and [4]Bureau of Economic Geology, Jackson School of Geosciences, The University of Texas at Austin, Austin, TX, USA

Abstract

This study examines detrital garnet compositions from five samples spanning a Late Miocene–Pliocene section of Himalayan sedimentary rocks (Surai Khola, Siwalik Group and central Nepal) to assess provenance and tectonic implications. A total of 100 detrital garnets were analysed for edge-to-edge compositional zoning, revealing distinct groups linked to specific hinterland regions. Manual classification identified garnet Groups 1 and 2 as grossular, Group 3 as spessartine, and Groups 4 through 7 as almandine, varying in XCa, XMg and XMn. Most garnets exhibit low XMg and flat zoning, with Groups 6* and 7* containing slightly higher XMg. Statistical clustering aligns broadly with manual groupings, which strengthens provenance interpretations. Comparisons with hinterland garnet compositions expand provenance options to magmatic garnets and rocks outside the Himalayan core units. Eight Siwalik Group garnets were modelled for pressure–temperature conditions and paths. Group 4 and 6 garnets, potentially linked to blueschist/eclogites or metamorphosed arc/Himalayan core rocks, record conditions of 510–538°C and 4.6–6.8 kbar, with isothermal burial over 0.5–2 kbar. Group 2 garnet, resembling compositions from North Himalayan granitic enclaves, yields core conditions of 480°C and 6 kbar and an N-shaped pressure–temperature path. Two Group 5 garnets with zoning like those in the High Himalayan leucogranites yield 520–528°C at 3.2–3.6 kbar. These findings provide insights into Himalayan erosion dynamics, hinterland exhumation and sediment transport pathways. Integrating garnet compositional zoning with statistical clustering and thermodynamic modelling is valuable for provenance studies of garnet-bearing sedimentary sections.

1. Introduction

The Himalayan orogen is one of the most rapidly eroding regions in the world, driven by ongoing uplift caused by the collision of India with Asia, intense monsoonal precipitation and active tectonics (Thiede *et al.* 2009; Owen, 2010; Olen *et al.* 2015). These processes continually strip away near-surface materials, progressively exposing deeper-seated rocks. Garnet-bearing metamorphic and igneous rocks exposed in outcrops of the Himalayan hinterland have long been used to unravel subsurface pressure–temperature conditions, and these data have been applied to develop models for their tectonic history (Hodges *et al.* 1988; Hubbard, 1989; Catlos *et al.* 2001; Kohn *et al.* 2001; Catlos *et al.* 2018, 2022). However, garnets now exposed in the Himalayan hinterland, informative as they are, reflect exhumation processes that operate over vastly different timescales, from rapid events like landslides to slow uplift over millennia (Vance *et al.* 2003; Zech *et al.* 2009). Our knowledge of Himalayan geological development is thus fundamentally limited if we only rely on conditions reported from garnets that appear in outcrop samples.

The Himalayan orogen is mapped as a fold-and-thrust belt, characterized by major lithotectonic units and bounding structures along its length (e.g. Le Fort, 1996). Its orogenic history is preserved in the foreland basin sediments of the Sub-Himalayan Sequence, known as the Siwalik Group. Figure 1 shows a geological map of the Himalaya, illustrating the regional context of the group. Figure 2 presents a cross-section through the central Nepal Himalaya to highlight the Siwalik Group's structural relationships. Since the mid-nineteenth century, numerous studies have examined the Siwalik Group from petrographic, palaeontological,
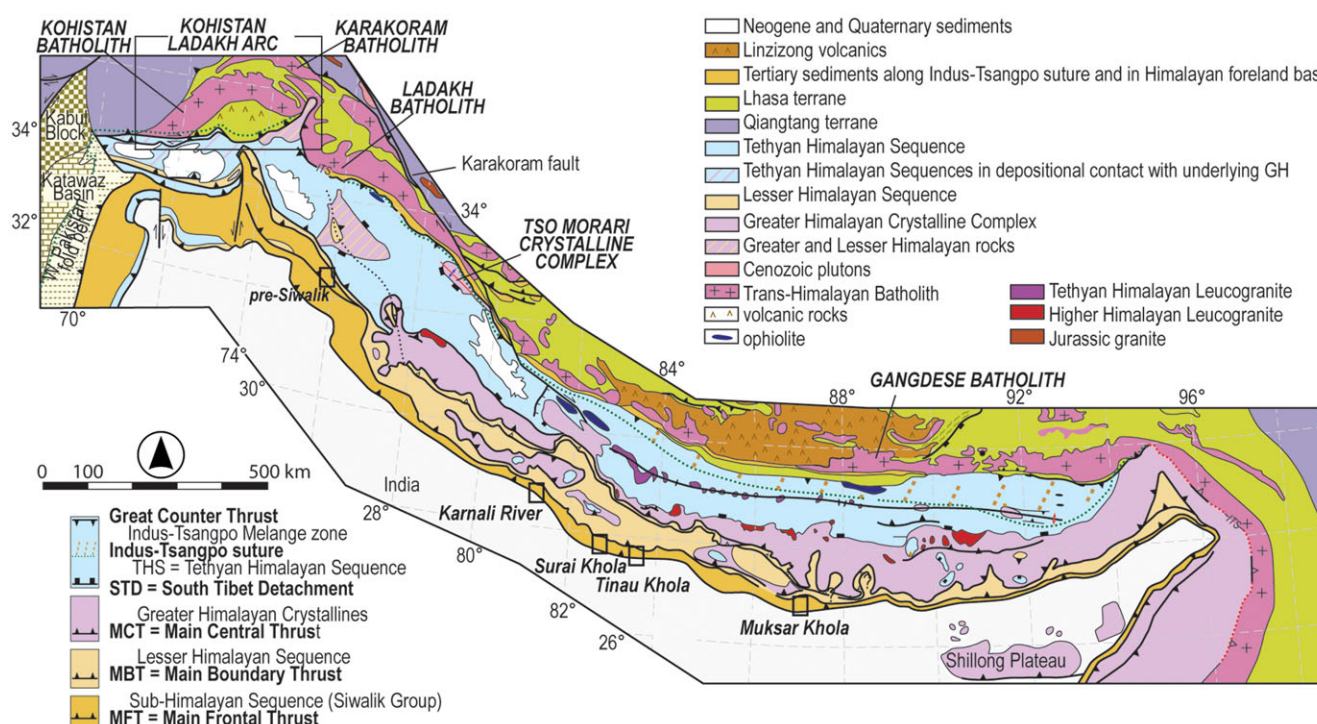
Figure 1. Geological map of the Himalaya, modified from Yin (2006).

stratigraphic, isotopic provenance, detrital thermochronological and paleohydrological perspectives (Pilgrim, 1910, 1913; see reviews in Patnaik, 2013; Flynn *et al.* 2016). These sedimentary rocks preserve records of erosion and exhumation associated with India–Asia collision, including the uplift of distinct lithological units at specific times and the progressive advancement of thrust belts into the foreland basin (e.g. Burbank *et al.* 1996; DeCelles *et al.* 1998; Singh *et al.* 2004; Jalal *et al.* 2011).

This paper aims to decipher the uplift and exhumation history of the Himalaya as recorded in the sedimentary archive of the Siwalik Group by exploiting the chemical zoning of detrital garnets. These zoning patterns reveal the full potential of garnet compositional variations to reconstruct tectonic histories. Pressure–temperature conditions and paths were modelled for Siwalik garnet grains that best preserve their prograde compositional zoning, assuming growth in a pelitic bulk rock composition. This approach bridges the gap between hinterland tectonic signals and sedimentary records in the foreland basin. By extensively characterizing Himalayan hinterland garnets, the study pioneers alternative methods for reconstructing tectonic histories preserved in foreland basin sediments.

2. Primary data: detrital garnet

Garnet is a cubic, isotropic mineral classified as a nesosilicate, meaning it consists of isolated silicate tetrahedra within its structure. The garnet unit cell has the structure of $X_3Y_2Z_3O_{12}$, where (commonly) X = Mg, Fe^{2+}, Mn or Ca, Y = Al, Fe^{3+}, Ti or Cr and Z = Si (Deer *et al.* 2009). Less commonly, X = Y, Y = Mn, V or Zr (Rickwood, 1968). One can expect to find a range of additional elements possibly present, including F, Na, Sc, Sn, Li, P, S, Cl, K, Ni, Zn, As, Sr, Nb, Te, Ba, REE, Hf, W and Th (Locock, 2008).

Garnet has several identified varieties, but the more commonly expressed end-members are pyrope ($Mg_3Al_2Si_3O_{12}$), almandine

($Fe_3Al_2Si_3O_{12}$), spessartine ($Mn_3Al_2Si_3O_{12}$) and grossular ($Ca_3Al_2Si_3O_{12}$). Andradite is the grossular end-member, but with the Y site occupied by Fe^{3+} and/ or Ti. Uvarovite is the grossular end-member with the Y site occupied by Cr. Hydrogrossular includes the addition of an OH component into the basic framework ($Ca_3Al_2Si_3O_8(SiO_4)_{1-m}(OH)_{4m}$.

The garnet series comprises two types: pyralspite (**pyr**ope, **al**mandine and **sp**essartine) and ugrandite (**u**varovite, **gr**ossular and **and**radite). In the pyralspite series, Mg, Mn and Fe have a 2+ oxidation state and similar size, substituting for each other in the X site of the garnet structure. In the ugrandite series, the X site is dominated by Ca. The two species have no continuous variations. When found as end-member compositions, spessartine garnets tend to form in pegmatites and highly fractionated granites (Kontak & Corey, 1988; Laurs & Knox, 2001; Sami *et al.* 2020), eclogitic metacherts (Cenki-Tok & Chopin, 2006) and metamorphosed Mn-rich rocks (Nyame, 2001). Calcium-rich garnets form in magmatic and metasomatic environments (Scheibner *et al.* 2007), kimberlite xenoliths (Kopylova *et al.* 2000), granulites (Petrakakis *et al.* 2018) and skarns and hornfels (Labotka, 1995). Almandine-rich garnets are typical of metamorphosed mudrocks, igneous and meta-igneous assemblages (Stone, 1988; Harangi *et al.* 2001). In terms of specific gravity, almandine is greater (4.32), followed by spessartine (4.19), uvarovite (3.90), andradite (3.86), grossular (3.59) and pyrope (3.58) (Suggate & Hall, 2014). Most garnets are solid solutions with the X site varying XMg, XFe, XMn and XCa components.

Garnet's durability, compositional diversity and geochemical characteristics make it a powerful mineral for revealing the provenance and geological history recorded within the sedimentary record (Suggate & Hall, 2014; Tolosana-Delgado *et al.* 2018; Stutenbecker *et al.* 2017, 2024). Garnet is relatively stable during surface weathering, transport and deep burial (Morton & Hallsworth, 1999; Andò *et al.* 2012) and is a common component
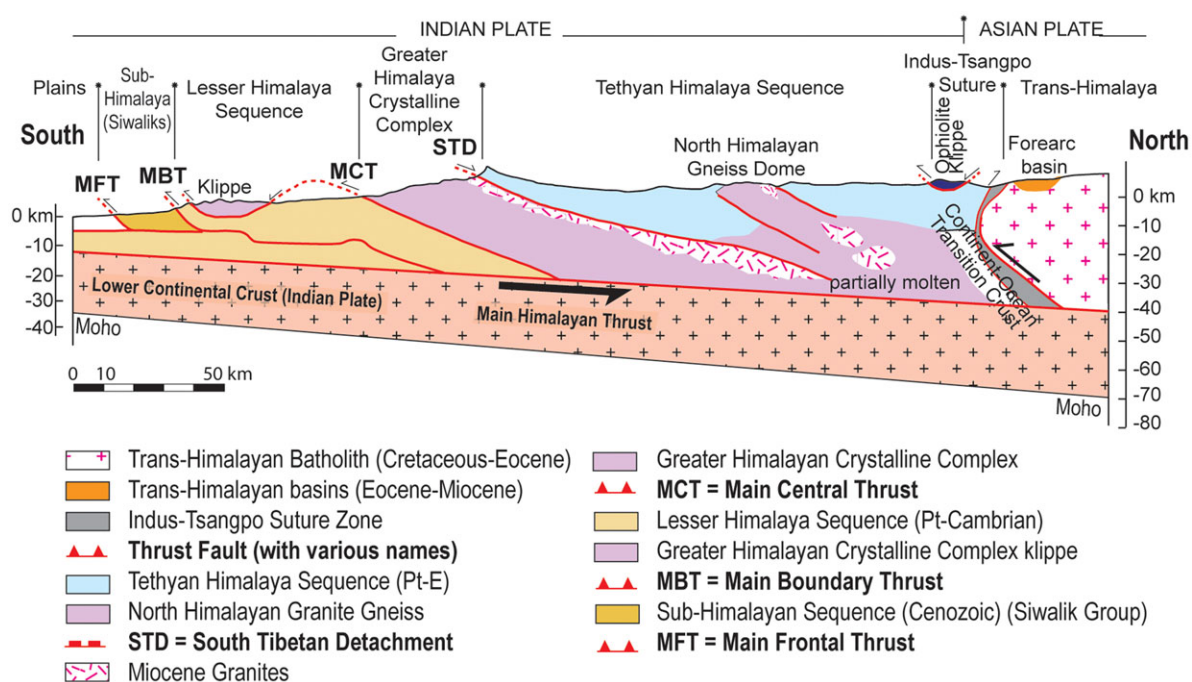
Figure 2. Cross-section of the Himalayan orogen, adapted from Sorkhabi (2010).

of some detrital sediment (Velbel, 1984; Suggate & Hall, 2014; Alizai *et al.* 2016; Stutenbecker *et al.* 2017; Tolosana-Delgado *et al.* 2018). Although garnets with higher Fe contents lend themselves to weathering and developing Fe-bearing alteration minerals [limonite, $FeO(OH) \cdot nH_2O$; goethite, $FeO(OH)$; gibbsite $(Al(OH)_3]$ even in rock outcrops (Velbel, 1984; Price *et al.* 2013), clay minerals, goethite and gibbsite can act as protective surface layers that assist in preservation (Price *et al.* 2013). Almandine-pyrope garnets are also harder than quartz by several GPa (Whitney *et al.* 2007). Almandine garnet is widely used as an abrasive due to its high fracture toughness and resistance to chemical weathering (Poon *et al.* 2020; Jamaludin *et al.* 2022). These properties suggest it can survive the chemical and physical processes associated with mass wasting. Grossular garnet is observed to be less stable than other compositions in conditions of elevated pore-fluid temperatures at deep burial (Morton, 1987; Morton & Hallsworth, 2007; Krippner *et al.* 2015).

Each element in the garnet structure is critical in tracking the mineral grain's growth history. Garnet is the only sink for Mn in many bulk rock compositions. Prograde garnet growth in pelitic bulk compositions will show higher XMn in their cores and decrease towards rims, creating a bell-shaped compositional profile. Any changes in the XMn across a garnet can be used to track additional stages of growth. Flat XMn zoning often indicates that the garnet experienced a higher temperature (>600°C), depending on grain size and the duration of thermal exposure. Because Mn is incompatible with other significant minerals in many rocks, some garnets exposed to higher temperatures will increase in XMn content at their rims.

Garnet XFe and XMg contents track temperature and are used in various thermometers, whereas XCa is often used to understand the pressure changes and is used in barometers. Spear (1995, Figure 17-10) showed that in pelitic bulk rock compositions, one can anticipate a garnet's burial history by tracking its XMn, XFe, XCa and XMg. This study investigates garnet compositions

edge-to-edge to uncover their growth history and evaluate their potential as proxies for tectonic processes. By integrating compositional trends with literature data, we aim to link detrital garnets to their hinterland sources, shedding light on Himalayan exhumation and uplift.

3. Himalayan geology: tectonic context of potential source areas

This section provides an overview of geological units that could contribute garnet to the Siwalik Group. Although the Surai Khola section of the Siwalik Group is thought to have received sediment from a limited number of Himalayan units (e.g. Baral *et al.* 2016), their compositions necessitated considering additional sources to explain the full range of garnet geochemical signatures.

3.a. Suture zone units and associated assemblages

The timing of the India–Asia collision is often cited as occurring during the Paleocene (Rowley, 1996; Yin & Harrison, 2000; Hu *et al.* 2016; Najman *et al.* 2017; Parsons *et al.* 2020). The Indus–Tsangpo suture zone (Indus-Yarlung-Tsangpo suture zone, Yarlung Zangbo Ophiolite Zone, Liu *et al.* 2010) is the collisional boundary between rocks of Indian and Asian affinities to the south and north, respectively (Figures 1 and 2). Suture zones often involve multiple fault systems, recording high-strain and incorporating a wide range of deformed rock materials (Dewey, 1977; O'Brien, 2001; Catlos & Çemen, 2023). Metamorphosed igneous rocks within the Indus–Tsangpo suture zone and its associated mélange include ophiolites, serpentinite gabbro, volcanic rocks, blueschists and syn-tectonic high-Si, peraluminous granites (e.g. Thakur, 1981; DiPietro *et al.* 1999). Several studies have reported garnet and its associated conditions from suture zone high-pressure amphibolites, deformed blueschist-facies quartz schists and eclogite-facies metapelites (Honegger *et al.* 1989; Guilmette

et al. 2008, 2009, 2012; Cai & Cao, 2013; Chen *et al.* 2021; Li *et al.* 2024).

Garnet-bearing assemblages are also found in deformed island arc rocks located between the Eurasian plate and the Indian plate along the Indus–Tsangpo suture zone. For example, the **Kohistan–Ladakh Arc** lies adjacent to the suture zone and represents an island arc that initially formed above a subduction zone within the Neo-Tethys Ocean (Fig. 1) (Shah *et al.* 2011; Petterson, 2019). Garnet-bearing assemblages within the Kohistan-Ladakh Arc include those associated with magmatic rocks, garnet–kyanite–staurolite gneisses and mafic–ultramafic gabbroic assemblages (Raz & Honegger, 1989; DiPietro *et al.* 1999; Petterson, 2010; Thanh *et al.* 2011; Sayab *et al.* 2016; Jagoutz *et al.* 2019; Petterson, 2019; George *et al.* 2022).

Garnet-bearing magmatic rocks are also exposed near the Indus–Tsangpo suture zone due to subduction-related magmatism before and after collision. These include garnets documented in anorthosites, two-mica granites, leucocratic dikes and leucosomes associated with the **Kohistan, Karakoram, Ladakh** and **Gangdese batholiths** (Fig. 1) (Reichardt *et al.* 2010; St-Onge *et al.* 2010; Ma *et al.* 2017; Ding *et al.* 2022; Dong *et al.* 2024).

Himalayan rocks exposed directly south of the suture zone are part of the **Tethyan Himalayan Sequence**, which consists of Paleoproterozoic to Eocene Indian shelf sedimentary rocks interbedded with Paleozoic and Mesozoic volcanic assemblages (Jadoul *et al.* 1998; Yin & Harrison, 2000; Yin, 2006; Bhargava & Singh, 2020). The **Tso Morari Crystalline Complex** in NW India is often spatially associated with the **Tethyan Himalayan Sequence** (e.g. Steck *et al.* 1998; Rao & Rai, 2006) (Fig. 1). Garnet-bearing rocks in eclogite-facies assemblages record ultra-high-pressure conditions closely associated with tectonic processes associated with collision (e.g. Wilke *et al.* 2015; Jonnalagadda *et al.* 2019). In contrast, upper structural levels of the Tethyan Himalayan Sequence in NW India contain garnet-bearing phyllites, schists, amphibolites and kyanite-biotite migmatites (Searle *et al.* 1993; Catlos *et al.* 2020; Kawabata *et al.* 2021; Sen *et al.* 2023). Some Oligocene to Miocene-aged **North Himalayan granitic bodies and gneiss domes** formed within the Tethyan Himalayan Sequence are garnet-bearing (Fig. 2) (Lee *et al.* 2000; Zhang *et al.* 2004; Smit *et al.* 2014; Wang *et al.* 2022a).

3.b. Himalayan core

The Tethyan Himalayan Sequence is separated from the underlying higher-grade schists and gneisses of the **Greater Himalayan Crystallines Complex (GHC)** by the north-dipping South Tibet Detachment (STD) (Figs. 1 and 2) (e.g., Burchfiel *et al.* 1992; Hodges *et al.* 1992; Kohn, 2014; Carosi *et al.* 2018; Kellett *et al.* 2019; Wang *et al.* 2024). The GHC is a unit of primarily kyanite to sillimanite grade gneisses intruded by **High Himalayan leucogranites (HHL)** in its upper portion (Upreti, 1999; Wu *et al.* 2020; Cao *et al.* 2022; Zhang, 2024). Both lithologies are garnet-bearing. The GHC protolith is suggested to be the pre-Himalayan, Indian plate margin sediments intruded by Cambrian–Ordovician granitoids that were thrust beneath Tibet during the early stages of the Himalayan collision (Catlos, 2023; Robinson & Martin, 2023). Garnets are also present in some HHL (Searle & Fryer, 1986; Weinberg, 2016; Wu *et al.* 2020; Shi *et al.* 2021).

The highest-grade assemblages associated with the GHC are granulite metapelites and coesite-bearing eclogites (O'Brien *et al.* 2001; Borghi *et al.* 2003; Zhang *et al.* 2022). The GHC may have experienced two metamorphic episodes (see review in

Catlos, 2023). The first Eohimalayan event (phase) occurred during the Eocene–Oligocene (ca. 52–30 Ma) and is marked by accretion and metamorphism (e.g., Kelly *et al.* 2022; Wang *et al.* 2022b). During the subsequent Miocene Neohimalayan event (phase), slip along the **Main Central Thrust (MCT)** was initiated, and Miocene HHL were generated (e.g., Wu *et al.* 2020).

At its base, the GHC is thrust over lower-grade metasedimentary rocks of the **Lesser Himalayan Sequence (LHS)** along the MCT (Figs. 1 and 2) (Upreti, 1999; Robinson & Martin, 2014). The lack of an apparent break in metamorphic grade between the GHC and LHS makes it challenging to place the boundaries of the MCT zone (e.g., Martin, 2017). The MCT zone is characterized by inverted metamorphism, where metamorphic grade increases toward structurally shallower levels (e.g., Catlos *et al.* 2001; Larson *et al.* 2016; Carosi *et al.* 2018; Pant *et al.* 2020). The LHS lies in the hangingwall of the MBT (Meigs *et al.* 1995; Mugnier *et al.* 1994), which places it structurally above the Siwalik Group. The LHS is mainly comprised of Paleoproterozoic sedimentary rocks associated with Gondwana and is intruded by granite dated to ~1.84 Ga and a narrow belt of younger (Permian to pre-Middle Miocene) rocks distributed in its southern margin (e.g., Mukhopadhyay *et al.* 1996; Miller *et al.* 2000; Mishra *et al.* 2019). To the south, the **Main Frontal Thrust (MFT)** forms the boundary between the Siwalik Group and the Indo-Gangetic Plain (e.g., Burgess *et al.* 2012; Srivastava *et al.* 2016).

The Siwalik Group is a thick succession of dominantly fluvial, coarsening upward, sedimentary rocks located along the entire 2400 km length of the Himalaya from Pakistan's Potwar plateau on the west to the Brahmaputra valley in the east (Fig. 1) (Burbank *et al.* 1996; Bora & Shukla, 2005; Bernet *et al.* 2006; Sanyal & Sinha, 2010; Khan *et al.* 2019; Dhamodharan *et al.* 2020). Siwalik sedimentary rocks primarily originated in the Himalaya, and sedimentation occurred in a foreland basin with alluvial fans, fluvial mega-cones, braided channels and flood plains, similar to those that developed the present-day Indo-Gangetic Plain (Parkash *et al.* 1980; Jain & Sinha, 2003). Its formation occurred due to the evolution of large river systems analogous to those associated with the Ganga River system (Jain & Sinha, 2003; Bora & Shukla, 2005; Sanyal & Sinha, 2010; Taral & Chakraborty, 2018; Khan *et al.* 2019; Dhamodharan *et al.* 2020). As Fig. 3 demonstrates major river systems, such as the Ganges, Indus and Brahmaputra, along with their tributaries, currently drain extensive areas of the Indian subcontinent. The deposits record a range of environments, including piedmonts, outwash plains, channels, floodplains and oxbow lakes, some of which have marine influence in older sections (Taral *et al.* 2019; Debnath *et al.* 2021; Khan *et al.* 2023). Siwalik Group sediment accumulation began in the Middle Miocene in a long foredeep near sea level (Bora & Shukla, 2005; Chakrabarti, 2016). The foreland basin developed as the subducting Indian plate flexed under the crustal load of the rising Himalaya (Lavé & Avouac, 2000; Rai, 2003; Valdiya, 2016; Dutta *et al.* 2019).

3.c. Potential Proterozoic mobile belt sources of the Indian plate

Although the dominant documented source of sediment in the Siwalik Group is from Himalayan core assemblages, rocks from the Indian Shield also have the potential to contribute through erosion and river transport (Khan & Tewari, 2015; Chakraborty *et al.* 2020). Figure 3 illustrates the **Indo-Gangetic Plain**, which lies south of the Himalaya and spans northern and eastern India, Bangladesh, parts of Pakistan and southern Nepal (Pant & Sharma,
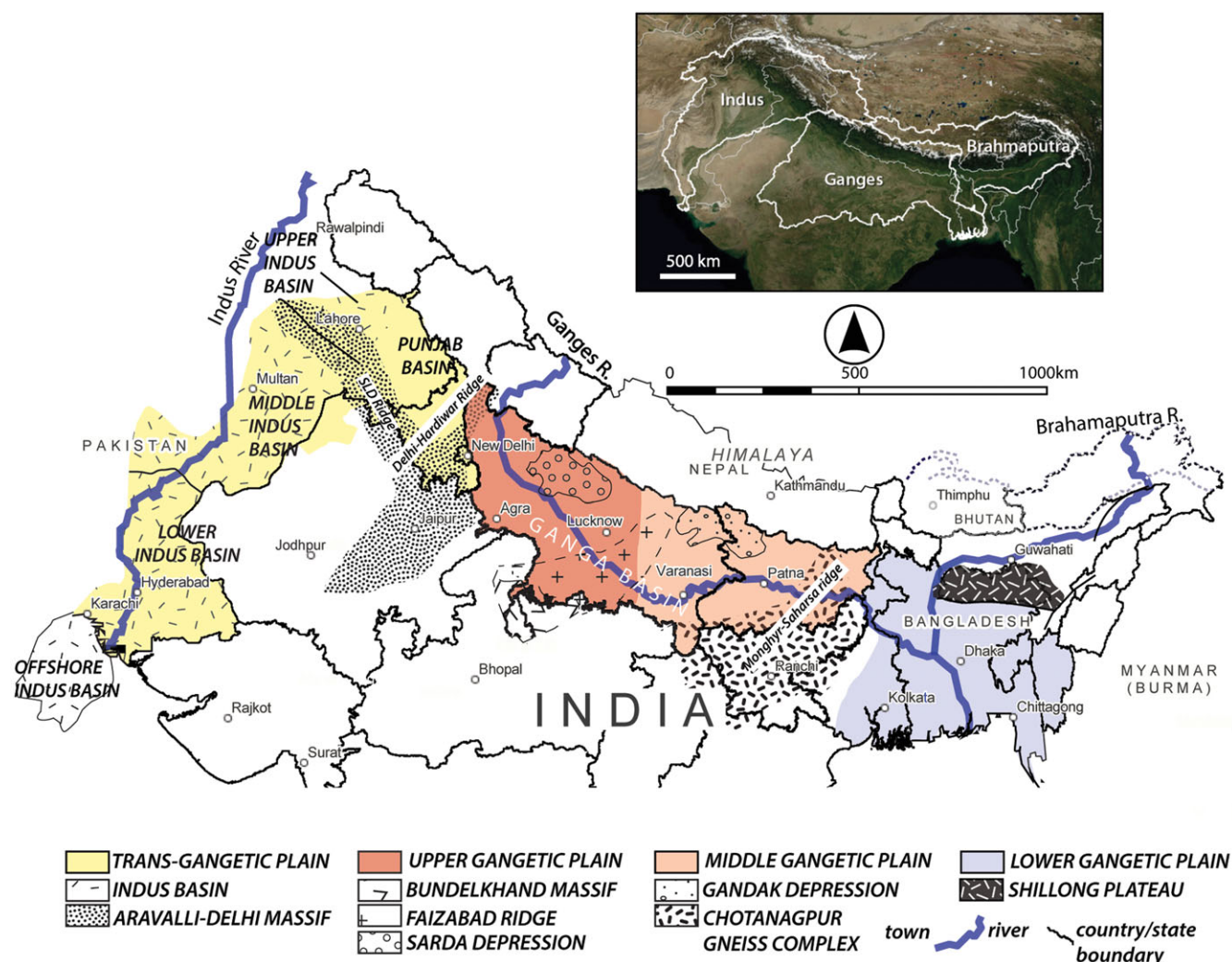
Figure 3. Primary basement structural features of the Indo-Gangetic Plain, after Catlos (2023).

1993; Pathak *et al.* 2014). The region is classified into distinct sections based on geography, river systems and climate (Pathak *et al.* 2014; Catlos, 2023). If contributions to the Siwalik Group include sediments from proximal sources south of the Himalaya, mixing Himalayan detritus with garnet-bearing Proterozoic mobile belt sources would reflect a dynamic interplay between interconnected river systems.

Ancient rivers may have had axial components that transported sediments eroded from Precambrian basement rocks, including granites, gneisses and schists, into the Himalayan foreland basin, where Siwalik sediments accumulated (Burbank *et al.* 1996; Ulak, 2005; Mandal *et al.* 2014). While the primary sources of garnet-bearing material in Siwalik exposures are linked to the Himalaya, some units in northwestern India contain similar mineralogical signatures. These include the Chotanagpur Granite Gneiss Complex (CGGC) (Sanyal & Sengupta, 2012; Dey *et al.* 2019), Aravalli-Delhi Fold Belt (Prakash *et al.* 2018) and Shillong-Meghalaya Plateau (Chatterjee *et al.* 2011; Chatterjee, 2017). These regions contain garnets that record ultra-high temperature conditions and share Proterozoic zircon dates in the Siwalik Group (Mukherjee *et al.* 2019; Singh *et al.* 2021; Nag *et al.* 2024). While these potential sources are considered, our primary focus is on assessing garnet compositions in the context of Himalayan provenance.

4. Previous work on Siwalik Group garnets

Detrital garnets have long been extensively documented throughout the Siwalik Group, comprising more than 60% of heavy mineral separates (Chaudhri, 1972; Chaudhri & Gill, 1981; Singh *et al.* 2004; Szulc *et al.* 2006). Garnet is present in Siwalik exposures across the range front, including Pakistan (Abid *et al.* 1983; Ullah *et al.* 2015; Zaheenullah *et al.* 2017; Ali *et al.* 2023), NW India (Kaul *et al.* 1983; Jassal *et al.* 2000; Najman & Garzanti, 2000; Ranjan & Banerjee, 2009), Nepal (Chaudhri & Gill, 1981; Nakajima *et al.* 2020; Rai *et al.* 2021) and NE India (Kundu *et al.* 2016). Early studies linked the presence of garnet to the erosion of hinterland metamorphic assemblages (Bhushan, 1973), although magmatic garnet is also present in the Himalaya (e.g., Searle & Fryer, 1986; Yu *et al.* 2021; Yan *et al.* 2022). Siwalik garnets are often described as angular to sub-rounded grains, suggesting shorter transport distances (Sinha, 1970; Singh, 2012; Goswami & Deopa, 2018; Ali *et al.* 2023). While rare, euhedral garnet has been noted in Siwalik Group rocks in Pakistan and the NW Indian Himalaya, implying limited transport distance and local sources in those areas (Sinha, 1970; Chaudhri, 1972; Abid *et al.* 1983). Along the Indus River, the grain size of heavy minerals decreases, and the degree of roundness increases downstream (e.g., Cerveny *et al.*, 1989). In some sections of the Siwalik Group (NW India), garnet abundance

increases from lower to upper stratigraphic levels (Ranjan & Banerjee, 2009). This trend is not consistently observed and has not been noted in the Surai Khola section.

The Himalaya are ideally situated to use garnets for Siwalik Group provenance because outcrop samples have long been targeted for chemical analyses and pressure–temperature estimates, and a few options exist for possible sources. The wide chemical diversity of garnets also facilitates the development of provenance hypotheses. However, the approach of previous work on Siwalik garnets relied on single-spot analyses, failing to capture chemical variations within individual grains. These studies suggest that Siwalik garnets are largely unzoned. For example, Nakajima *et al.* (2020) analysed over 1,000 Siwalik garnets and found only two grains with more than a 5 mol% difference between the geometric core and rim.

Almandine is the most common garnet composition reported from Siwalik sedimentary rocks and Himalayan fluvial-deltaic sands (Andò *et al.* 2009; Nakajima *et al.* 2020; Yoshida *et al.* 2021; Rai *et al.* 2021). Although large proportions of low-grossular ($XCa_{<10}$) and high-pyrope ($XMg_{20\%}$) garnets are often reported in detrital sediments (Sabeen *et al.* 2002), this is not the case for Siwalik garnets, which are dominated by lower XMg and higher XCa contents (Yoshida *et al.* 2015; Nakajima *et al.* 2020; Yoshida *et al.* 2021).

Studies of detrital garnet compositions associate their chemistry with the exhumation of a limited number of hinterland source terranes, focusing on tracking the exhumation of the GHC via the onset of MCT activity. GHC garnets exhibit a range of compositions, but the appearance of higher XMg Siwalik garnets is consistently linked to the exhumation of deeper GHC levels associated with MCT movement (Nakajima *et al.* 2020; Yoshida *et al.* 2021).

One of the first studies of Siwalik garnet compositions focused on Middle–Late Miocene sandstones of the Tinau Khola in central Nepal (Yoshida *et al.* 2015). The Tinau Khola is a key locality for compositional analysis of Siwalik garnets (see also Nakajima *et al.* 2020; Yoshida *et al.* 2021), though it exposes only the Lower and Middle Siwalik sedimentary rocks (Gautam *et al.* 2012). Garnet was analysed using Energy Dispersive Spectrometry, which has been cited as problematic for low-Z elements but can yield comparable results to Wavelength Dispersive Spectrometry for garnet (Çubukçu *et al.* 2008; Jayabun *et al.* 2021). Garnets from the Arung Khola (12–9.1 Ma) and Binai Khola (9.1–7.3 Ma) Formations transition from low XMg (low XCa and higher XFe and XMn) to higher XMg, linked to a shift from the erosion of low- to medium-grade metasedimentary rocks to granulite- and amphibolite-facies rocks. Yoshida *et al.* (2015) interpreted this as a change in sediment sources from shallower to deeper exhumed GHC material. The lower part of the Arung Khola Formation also yielded fewer garnets overall, supporting this interpretation. The study suggested that higher-grade metamorphic garnets first appeared at 12 Ma in the Tinau Khola section, with an increased input of MCT-zone metamorphic rocks between 11 and 10 Ma, followed by a decline in garnet supply after 9 Ma.

A similar provenance shift from shallower to deeper GHC sources was observed by Nakajima *et al.* (2020) and Yoshida *et al.* (2021) in Lower Siwalik samples from the Karnali River (western Nepal) and Tinau Khola (central Nepal). Here, the change in garnets from $XMg_{<10}$ and $XCa_{10–20}$ to those with $XMg_{10–25}$ and $XCa_{<10}$ again was cited to reflect the transition from the erosion of lower- to higher-grade GHC metamorphic rocks associated with the MCT motion. Additionally, the lower-pyrope

and higher-grossular garnets were associated with a zircon-tourmaline-rutile heavy mineral assemblage, whereas staurolite appeared in the higher-pyrope and lower-grossular garnet group, consistent with the exhumation model. This change in garnet chemistry occurred in the Karnali River at 14–12 Ma but later along the Tinau Khola at 11–10 Ma, suggesting a progressive eastward unroofing of the GHC, with denudation advancing from west to east. These dates are significant in that Surai Khola εNd(T) values suggest that erosional breaching of a large duplex in the northern part of the Lesser Himalayan zone had occurred by ~11 Ma (Huyghe *et al.* 2001; Robinson *et al.* 2001).

Yoshida *et al.* (2021) noted that Siwalik Group garnets from the Tinau Khola section exhibit a relatively constant composition throughout the Late Miocene, whereas garnets from the Karnali River section, derived from sandstones spanning both the Middle and Late Miocene, display a broader compositional range. These compositions suggested that the Karnali River garnets were derived from pelitic and calcareous metamorphic rocks and the Tinau samples were likely sourced from amphibolite-facies metasedimentary and felsic igneous rocks. The lower variability in garnet compositions also led to speculation that the catchment area supplying Tinau Khola Siwalik sandstones was smaller than that of the Karnali River.

In the Muksar Khola section of the Siwalik Group in eastern Nepal, detrital garnet compositions indicate that erosion of higher XMg6-25 and low XCa (<10) was sourced from shallower GHC gneiss and leucogranite sources before 7.7 Ma (Rai *et al.* 2021). After 7.7 Ma, an increase in moderate Ca-rich garnets (Grs + And 35–50) and negative εNd(T) suggest that the MCT zone became a dominant sediment source, with its exhumation starting after 7.5 Ma. By 4.0 Ma, detrital garnet compositions shifted again, with a resurgence of Mg-rich, low-Ca garnets and increased detrital kyanite and sillimanite, indicating a return to deeper GHC sources. Including leucogranite sources was a novel consideration, suggesting that additional lithologies, besides GHC, LHS and MCT zone assemblages, could be considered. The pattern of changing detrital mineral compositions also supported a progressive exhumation history, with alternating contributions from the MCT zone and the deeper levels of the GHC units.

Interpretation of these results has traditionally relied on ternary diagrams, which are commonly used to assess garnet provenance in the Siwalik Group and other settings (Wright, 1938; Morton, 1985; Preston *et al.* 2002; Morton *et al.* 2004; Teraoka *et al.* 1997, 1998; Sabeen *et al.* 2002; Suggate & Hall, 2014; Alizai *et al.* 2016). Krippner *et al.* (2014) argue that these diagrams are helpful only for garnets derived from the mantle, granulite-facies metasedimentary rocks and felsic igneous rocks. Based on an analysis of more than 3,000 garnets, they also note that ternary discrimination diagrams are imprecise for definitively identifying garnet host rocks. We employ an alternative approach that analyses garnet compositions edge-to-edge, incorporating both manual and statistical methods to refine provenance interpretations.

5. Materials and methods

5.a. Stratigraphic context and sample overview

Ten sandstone samples from the Lower (SK1, SK2 and SK3), Middle (SK4, SK5, SK7, SK8 and SK11) and Upper (SK16 and SK17) Siwalik Group were collected from the Surai Khola section, one of the most representative and complete Siwalik Group

successions in terms of sediment thickness and age (Middle Miocene through Pleistocene). Figure 4 illustrates the location map and stratigraphic column, along with the sample sites. Of these, five samples (SK7, SK8, SK11, SK16 and SK17) yielded detrital garnets and were selected for geochemical analyses. Most samples were analysed for bulk geochemical composition to support provenance interpretations (see Supplementary files).

The stratigraphic column is estimated to be 5,650 metres thick and is accessible through continuous exposures along the East-West Highway in western Nepal. An abundance of data on various geological aspects has been documented in the section, including biostratigraphy and palynology (Corvinus, 1988; Corvinus, 1993; Corvinus & Nanda, 1994; Hoorn *et al.* 2000; Corvinus & Rimal, 2001) and magnetic polarity stratigraphy (Appel *et al.* 1991; Rösler *et al.* 1997; Rösler & Appel, 1998; Gautam & Rösler, 1999; Gautam, 2008; Ojha *et al.* 2009). The sequence has been mapped for its composition, structure, paleoenvironment and palaeohydrological properties (Dhital *et al.* 1995; Quade *et al.* 1995; Nakayama & Ulak, 1999; Ulak, 2005; Szulc *et al.* 2006; Dhital, 2015) and units subjected to provenance and thermochronological analyses (Bernet *et al.* 2006; van der Beek *et al.* 2006; Baral *et al.* 2016). Geochemical, mineralogical and petrographic data are available (Critelli & Ingersoll, 1994; Sanyal *et al.* 2005; Szulc *et al.* 2006). Its sedimentary facies and slope movements have also been documented (Nakayama & Ulak, 1999; Ulak, 2005; Tamrakar & Yokota, 2008).

We report formation boundaries and thicknesses supplemented with approximate magnetostratigraphic dates derived by renewed correlation of the magnetic polarity sequence of Appel *et al.* (1991) with slight modifications by Rösler *et al.* (1997) and a recent Geomagnetic Polarity Time Scale included in the Geologic Time Scale 2020 (GTS2020: Gradstein *et al.* 2020). Based on the updated correlation, the boundaries between formations and their associated magnetic polarity chrons are as follows: the Bankas–Chor Khola boundary corresponds to Chron C5r.2r (11.592–11.188 Ma), the Chor Khola–Surai Khola boundary to Chron C3Br.2r (7.456–7.305 Ma), and the Surai Khola–Dobata boundary to Chron C3n.2n (4.631–4.493 Ma) (Gradstein *et al.* 2020). The approximate dates of the boundaries are indicated in Fig. 4b. Age assignments following the magnetic polarity sequence of Ojha *et al.* (2009) or the different versions of the global magnetic polarity scales other than the GTS2020 for correlations are likely to result in some differences. However, those would be minor (see Szulc *et al.* 2006 for comparison), and our primary conclusions will not be affected.

All samples are fine- to medium-grained sandstones collected from fresh exposures and selected for their stratigraphic position and lithologic comparability with previous paleohydrological and provenance studies. The five horizons yielding garnets are the primary focus of this study, and their estimated magnetostratigraphic sediment deposition ages are SK7 (9.5 Ma) and SK8 (8.8 Ma) within the Shivagarhi Member of the Chor Khola Formation; SK11 (6.8 Ma) within the Surai Khola Formation and SK16 (4.0 Ma) and SK17 (3.8 Ma) within the Dobata Formation (see Dhital, 2015 for a review of these lithologies). These time frames for the horizons with garnet are consistent with when most researchers would indicate significant GHC input to the Siwalik Group was well underway in Nepal (Huyghe *et al.* 2001; Robinson *et al.* 2001; Szulc *et al.* 2006; Nakajima *et al.* 2020; Yoshida *et al.* 2021). Geochemical analyses were conducted on all garnet-bearing samples except SK16, as well as on additional sandstones from the Bankas Formation (SK1, SK2 and SK3), Jungli Khola Formation (SK4, SK5 and SK6) and Surai Khola Formation (SK13, SK14 and SK15) (see Supplementary File, Figure S1).

5.b. Garnet extraction and identification

Garnets were extracted and identified through a combination of physical, optical and density-based methods designed to isolate and verify detrital grains from the Siwalik sandstones. Initially, samples were crushed and sieved to isolate grains within a target size fraction (260 µm) for heavy mineral separation. We used a sieve size that aimed to retain grains larger than 63 µm and remove grains larger than 260 µm, which enriched the heavy mineral fraction while minimizing fines and oversized clasts. While this range was effective for garnet recovery in the Siwalik Group, future studies may benefit from testing larger grain-size fractions, which could capture additional material. This preliminary separation involved using a water table to concentrate the heavy mineral fraction, which facilitated the removal of light minerals and potential organic matter, yielding a denser concentrate enriched in garnet and other heavy minerals. Subsequent separation employed heavy liquids to further isolate the garnet-rich fraction. While bromoform ($CHBr_3$) has traditionally been used in heavy liquid separation due to its high density, health and safety concerns have led to the adoption of sodium polytungstate ($Na_6[H_2W_{12}O_{40}]$) as a safer alternative with a comparable density (2.9 g/cm^3; Andò, 2020; Stutenbecker *et al.* 2024). Bromoform was used in this study due to its availability. After heavy liquid separation, the remaining concentrate was subjected to magnetic separation using a Frantz Isodynamic Separator. The sequence of magnetic separation after heavy liquids aimed to refine the garnet fraction by removing ferromagnetic and paramagnetic minerals. The magnetic separation settings were adjusted to focus on a range suited for garnet recovery (between 0.1 and 1.5 A), considering that garnets can vary in magnetic susceptibility based on composition and alteration state.

In the fraction isolated from the magnetic separation, garnets were identified based on their colour, high relief, isotropic optical character and roughly spherical shape. Garnets can exhibit a wide range of shapes and colours (Mange & Maurer, 1992). Euhedral forms, sharp, irregular fragments and sub-rounded to rounded grains are common. Uneven and conchoidal breakage patterns and dissolution features like pits and etch facets may develop. Garnet colour is related to composition. Pyrope and almandine are truly isotropic, though spessartine may display slight anisotropy. Grossular may show weak birefringence.

In this study, red garnets were the most readily identifiable grains, so we focused on these for consistency. Other garnet compositions may show different colours (Mange & Maurer, 1992). While this approach might limit the inclusion of other garnet varieties, it aligns best with the project's scope. Garnets were confirmed to be isotropic under polarized light, and their approximately spherical morphology was noted, as is typical for garnet grains in these sediments. The selected grains were then mounted in epoxy and polished to expose their cross-sections for further mineralogical and compositional analysis. If more than one garnet mount was created, we labelled the garnets with an additional letter (e.g., SK16A-garnet number).

5.c. Geochemical analyses

Whole-rock mineralogical analysis (XRD data) was obtained from all samples in the Department of Earth and Planetary Sciences at The University of Texas at Austin (UT Austin) (Fig. 4c). Whole-rock samples were manually homogenized, ground and sieved to a 200 µm mesh size. XRD analyses were performed using a Bruker D8 instrument equipped with Cu Kα radiation, a nickel filter, and a
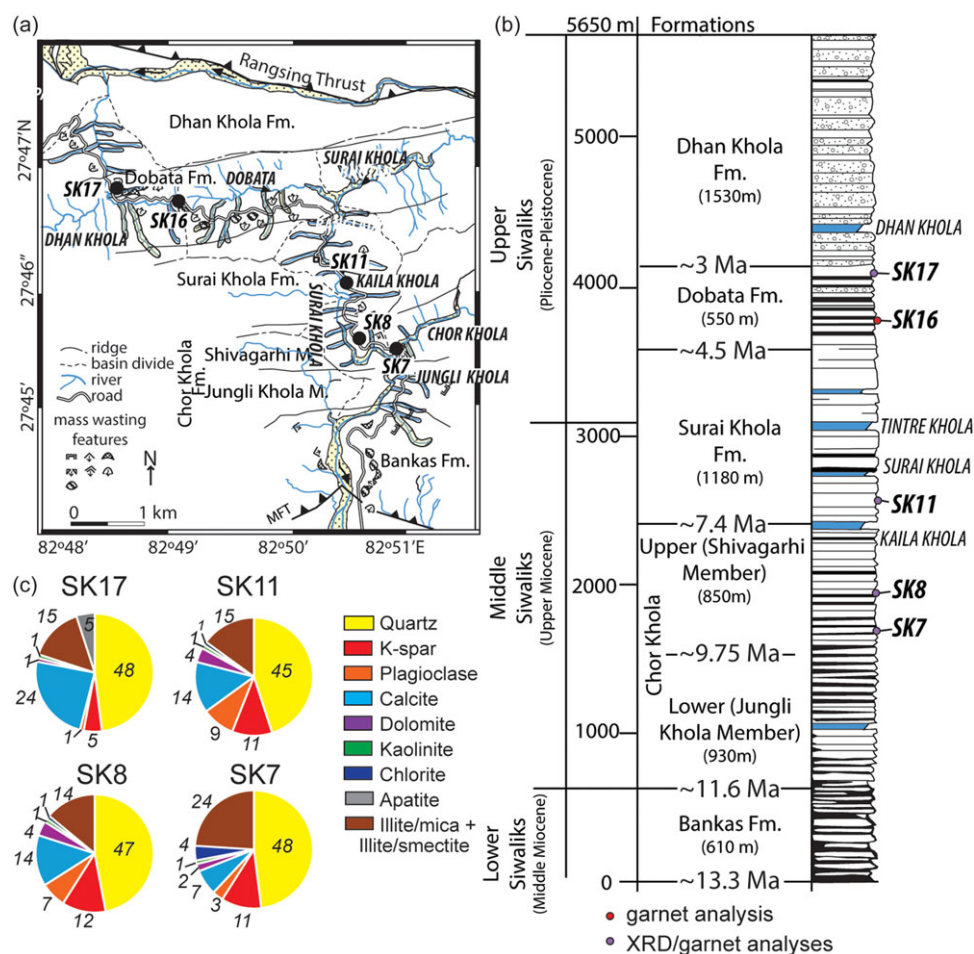
Figure 4. (a) Map of the Surai Khola area showing sample locations, modified from Tamrakar and Yokota (2008). (b) Stratigraphic section of the Siwalik Group with sample numbers indicated, adapted from Corvinus and Rimal (2001). (c) Mineral proportions in samples SK17, SK11, SK8 and SK7, shown as pie charts.

LYNXEYE solid-state detector. The instrument operated at 45 kV and 40 mA, utilizing a 2θ scan range of 3° to 70° with step increments of 0.0195° (2θ) and a 1-second acquisition per step. Whole-rock X-ray patterns were determined through Rietveld refinement using Bruker TOPAS 4.2 software.

Each garnet mount was imaged and analysed using a Hitachi SU-8700 Field Emission Scanning Electron Microscope (SEM) with Bruker Corporation's AMICS automated mineralogy system software package. The SEM operated at an accelerating voltage of 15 kV, emission current of 87 μm and acquisition time of 30 milliseconds for each Energy Dispersive Spectroscopy (EDS) spectrum. The spatial resolution was set to 100 μm, and mineral identification was refined using the AMICS Process software. The EDS spectra provided mineralogical classification and facilitated garnet identification for further compositional analyses.

Garnets were analysed edge-to-edge using a JEOL JXA-8200 electron microprobe at UT Austin. All compositional data are provided in a supplementary dataset (Dataset S1). Most garnet analytical totals were acceptable for this mineral (99–102.5%, Kohn, 2014). For calculating atoms per formula unit from weight per cent totals, we followed Deer *et al.* (2009) instead of Rickwood (1968) or Locock (2008). Alternative approaches would not significantly alter the observed trends in elemental distribution.

Spot analysis was performed at a distance of ~20 μm or less across the garnet to capture compositional variations. We obtained a maximum of 14 data points across the largest grains. A total of 89 garnet grains were analysed (SK7 = 15 garnets, SK8 = 11 garnets,

SK11 = 27 garnets, SK16 =15 garnets and SK17 = 21 garnets). Additionally, seven central section spot analyses were conducted on garnets in sample SK16.

Only ten garnets exhibited higher Mn in their cores, as shown in Fig. 5. Of these, eight garnets were successfully modelled to reconstruct their thermobarometric histories, including those from samples SK11 (SK11-1, SK11-9, SK11-14 and SK11-24), SK16 (SK16C-3 and SK16B-14) and SK17 (SK17-13 and SK17-19). The remaining two garnets (SK11-17 and SK17-10) were excluded from thermodynamic modelling due to their spessartine-rich compositions because we lacked suitable solution models and bulk-rock compositions. Samples exhibiting flat zoning profiles were also excluded from thermodynamic modelling, as such profiles are typically interpreted to reflect diffusional re-equilibration of primary garnet compositions.

5.d. Garnet grouping and classification approach

Initially, garnets were manually categorized into primary end-member groups based on spessartine (XMn), almandine (XFe), pyrope (XMg) and grossular (XCa) distributions. Following this initial classification, we refined their groupings by determining the relative proportions of additional mole fraction end-members. This framework allowed us to establish a general group classification scheme, ultimately identifying seven (or nine, depending on XMg contents) compositional groups within the garnet samples. Figure 5 shows representative examples of the classification grouping, with details for all samples listed in Table 1.
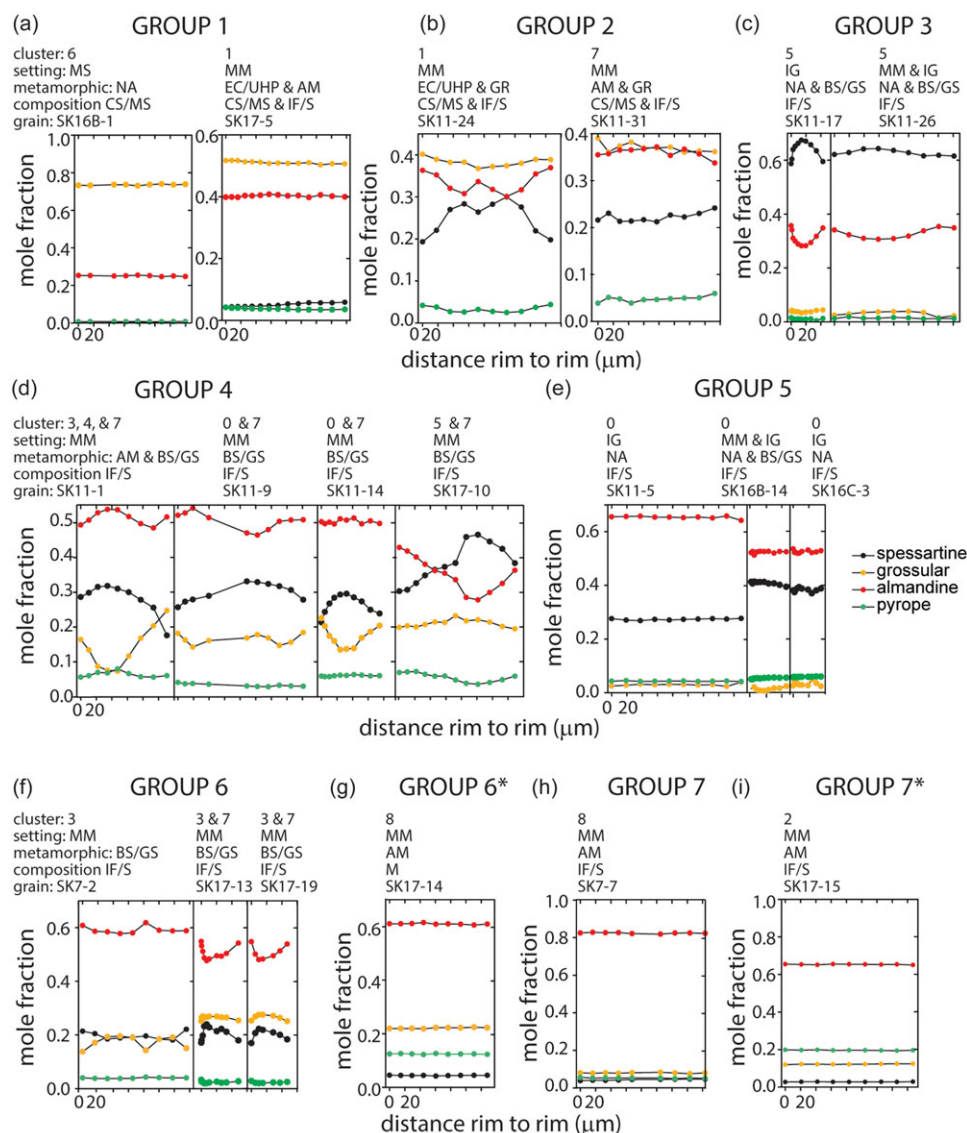
**Figure 5.** Garnet transects from the largest grains of each group. Group and cluster numbers, as well as setting, metamorphic and compositional classes, are indicated (after Schönig *et al.* 2021). Abbreviations: MS = metasomatic rocks; IG = igneous rocks; MM = metamorphic rocks; BS/GS = blueschist/greenschist-facies; AM = amphibolite-facies; GR = granulite-facies; EC/UHP = eclogite/ultrahigh-pressure facies; CS = calc-silicates; IF/S = intermediate–felsic/metasedimentary; M = mafic.

Table 1. Summary groupings from garnet compositions

Sample/Group	Group 1	Group 2	Group 3	Group 4	Group 5	Group 6/Group 6*	Group 7/Group 7*	Sum
High	XCa>Fe	XCa+Fe+Mn	XMn>Fe	XFe>Mn>Ca	XFe>Mn	XFe	XFe	
Low	XMn+Mg	XMg	XCa+Mg	XMg	XCa+Mg	XCa+Mn>XMg	XMn+Ca+Mg	
Total Garnets	14	4	2	8	26	15/1*	22/8*	100
Analyses Total	88	42	19	84	228	126/9*	138/70*	804
% Total analyses	11	5	2	10	28	16/1	17/9	100%
XFe (±1σ)	0.244 (0.118)	0.320 (0.034)	0.320 (0.024)	0.476 (0.059)	0.582 (0.045)	0.512 (0.064)/ 0.610 (0.002)	0.706 (0.092)/ 0.723 (0.082)	
XMn (±1σ)	0.026 (0.020)	0.247 (0.066)	0.633 (0.024)	0.305 (0.049)	0.325 (0.057)	0.186 (0.039)/ 0.045 (0.001)	0.109 (0.079)/ 0.020 (0.022)	
XCa (±1σ)	0.713 (0.149)	0.399 (0.090)	0.035 (0.007)	0.170 (0.041)	0.046 (0.026)	0.251 (0.044)/ 0.221 (0.002)	0.097 (0.061)/ 0.047 (0.034)	
XMg (±1σ)	0.017 (0.018)	0.034 (0.017)	0.012 (0.003)	0.049 (0.013)	0.048 (0.013)	0.050 (0.018)/ 0.124 (0.001)	0.088 (0.043)/ 0.210 (0.056)	

*This symbol classifies garnets with higher XMg. We include data for both the lower/higher Mg samples.
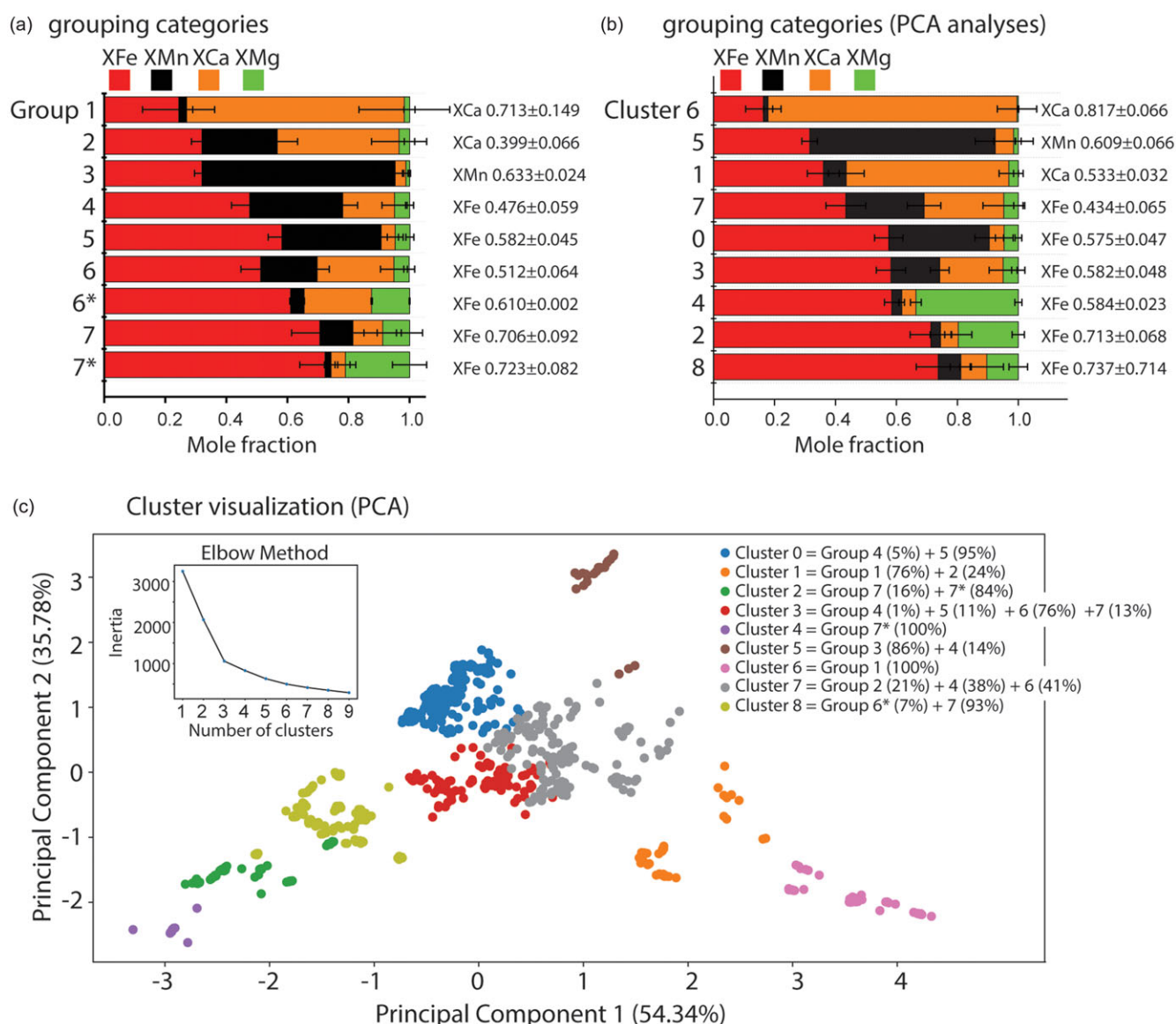
Figure 6. (a) Bar diagram showing the manual group classifications per sample, showing the dominant mole fractions. (b) PCA-based grouping per sample. (c) PCA scatter plot with clusters coloured by group. The inset displays the results of the elbow method. All data, including those from zoned garnets, are included in this diagram.

Zoned garnets are found in all manual garnet groups except for 1, 6*, 7 and 7*.

Clustering was also performed using XMn, XCa, XFe and XMg, combining Principal Component Analysis (PCA) and k-means. Figure 6 shows the results of the PCA and their relationship to the grouping categories. Before clustering, the dataset was pre-processed by standardizing all features using the StandardScaler, ensuring each feature contributed equally to the analysis by removing the effects of differing units or scales. PCA was then applied to reduce the dimensionality of the dataset from four features to two principal components. The first principal component (PC1) captured the largest variance in the data, while the second principal component (PC2) captured the second-largest variance orthogonal to PC1. For PC1, the contributions of the features are most strongly influenced by Fe (-0.6340) and Ca (0.5786), with lower contributions from Mn (0.0722) and Mg (-0.5080). PC2 is primarily influenced by Mn (0.8092) and Ca (-0.4361), with smaller contributions from Fe (-0.0095) and

Mg (-0.3936). For PC3, the contributions are driven by Mg (-0.7420) and Fe (-0.5651), with moderate contributions from Mn (0.3606) and minor contributions from Ca (-0.0128). Finally, for PC4, the feature contributions are Mn (-0.4582), Ca (-0.6891), Fe (-0.5278) and Mg (-0.1913). PC4 is predominantly influenced by Ca, with moderate contributions from Fe and Mn. PC1 explains the most variance, accounting for 54.3%, followed by PC2 with 35.8%, PC3 with 9.9% and PC4 with a negligible 0.01%. Because PC1 and PC2 capture most of the variance (90.12% combined), they form the basis for our two-dimensional clustering and data visualization shown in Fig. 6c.

The optimal number of clusters was determined using the Elbow Method, which involves plotting the number of clusters (k) against the inertia (the within-cluster sum of squared distances) (Fig. 6c, inset). The point at which the inertia curve showed a significant reduction in slope (the 'elbow') was identified as the optimal k. Although the elbow method suggests using three clusters (k=3), we opted for nine clusters to disentangle

overlapping groups better and capture subtle differences within the dataset. The elbow method, while effective, often oversimplifies complex data, potentially merging variability or outliers into larger clusters. Increasing the number of clusters ensures a better representation of the dataset's structure. Based on the cluster visualization, we identified seven to nine clusters suitable for representing the data. Nine clusters were chosen as they align with the manual approach and allow a comparison.

We also applied the host-rock discrimination scheme of Schönig et al. (2021), which is based on a random forest machine-learning algorithm trained on a large dataset of chemical analyses of garnet from a wide range of lithologies. The setting and metamorphic classes classification scheme of Schönig et al. (2021) predicts the correct classification for 88% of all observations in the database, whereas the composition model predicts the correct class for >92%. Supplementary Dataset S3 presents the quantitative results from this analysis.

Multiple other approaches are available to ascertain the provenance of Siwalik garnets. These include using bi-plots (Krippner et al. 2014), alternative compositional databases (Suggate & Hall, 2014) or three-dimensional calculations (Knierzinger et al. 2019). The compositional analysis combined with Lu-Hf and U–Pb geochronometry (Mark et al., 2023) and dating of garnet inclusions has recently been applied (Schönig et al. 2018). Trace element data are also valuable for interpreting provenance and metamorphic histories (Raimondo et al. 2017; Rubatto et al. 2020; Hong et al. 2020). However, more major element data is available for Himalayan hinterland garnets than trace elements, which limits provenance interpretations. We note with some caution that trace elements should not be considered event markers recording simultaneous rock-wide changes as they may only record local changes or transient disequilibrium (Chernoff & Carlson, 1999).

5.e. Thermobarometric approach

We created isochemical phase diagrams for garnet regions with elevated Mn concentrations near their centres (not necessarily true cores, as zoning geometries could not be confirmed). These were based on a probable LHS rock bulk composition (sample MA43 from Catlos et al. 2001; 2018), using the software package Theriak-Domino (de Capitani & Brown, 1987; de Capitani & Petrakakis, 2010), the thermodynamic dataset of Holland and Powell (1998, with solution model updates through 2010) and appropriate mixing models in the $MnO–Na_2O–CaO–K_2O–FeO–MgO–Al_2O_3–SiO_2–H_2O–TiO_2$ system. We assumed the presence of water (activity of $H_2O = 1.0$) and the Fe oxidation state of 2+. The MA43 bulk composition was modified until the isopleths of ±0.02 mole fraction spessartine, almandine, pyrope and grossular, corresponding to the analysis of the highest Mn content, intersected in the phase diagram. The specific solid solution models were chosen based on options of minerals in a pelitic bulk composition (feldspar, Baldwin et al. 2005; Holland & Powell, 2003; garnet, Mahar et al. 1997; White et al. 2000, 2005; Zeh & Holness, 2003; biotite, Powell & Holland, 1999; White et al. 2000; white mica, Coggon & Holland, 2002; ilmenite, ideal Mn-Mg-Fe solution; chlorite, Holland et al. 1998; staurolite, Holland & Powell, 1998; Mahar et al. 1997; chloritoid, Mahar et al. 1997; White et al. 2000).

We explored various effective bulk rock compositions until we observed the intersection of the isopleths. The intersection point defined the pressure–temperature condition of the central section. To develop the pressure–temperature paths, electron microprobe compositions were used, but 1–2 data points were added between the analyses, assuming no significant changes in chemistry occurred in the garnet where no data were collected. The use of additional data maintains computational stability and faster fits with the Nelder-Mead search routine of the MATLAB programme. The MATLAB script was applied to the Theriak-Domino programme to search the pressure-temperature grid for a minor misfit between the modelled garnet composition and the measured composition and to calculate the portion of the bulk composition that should be sequestered in the next step of garnet growth. The process repeats all steps across the garnet profile, estimating the pressure–temperature conditions for each data point and the change in effective bulk composition. All data for the pressure–temperature paths are provided as supplementary files (Table S5).

We generated pressure–temperature paths for the SK11 garnets, SK16C-3 and SK17-19, which have higher Mn concentrations in their central sections. In some cases, two pressure–temperature paths were generated for the garnets with symmetrical zoning patterns from their central sections to the edge. Garnets SK16B-14 and SK17-13 did not yield enough compositional variations across the garnet to develop a pressure–temperature path.

6. Results for equivalent samples

6.a. Garnet grain size and comparison to palaeohydrological indicators

Table 2 summarizes palaeohydrological results from samples collected from locations equivalent to those in this study (Ulak, 2005). These data provide insights into sediment transport dynamics and offer an understanding of the environmental conditions during deposition. We include our measured garnet grain sizes from these samples, allowing for a direct comparison to the D50 and D95 values from equivalent samples. D50 represents the median grain size, where 50% of the sediment sample (by weight) is fine-grained, and 50% is coarse-grained, while D95 represents the fine end-member grain, where 95% of the sediment sample is finer and only 5% is coarser.

This study separated garnet grains using a sieve-based method, with a maximum observable size of 260 μm. However, only two samples (SK17 from the Dobata Formation and SK11 from the Surai Khola Formation) contained garnets that reached this size, suggesting that garnets from these rocks were large enough to be transported alongside the coarsest fraction of the sediment. In contrast, the maximum garnet size in other samples was significantly smaller than the D50 and D95 values of equivalent samples, which have implications for sediment sorting, transport behaviour and provenance interpretations.

For example, the sample from the same location as SK7, within the Shivagarhi Member, records the highest-energy conditions, characterized by the greatest discharge (3,430 m³/s), steepest slope (5.49%) and highest upper-velocity limit (2.8 m/s). These conditions are consistent with an environment capable of transporting coarse sediments from an actively uplifting hinterland. This sample has the greatest flow depth (4.7 m), indicative of substantial fluvial power and a well-developed system. However, in SK7, the largest observed garnet was 163 μm, significantly finer than the equivalent sample's median grain size (D50 = 390 μm) and much smaller than the coarsest transported grains (D95 = 670 μm). This size discrepancy suggests that garnets were

Table 2. Summary of paleohydrology estimates for sampled locations (data after Ulak, 2005)

Sample	SK17	SK16	SK11	SK8	SK7
Ulak (2005) sample number	SC20a	SC19a/ SC19b	SC12a/ SC12b	SC09a/ SC09b	SC08a
Bedding*	PCB	TCB	TCB	RL/TCB	TCB
Depth (m)	2.4	1.8/1.2	2.1/1.3	0.9/0.4	4.7
Slope (%)	4.26	1.55/ 0.69	2.45/ 1.52	1.05/ 0.47	5.49
Discharge (m³/sec) and velocities (m/sec)†					
Discharge	679	339/128	492/ 15.5	63.8/ 90.4	3430
Ucr	0.34	0.23/ 0.18	0.27/ 0.25	0.24/ 0.21	0.3
Urd	0.74	0.6/1.02	1.04/ 1.22	0.54/ 0.46	1.16
Uup	0.67	0.63/ 0.39	1.58/1.1	0.83/ 0.43	2.8
AV	0.72	0.62/0.6	1.4/1.14	0.39/ 0.44	2.25
Grain sizes (garnet data from this paper) (µm)§					
D50	360	170/520	420/720	170/190	380
D95	690	230/990	960/ 1550	290/360	670
Average garnet size (±1σ)	125 (72)	82 (62)	136 (59)	46 (17)	72 (51)
Largest garnet	260	194	259	70	163
Smallest garnet	7	21	42	21	9

*PCB = Planar Cross-Bedding, TCB = Trough Cross-Bedding, RL = Ripple Lamination

†Ucr = Upper Critical Velocity, Urd = Upper Regime Deposition Velocity, Uup = Upper Unidirectional Flow Velocity, AV = Average velocity

§D50 = Median grain size, in which 50% of the sediment sample (by weight) is finer and 50% is coarser. D95 = Coarse end-member, the grain size at which 95% of the sediment sample is finer and only 5% is coarser.

deposited with finer-grained material rather than the dominant sand fraction. Possible explanations include selective sorting due to the garnet's higher density and differential transport behaviour compared to lower-density grains (quartz, feldspar or lithic fragments) or a provenance signal indicating a limited supply of coarser-sized garnets.

Sample SK17, collected from our uppermost stratigraphic level of the Dobata Formation, retains high-energy transport characteristics, but with more moderate discharge, slope and velocity than SK7 (Table 2). The channel depth is lower than that of SK7 but still indicates a moderate fluvial system capable of transporting sand-sized sediments. Garnets from SK17 reached the maximum sieve size (260 µm), suggesting they were transported alongside the dominant sand fraction rather than being selectively sorted into finer sediments. Notably, SK17 was the only sample to exhibit planar cross-bedding structures, consistent with the migration of large sandbars or dunes under moderate- to high-energy conditions. This observation supports the interpretation that SK17 represents a dynamic but less extreme depositional setting than SK7.

Data from samples between these stratigraphic levels, including those equivalent to SK8 (Shivagarhi Member), SK11 (Surai Khola

Formation) and SK16 (Dobata Formation), indicate lower and more variable transport energies compared to SK17 and SK7 (Table 2). Ulak (2005) reports data from two samples at each location, suggesting episodic variations in flow energy. For instance, one sample from the SK16 location indicates fine-grained deposition, whereas another is associated with coarser sediments and more variable transport energy. This variability could reflect deposition in different fluvial sub-environments, such as floodplains, channels, levees or crevasse splays. The reported discharge values for these locations are 128 and 339 m³/s, significantly lower than those of SK7 and SK17, further supporting the interpretation of reduced flow energy. In sample SK16, the largest observed garnet was 194 µm (Table 2). When compared to bulk sediment grain-size distributions, garnets were slightly coarser than the median (D50 = 170 µm) in one equivalent sample but significantly finer than the median (D50 = 520 µm) in another. Similarly, garnet size approached the D95 value (230 µm) in the finer-grained dataset, whereas it was much finer than the D95 value (990 µm) in the coarser-grained dataset. These results indicate that garnets in SK16 were transported under variable hydrodynamic conditions, depending on local depositional energy and grain-size distributions. In finer-grained sediments, garnets would have been among the coarser components. However, garnets were significantly finer than expected based on the D50 and D95 values characterizing the coarser-grained sediments. This pattern suggests that garnets were deposited under flow conditions capable of moving medium- to fine-grained sand but not necessarily the coarsest fraction. Such variability may reflect differences in local depositional energy, sediment input or selective sorting processes.

Discharge estimates for two samples from the SK11 location varied significantly (16 and 492 m³/s), consistent with the episodic flow energy variations observed. This sample also contained garnets that reached the maximum sieve size, suggesting that at least some garnets were transported alongside the dominant sand fraction. In contrast, data from rocks from the SK8 location exhibited the lowest transport energy in the dataset. These samples contained finer-grained sediments, with the lowest discharge rates and slopes recorded. Additionally, one equivalent sample displayed ripple laminations commonly associated with overbank deposits or shallow water environments (Taral *et al.* 2017; Rai & Yoshida, 2021). In sample SK8, the largest observed garnet was only 70 µm in diameter. Compared to bulk sediment grain-size distributions, garnets were significantly finer than the median grain size (D50 = 170–190 µm) and much finer than the D95 values (290–360 µm). This observation suggests that garnets were deposited under conditions favouring fine-particle transport, potentially due to selective sorting or differences in the original grain size of the source material.

Palaeocurrent directions in the Surai Khola section indicate that transverse rivers, flowing perpendicular to the mountain front (N-S), became the primary sediment suppliers in the later stages of the Middle Miocene (Burbank *et al.* 1996). Szulc *et al.* (2006) suggest that the Surai Khola lacks evidence for sustained axial flow (WNW or ESE). However, their dataset includes only one direction from the Dobata Formation, which showed NE-directed flow. This observation suggests that a transverse river was possible at that specific location. The dataset from Nakayama & Ulak (1999) and Ulak (2005) includes numerous samples with paleoflow indicators that support the presence of an axial drainage system in the Dobata and Dhan Khola units, as well as intermittently throughout the section, particularly in the lower part of the Surai Khola Formation.

Their results are consistent with a possible transverse river input by ~4 Ma, persisting into the Dhan Khola Formation.

Quade *et al.* (1995) and Hoorn *et al.* (2000) documented a major environmental shift from C₃- to C₄-dominated ecosystems in the upper part of the Middle Siwalik (MS1) around 6.5 Ma. This transition occurs at a stratigraphic level slightly above the Surai Khola marker, as shown in Fig. 4b. The more recent identification of a second phase of vegetation change, characterized by the expansion of C₃ plants during the last 3 Myr, appears unique to the Surai Khola section and may have been influenced by sediment recycling at 3–4 Ma (Charreau *et al.* 2021; Roy *et al.* 2020). This recycling could be linked to a shift from an extensive, trans-Himalayan river system to one primarily draining the LHS and a Siwalik piedmont (Charreau *et al.* 2021).

Overall, the reported paleohydrology results indicate that sediment transport within the Surai Khola Siwalik section was episodic and spatially variable (Table 2). Specific samples (e.g., SK7 and SK17) record high-energy transport, likely linked to hinterland exhumation and localized shifts in discharge or slope. In contrast, others (e.g., SK8 and SK16) reflect lower-energy conditions. Given the depositional ages of SK7 and SK17 (9.5 Ma and 3.8 Ma, respectively), these events likely occurred under differing climatic and tectonic conditions. The 6.5 Ma vegetation shift (e.g., Quade *et al.* 1995; Hoorn *et al.* 2000) marks an important climatic transition; however, sediment transport intensity may also be modulated by local slope dynamics, discharge variability or tectonic uplift. These variations may reflect transient sediment routing responses to changing sediment supply and transport capacity within a dynamic fluvial system. This episodic behaviour aligns with that of modern Himalayan rivers, where peak discharges, often driven by the monsoon, can periodically flush large volumes of sediment downstream (Singh *et al.* 2007; Clift, 2020). While regional climate likely influenced discharge patterns, the garnet-bearing samples appear to reflect tectonic controls on sediment availability and grain size. Larger garnets are generally found in samples associated with higher-energy, coarser-grained environments (e.g., SK17), while smaller grains dominate finer-grained, lower-energy settings (e.g., SK8 and SK7).

6.b. Geochronological constraints on sediment provenance and exhumation

Detrital white mica 40Ar/39Ar, zircon U–Pb, and zircon and apatite fission track (ZFT and AFT) dates from equivalent samples of the Surai Khola section have been previously reported in isolation (Bernet *et al.* 2006; Szulc *et al.* 2006; van der Beek *et al.* 2006; Baral *et al.* 2016). This section synthesizes these independent datasets relevant to the samples in this study. By integrating existing age constraints with palaeohydrological records, we can better assess their provenance and how fluvial processes modulated sediment flux from the hinterland to the foreland basin.

Szulc *et al.* (2006) report detrital white mica 40Ar/39Ar dates from the same stratigraphic level as SK16 (4 Ma) and samples closely matching the depositional ages of SK11 (6.8 Ma; equivalent sample at 7 Ma), SK8 (8.8 Ma; equivalent sample at 8.9 Ma) and SK7 (9.5 Ma; equivalent sample at 10 Ma). The youngest mica 40Ar/39Ar dates for each sample fall within the Middle to Late Miocene at 16.1±0.3 Ma (SK8), 13.8±3.4 Ma (SK11), 12.1±0.1 Ma (SK16) and 11.4±1.2 Ma (SK7). These results indicate that no detrital white mica grains record active exhumation synchronous with deposition. Instead, the sediment was derived from previously exhumed and cooled source terrains. Lag times, estimated as the

difference between the youngest mica cooling age and depositional age, vary among the samples: ~2 Myr (SK7), ~7 Myr (SK11), ~7.2 Myr (SK8) and ~8 Myr (SK16). The shorter lag time of SK7 is consistent with the observation that it was deposited under the highest-energy conditions. The longer lag times in the other samples reflect the variable depositional energy conditions, as described in the previous section.

These lag times differ from those estimated using AFT dates, which suggest a constant lag time of 0.8±0.5 Myr due to rapid source-area exhumation rates of ~1.8 km/Myr since ~7 Ma (van der Beek *et al.* 2006). The difference likely reflects the sensitivity of these thermochronometers to different closure temperatures, with AFT recording more recent cooling histories. Detrital white mica grains were sourced from previously exhumed rocks, whereas AFT records more recent cooling closer to the depositional period. The AFT and mica geochronology studies indicate that the Surai Khola section underwent sediment recycling, with the Upper Siwalik sedimentary rocks more strongly affected than the underlying units (Szulc *et al.* 2006; van der Beek *et al.* 2006).

Figure 7 presents the detrital 40Ar/39Ar white mica dates from equivalent samples in a radial plot, illustrating their distribution, age peaks, and central and weighted mean dates. A radial plot enables the comparison of age estimates of varying precision and the visualization of mixed-age populations while accounting for individual uncertainties. It is beneficial for identifying outliers (Galbraith, 1990; Vermeesch, 2009). Central peak and calculated weighted mean dates highlight dominant exhumation phases. Data from samples SK16, SK11 and SK7 indicate a primary sediment source with exhumation pulses in the Middle Miocene, whereas SK8 suggests derivation from regions that cooled during the Late to Middle Miocene. The consistent Middle Miocene dates (~14–19 Ma) across all samples suggest a common source region. The dates also align with ZFT dates from the section (~16 Ma) (Bernet *et al.* 2006). The absence of younger white mica 40Ar/39Ar dates (<10 Ma) also indicates that by ~9.5–4 Ma, actively exhuming regions were not significantly contributing to the sediment load. Instead, sediment was sourced from terrains that had already undergone exhumation and cooling by the Middle Miocene.

Older 40Ar/39Ar age peaks in each sample (e.g., 21–26 Ma, 31–45 Ma) may reflect contributions from additional sources or excess argon, yielding artificially older apparent dates. Caution is needed in interpreting detrital white mica 40Ar/39Ar dates. However, these older ages are not uncommon in the Himalaya, and muscovite is generally less prone to incorporating atmospheric Ar than other minerals (Stuart, 2002).

U–Pb zircon dates are also reported from equivalent sample locations in the Surai Khola section (Bernet *et al.* 2006; Baral *et al.* 2016). We focus on data from Baral *et al.* (2016) due to the large number of zircon dates from samples at the same stratigraphic level as SK11 as well as the same formation and nearby locations for SK8 and SK16. Fig. 8a–c shows radial plots for these samples that show dispersion consistent with a mixed population. However, each sample exhibits consistent age peaks at ~550 Ma, 900 Ma, 1.2 Ga, 1.8 Ga and 2.5 Ga. These age distributions closely resemble those of previous studies, which show that Siwalik sedimentary rocks in western Nepal yield U–Pb zircon populations of 460–530 Ma, ~850–1200 Ma, ~1.8–2.0 Ga and ~2.5 Ga (DeCelles *et al.* 1998). Zircons from the Tethyan Himalayan Sequence are typically associated with U–Pb age peaks at ~500 Ma and 1 Ga, while those from the GHC sequence cluster around ~1.1 Ga, with minor peaks at ~1.50 Ga, 1.7 Ga and 2.5 Ga. Upper formations of the GHC and granitic rocks
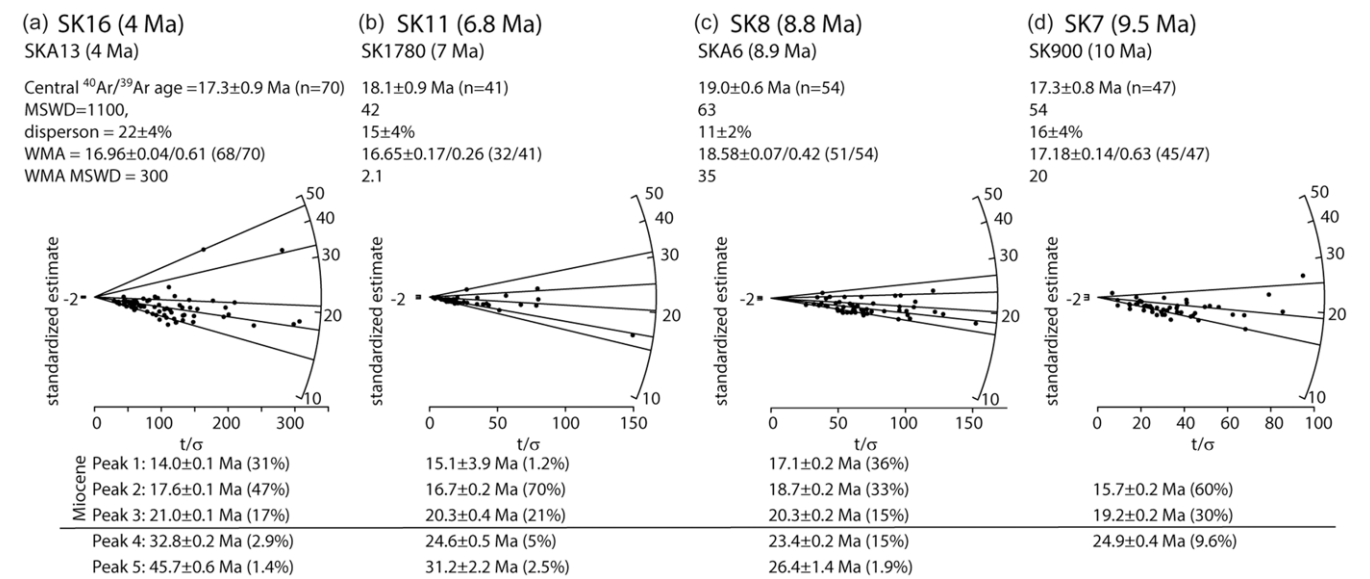
Figure 7. Radial plots for $^{40}Ar/^{39}Ar$ mica dates on data from Szulc *et al.* (2006). Sample numbers include both SK identifiers and those from original publications. Central and peak ages are labelled. WMA = Weighted Mean Ages.
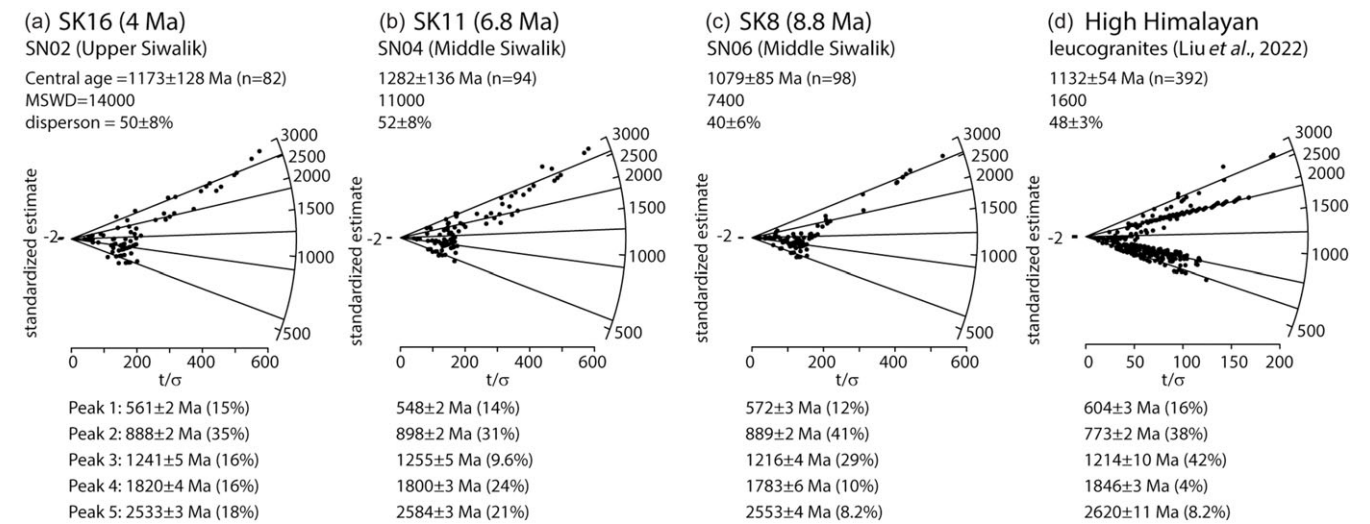
Figure 8. (a–d) Radial plots for U–Pb zircon dates from Baral *et al.* (2016), showing central and peak ages. Both our sample numbers and previously reported sample identifiers are included for reference. (d) U–Pb zircon dates from High Himalayan leucogranites, after Liu *et al.* (2022). All analyses yield $p(\chi^2) = 0$.

from the LHS also yield U–Pb zircon dates ~500 Ma (DeCelles *et al.* 2000, 2004; Gehrels *et al.* 2011).

Overall, past geochronological work in the Surai Khola on samples taken from stratigraphic levels similar to those in this study (<9.5 Ma) suggests that sediment source regions remained broadly consistent over time. This indicates long-term stability in sediment routing, with shifts primarily reflecting changes in the relative mixing proportions of different source terrains rather than abrupt provenance changes.

7. Results from Siwalik Group analyses

7.a. Garnet compositions and groupings

Garnet compositional profiles are categorized into nine groups based on both manual classification (zoning-based) and PCA

clustering. Most garnets exhibit low XMg values (<0.1) and display flat zoning. Those garnet groups that show higher XMg (>0.1) are denoted by an asterisk (*). Figure 5 is intended to be representative of the range of zoning profiles and, therefore, highlights garnets with compositional variation. Specifically, garnets that do not exhibit flat zoning are from Groups 2–6 and include samples SK11-24, SK11-17, SK11-1, SK11-9, SK11-14, SK17-10, SK16C-3, SK16B-14, SK17-13 and SK17-19. These garnets were selected for modelling their pressure–temperature conditions and paths.

Groups 1 and 2 are Ca-rich garnets found exclusively in SK11, SK16 and SK17 (Fig. 5a and b). Group 1 garnets have XCa > XFe with low XMn + XMg, while Group 2 garnets show more variability in their XFe, XMn and XMg contents. These Ca-rich garnets are low in Cr and Ti, consistent with previous findings that disregarded the uvarovite and hydrogrossular end-members (Yoshida *et al.* 2021). Group 3 garnets are spessartine (SK11),
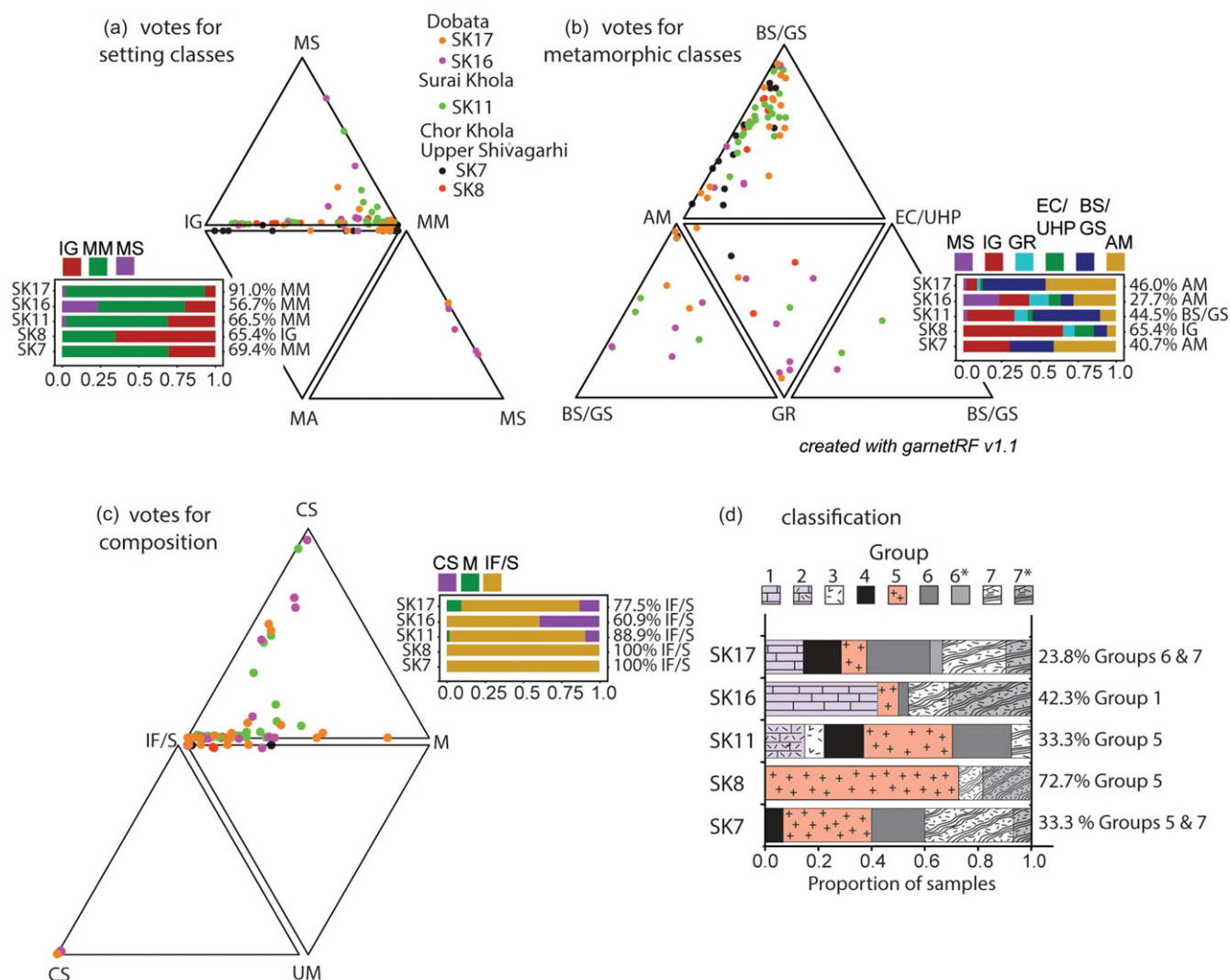
Figure 9. Kernel density plots showing distribution of classification votes for: (a) Setting classes; (b) Metamorphic facies; (c) Composition types, based on Schönig *et al.* (2021). Abbreviations: MS = metasomatic; IG = igneous; MA = mantle; MM = metamorphic; BS/GS = blueschist/greenschist; AM = amphibolite; GR = granulite; EC/UHP = eclogite/ ultrahigh-pressure; CS = calc-silicates; IF/S = intermediate–felsic/metasedimentary; UM = ultramafic; M = mafic. (d) Bar plot showing maximum percentage of each manual group per sample.

characterized by high MnO (26–28 wt%), low CaO and MgO contents and mixed zoning, with one grain exhibiting flat zoning and the other displaying a bell-shaped profile (35μm in diameter).

Groups 4–7 garnets are almandine with varying XMn, XCa and XMg. Most have low XMg, except for those designated in Group 6* (n=1) and 7* (n=8) (Fig. 5). Group 4 and Group 5 garnets are almandine-spessartine but differ in XCa. Group 4 garnets were found in samples SK7, SK11 and SK17. Group 5 and 7 garnets were present in all samples. Group 6 garnets were found in all samples except SK8. Group 6 and Group 7 garnets are similar but differ in their XCa and XMn compositions. These are almandine and possess higher XFe contents than the other garnet groups.

Figure 5 provides examples of the relationship between clustering and grouping for specific garnet analyses, whereas Figure 6c shows the percentage distribution of garnets across the classification approaches. Some garnet clusters were exclusively linked to manual groups (i.e. Cluster 4 and 6 are linked to Groups 7* and 1, respectively, Fig. 6c). However, garnet groups with compositional zoning from rim-to-rim are part of multiple clusters (i.e. Group 4 garnets are assigned in Clusters 0, 3, 4, 5 and

7, Fig. 5d). These observations indicate that the PCA prioritizes compositional variance over zoning trends that are best observed manually.

7.b. Garnet discrimination approaches

Figure 9 illustrates the results of garnet groups using the approach of Schönig *et al.* (2021). The 'setting' scheme discriminates for garnet sourced from mantle rocks (MA), igneous rocks (IG), metasomatic rocks (MS) and metamorphic rocks (MM) based on the votes for each class. Siwalik garnets exhibit votes from the MM, IG and MS categories (Fig. 9a). The metamorphic category dominates in all samples except SK8, which shows more igneous affinities. The classification scheme also classifies some metasomatic garnets in samples SK11, SK16 and SK17, although at lower amounts (2.6%, 23.4% and 2.0%, respectively).

The Schönig *et al.* (2021) metamorphic classes classification scheme shows that a wide variety of possible metamorphic classes are present in Siwalik samples (Fig. 9b). This scheme allocates analyses in the MS and IG categories but also includes possible

sources from granulite (GR), eclogite/ultrahigh-pressure terranes (EC/UHP), blueschist/greenschist rocks (BS/GS) and amphibolite-facies rocks (AM). This scheme suggests we should anticipate finding igneous garnets in all samples and metasomatic garnets in samples SK11, SK16 and SK17. It further suggests that AM and BS/GS-sourced garnets are present in all samples. GR and EC/UHP garnets appear in all samples except SK7. In the compositional classification, garnets with intermediate-felsic/metasedimentary (IF/S) dominate in all samples, with calc-silicate garnets appearing at higher structural levels in samples SK11, SK16 and SK17 (Fig. 9c). We also see the potential for mafic garnets in samples SK11 and SK17, although at low abundance (1.8% and 9.5% respectively).

7.c. Other minerals and lithological context

Bulk mineralogical analyses were performed on select Surai Khola samples using XRD (Fig. 4c). These data provide context on whole-rock mineralogy, support general interpretations of provenance and depositional environments, and help differentiate quartz- and carbonate-rich units. The XRD mineralogical analysis reveals the presence of quartz, K-feldspar, calcite, illite/mica and illite/smectite across all analysed samples. Notably, certain mineral phases are absent in specific samples: dolomite is absent in sample SK1, chlorite is absent in sample SK17 and both plagioclase and kaolinite are absent in sample SK18. Apatite is uniquely detected in sample SK17. Based on their mineralogical compositions, samples SK1, SK2, SK3, SK4, SK7, SK8 and SK11 are classified as sandstones. In contrast, samples SK5, SK17 and SK18 are classified as calcareous sandstones due to their significantly elevated calcite contents.

Observations of the mineralogical assemblage align with findings from previous studies on Surai Khola sedimentary rocks. For example, Szulc *et al.* (2006) found zircon, tourmaline, rutile, sphene, garnet and staurolite in all equivalent samples. However, kyanite and sillimanite appeared at stratigraphically higher levels in samples equivalent to SK16 and SK11. Baral *et al.* (2016) reported that samples from the Lower and Middle Siwalik sedimentary rocks are dominated by quartz (91% and 85%, respectively), with feldspar, lithic fragments and phyllosilicates, including muscovite, biotite and chlorite, comprising the matrix. Lithic fragments with calcite cement included carbonate, chert, phyllite, schist and gneiss. Critelli and Ingersoll (1994) attributed this detritus to a recycled orogenic source, primarily derived from low- to medium-grade metamorphic rocks within the suture belt with contributions from volcanic and ophiolitic rocks. However, they reported ophiolitic material only in the Siwalik Group exposures in Pakistan, which are sourced from the palaeo-Indus drainage system and, therefore, expected to contain detritus from the suture zone. Although current petrographic and detrital zircon datasets do not support significant suture zone input in the Siwalik Group of central Nepal (Szulc *et al.* 2006; Bernet *et al.* 2006), the presence of chromium spinel and high XCa garnets in the eastern Nepal Siwalik Group has been linked to ophiolites of the Indus–Tsangpo suture zone provenance (Rai *et al.* 2021).

7.d. Detrital garnet pressure–temperature conditions and paths

Figures 10 and 11 show estimated pressure–temperature conditions from Siwalik Group garnets that preserve higher Mn in their central sections and hinterland examples with similar zoning patterns. The coloured bars in the figures are isopleths of Siwalik garnet compositions ±0.2 XMn, XCa, XMg and XFe from the central section. The isopleth intersection provides our best estimates of the central section pressure–temperature conditions.

Table 3 summarizes the effective bulk compositions used for the samples adapted from an LHS rock (sample MA43; Catlos *et al.* 2001, 2018). The MA43 composition was adjusted for the garnet groups, except Group 6. For instance, adjustments for Group 4 garnets involved decreasing the Fe_2O_3 (−2 mol%) and CaO (−0.3 mol%) and increasing the MnO (+0.1 mol%) and MgO (+2 mol%) content of the MA43 composition. Group 2 garnets are the most Ca-rich garnets, and the MA43 composition was modified by adding CaO (+1 mol%), MnO (+0.1 mol%), SiO_2 (+0.5 mol%) and MgO (+1.5 mol%) while decreasing the Fe_2O_3 (−2.8 mol%). Changes in the MA43 composition were required for the intersection of central section XFe, XMg, XCa and XMn isopleths. Without these adjustments, intersections would not occur, impeding the estimation of central section pressure–temperature conditions. Notably, this challenge was encountered with spessartine Group 3 garnet SK11-17 and Group 4 garnet SK17-10. The chosen MA43 effective bulk composition and solution models were unsuitable for garnets with higher XMn contents.

Table 4 outlines the estimated pressure–temperature conditions and mineral assemblages for the garnet central sections. Notably, Group 2 garnet SK11-24 exhibited overlapping isopleths at the lowest temperature (480°C), with pressure similar to that of Group 4 and Group 6 garnets (~6 kbar). Sample SK11-24 also suggested higher CaO contents and uniquely included titanite in its mineral assemblage.

Group 4 garnets share the mineral assemblage of plagioclase + garnet + biotite + muscovite + ilmenite + chlorite + quartz + H_2O and similar initial thermal conditions of 520–535°C. However, modelled pressure conditions recorded by the garnets differ by 2 kbar among the samples. Sample SK11-1 had the lowest pressure of 4.6 kbar, whereas SK11-9 and SK11-14 were similar, with core conditions of ~6 kbar (Fig. 10a–c).

Group 5 garnets and sample SK17-19 from Group 6 share the Group 4 mineral assemblage. The central section of sample SK17-13 lacks plagioclase but contains the other minerals (Table 4). Group 5 garnets share the central section conditions of 520–525°C and a lower pressure of 3.2–3.6 kbar (Fig. 11a, b). Despite a different mineral assemblage, Group 6 garnets are of similar temperature (505°C) but differ in pressure (6.8 vs. 5.9 kbar) (Fig. 11c, d).

Due to limitations in zoning preservation for some smaller samples, pressure–temperature paths were constructed for only six garnets. Most samples exhibited isothermal burial over 0.5–2 kbar, except for Group 2 garnet SK11-24, which showed an N-shaped path fluctuating over 0.5 kbar (Fig. 10d). This path type may reflect small-scale pressure fluctuations during garnet growth, possibly caused by local tectonic or erosional processes (Catlos *et al.* 2018, 2022). The shape could indicate burial followed by rapid unloading due to erosion, followed by renewed burial or tectonic compression. Alternatively, it may reflect minor variations in the bulk composition of the garnet-bearing assemblage during growth, leading to apparent variations in the modelled path. Fluctuations are small and within the uncertainty of the modelling.

8. Discussion

8.a. Classification and compositional trends of Siwalik Garnets

High-resolution transects across individual grains is an approach commonly used in metamorphic studies to obtain detailed insights
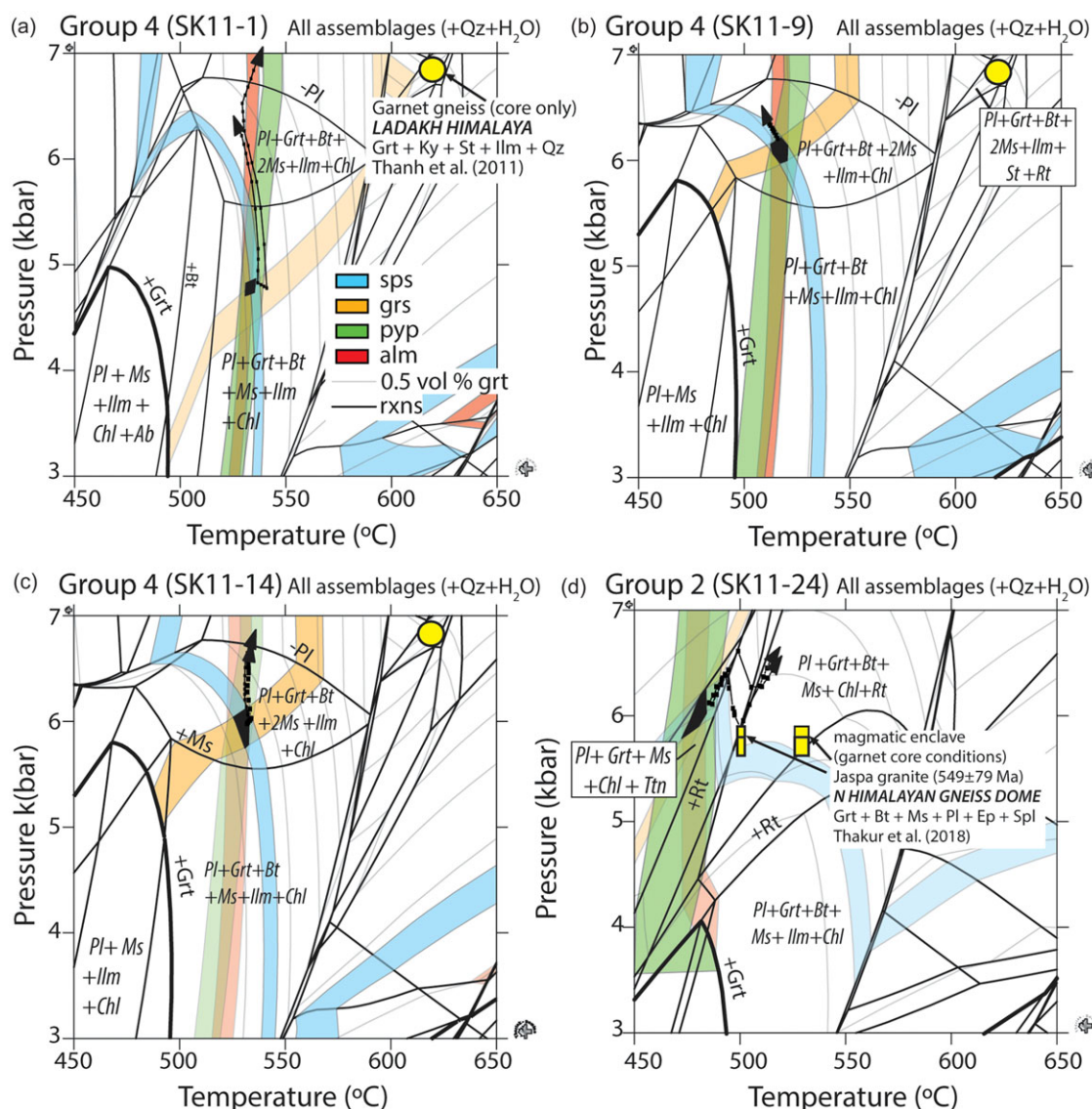
Figure 10. Pressure–temperature diagrams showing the central section conditions and paths for samples (a) SK11-1, (b) SK11-9, (c) SK11-14 and (d) SK11-24. Coloured bars are isopleths and indicate the garnet compositions ±0.2 mole fraction of spessartine, grossular, pyrope and almandine from the central section. Where they intersect is the best estimate of the garnet central section pressure–temperature condition. Some fields are labelled with the relevant mineral assemblages, and the garnet-in reaction boundary is indicated in bold. The volume % of garnet growth is also provided in 0.5 vol %. See Table 3 for the bulk composition used to create the diagrams. Fig. 5b and d show the zoning profiles for these garnets. We include examples of conditions from garnets with similar zoning in each panel.

into garnet growth histories in both metamorphic and igneous rocks (Fig. 5). Although these zoning profiles are from garnet fragments and likely record only portions of their overall compositional distributions, the consistency in zoning within groups suggests that they could be as credible or valuable as the options traditionally provided in ternary diagrams.

Our interpretation of the garnet compositions incorporates manual grouping and PCA-based clustering. While both approaches identify nine major groups and clusters, they differ in how the individual analyses are assigned. Some agreements exist between groups and clusters, as Group 3 maps exclusively to Cluster 5, and the analyses designated as Group 6* are entirely placed in Cluster 8. Group 5 mostly belongs to Cluster 0 (95.8%), with a small fraction in Cluster 3 (4.2%). However, more complex distributions occur among the strongly zoned garnets (Figs. 5 and 6). For example, Group 4 garnets are divided among Cluster 7

(77%), Cluster 0 (17.6%), Cluster 5 (4.1%) and Cluster 3 (1.4%), and Group 7 garnet spans Cluster 8 (84.2%), Cluster 3 (8.6%) and Cluster 2 (7.2%).

The relationship between PCA clusters and manual groups is also seen within single crystals. For example, zoned garnet SK17-10, characterized by a high X_{Mn} and lower X_{Fe} core, and a high X_{Fe} rim and lower X_{Mn} core, falls into our Group 4 category (Fig. 5d). However, the PCA separates the analyses into Clusters 5 and 7. Similarly, two zoned garnets, which we classify as Group 6 (SK17-13 and SK17-19), exhibit low X_{Fe} cores and higher X_{Fe} rims and would be placed in Clusters 3 and 7 by the PCA (Fig. 5f).

Both manual clustering and PCA rely on the same dataset, but PCA rigorously quantifies variance, identifying specific compositions without regard for crystal-scale compositional changes. The PCA approach treats each microprobe spot as a separate data point, which may seem appropriate for garnets lacking
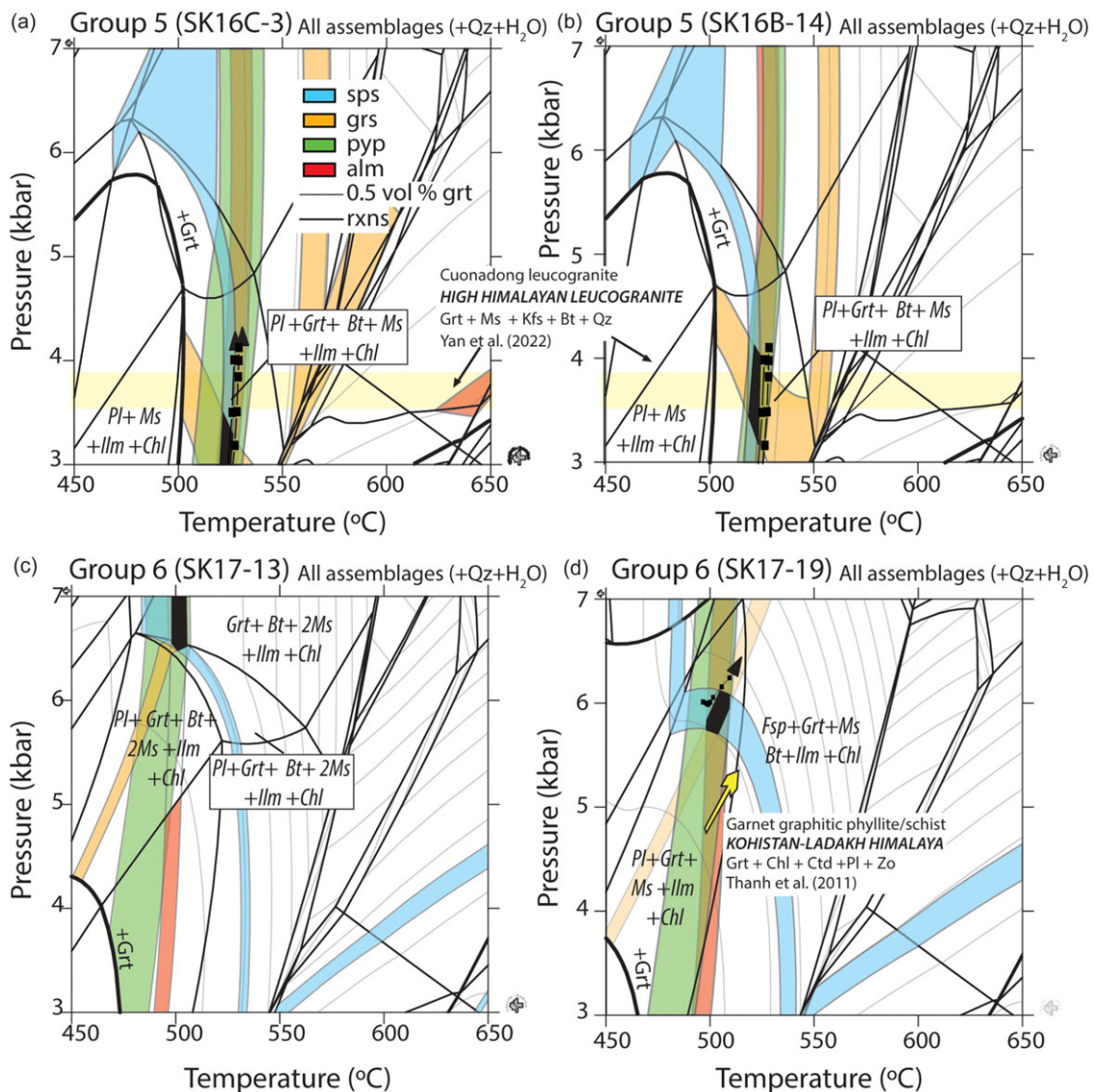
Figure 11. Pressure–temperature diagrams showing the central section conditions and paths for samples (a) SK16C-3, (b) SK16B-14, (c) SK17-13 and (d) SK17-19. The coloured bars are isopleths and indicate the garnet compositions ±0.2 mole fraction of spessartine, grossular, pyrope and almandine from the central section. Where they intersect is the best estimate of the garnet central section pressure–temperature condition. Some fields are labelled with the relevant mineral assemblages, and the garnet-in reaction boundary is indicated in bold. The volume % of garnet growth is also provided in 0.5 vol %. See Table 3 for the bulk composition used to create the diagrams. Fig. 5e and f show the zoning profiles for these garnets. We include examples of conditions from garnets with similar zoning in panels (a), (b) and (d).

compositional zoning but risks interpreting zoned garnets as multiple distinct 'sources' rather than unified crystals with internally evolving compositions. In this way, PCA effectively treats each composition as if it were an entirely separate provenance signal.

The same issue was found with the approach of Schönig *et al.* (2021), which uses a random forest machine-learning algorithm for garnet host-rock discrimination (Fig. 8). By integrating this machine-learning-based method, we gained greater confidence in our provenance interpretations but observed that minor compositional variations occasionally pushed individual spot analyses into different classification categories, even in broadly 'flat' zoned garnets (Fig. 5). Overall, ~ 35% of individual garnet grains contained spot analyses falling into different metamorphic settings, facies or composition categories, even though they were taken from the same crystal. Examples are shown in Fig. 5. The

category shifts reflect subtle compositional heterogeneities rather than indicating multiple distinct events within a single garnet. Variability can arise from subtle zoning, borderline compositional values, or simply the thresholds used by the classification algorithm.

These findings highlight the complexity of garnet growth histories and underscore the importance of the manual classification approach, which considers an entire garnet's compositional profile and geological context rather than treating each microprobe spot as a separate metamorphic or provenance signal. The manual approach captures patterns, allowing us to consider a garnet's entire growth history as a single entity linked to a potential provenance. Combining manual and statistical methods preserves the nuances of garnet zoning while still benefiting from a rigorous classification.

Table 3. Bulk compositional data (mol%) used to generate the core phase diagrams

Group	N/A	4	4	4	2	5	5	6	6
Sample	MA43*	SK11-1	SK11-9	SK11-14	SK11-24	SK16C-3	SK16B-14	SK17-13	SK17-19
SiO_2	60.700	61.200	61.200	61.200	61.200	60.000	60.000	61.200	60.700
Al_2O_3	23.293	23.293	23.293	23.293	23.293	24.623	24.623	24.293	23.293
Fe_2O_3	5.439	3.639	3.639	3.659	2.639	3.639	3.639	3.639	3.639
MnO	0.107	0.207	0.207	0.207	0.207	0.207	0.207	0.207	0.207
MgO	1.759	3.259	3.259	3.259	3.259	3.259	3.259	2.259	2.259
CaO	0.429	0.129	0.129	0.129	1.129	0.019	0.019	0.129	0.629
Na_2O	2.610	2.610	2.610	2.610	2.610	2.610	2.610	2.610	2.610
K_2O	5.077	5.077	5.077	5.077	5.077	5.077	5.077	5.077	5.077
TiO_2	0.528	0.528	0.528	0.528	0.528	0.528	0.528	0.528	0.528
$P2O5$	0.058	0.038	0.038	0.038	0.058	0.038	0.038	0.058	0.038
Total	100	100	100	100	100	100	100	100	100

*Sample MA43 composition was taken from Catlos *et al.* (2018).

Table 4. Summary of the central section and edge pressure–temperature conditions and mineral assemblages

Sample	Size μm	Core T (°C)	Core P (bars)	Core mineral assemblage*	Rim T (°C)	Rim P (bars)	Rim mineral assemblage*
Group 2							
SK11-24	166	480	6000	Pl + Grt + Ms +Chl + Ttn	515	6530	Pl + Grt +Bt + Ms + Chl + Rt
Group 4							
SK11-1	111	535	4600	Pl + Grt + Bt + Ms + Ilm + Chl	538	6986	Grt + Bt + 2Ms + Ilm + Chl
SK11-9	161	520	6050	Pl+ Grt + Bt + 2Ms + Ilm + Chl	510	6414	Pl + Grt + Bt + 2Ms + Ilm + Chl
SK11-14	75	530	6000	Pl + Grt + Bt + 2Ms + Ilm + Chl	534	6671	Grt + Bt + 2Ms + Ilm + Chl
Group 5							
SK16C-3	36	525	3200	Pl +Grt + Bt + Ms + Ilm + Chl	528	4197	Pl + Grt + Bt + Ms + Ilm +Chl
SK16B-14	46	520	3600	Pl +Grt + Bt + Ms + Ilm + Chl	–	–	–
Group 6							
SK17-13	49	505	6800	Grt + Bt + 2Ms + Ilm +Chl	–	–	–
SK17-19	47	505	5900	Pl +Grt + Ms + Ilm + Chl	513	6325	Pl + Grt + Ms + Bt + Ilm + Chl

*All mineral assemblages have Qz + H_2O. Mineral abbreviations after Whitney and Evans (2010).
–not determined.

8.b. Pressure–Temperature conditions and metamorphic history

Many Surai Khola garnet grains exhibit flat zoning profiles, suggesting that the metamorphism of Himalayan units reached thermal conditions high enough to facilitate diffusive zoning or that garnet growth occurred rapidly (Fig. 5) (Ague & Carlson, 2013). Since flat zoning was observed in larger garnet grains, we favour the interpretation of diffusive modification. Garnets that deviate from this trend provide valuable constraints for pressure–temperature modelling (Figs. 10 and 11). Table 5 lists Himalayan outcrop garnets used as comparisons for possible provenance for each group. Hinterland garnets were also analysed for their pressure–temperature conditions, which can be compared to the results generated for the Siwalik garnets or provide potential options for those in which conditions could not be ascertained using the modelling approach

applied in the paper. In addition, the isochemical phase diagrams provide options for the mineral assemblage of the host rock from which the garnet eroded. Table 4 lists these assemblages, which can be compared to those reported for their potential source region.

Group 2 garnets exhibit zoning patterns where XCa + XFe + XMn > XMg (Fig. 5). The pressure–temperature conditions for one representative Group 2 SK11 garnet indicate a central section temperature of 480°C at 6.0 kbar and an edge temperature of 515°C at 6.5 kbar (Fig. 10d). The pressure–temperature path is N-shaped with minor pressure variations, which may reflect erosional exhumation rather than tectonic activity (Catlos *et al.* 2018, 2022). Himalayan garnets with similar zoning patterns and compositions have been identified in rim analyses of garnet-bearing blueschists and granite enclaves and xenoliths within a North Himalayan granite in the Tethyan Himalayan Sequence (Honegger *et al.* 1989; Thakur *et al.* 2018). The mineral assemblage inferred from the

Table 5. Options for provenance for Siwalik garnet groups

Group	Characteristics	Himalayan unit*	Lithology	Pressure–Temperature (P-T) Range	Reference(s)
1	XCa>Fe low XMn + Mg	MCT, Indian Proterozic mobile belt, GHC	Calc-silicates, granulites	P: 5.5–6.5, 10–12 kbar	Groppo et al. (2013); Choudhury et al. (2023); Neogi et al. (1998); Dey et al. (2019)
				T: 650–750, 780–890°C	
2	XCa + Fe + Mn, low Mg	ITSZ, NHG	Blueschist, magmatic enclaves	P: 4.5–7.3, 11 kbar T: 350–500°C	Honegger et al. (1989); Thakur et al. (2018)
3	XMn>Fe, low XCa + Mg	HHL, ITSZ, Gangdese arc	Tourmaline granites, high-P metagreywacke, mafic migmatite, pegmatites	P: 3.5, 14–17 kbar	Visonà and Lombardo (2002); Ma et al. (2017); Yu et al. (2021); Xie et al. (2020)
				T: 600–850°C	
4	XFe>Mn>Ca, low XMg	ITSZ, GHC	Garnet schist, gneiss	P: 8.5–8.9 kbar	Johnson et al. (2021); Thanh et al. (2011)
				T: 572–650°C	
5	XFe>Mn, low XCa + Mg	HHL, N. Himalayan Gneiss dome, Gangdese arc	Magmatic garnet	P: 3.8, 15–17 kbar, T: <710–850°C	Thakur and Patel (2012); Yan et al. (2022); Ma et al. (2017); Xie et al. (2020); LingSen et al. (2019)
6	XFe> low XCa + Mn>Mg	ITSZ, GHC, Kohistan-Ladakh arc, Upper LHS	Blueschist, augen gneiss, schist, graphitic schist, eclogite	P: 5.3–5.4, 6.6–8.4, 9–10, 17–20 kbar	Chatterjee and Ghose (2010); Kawabata et al. (2021); Johnson et al. (2021); Sayab et al. (2016); Catlos (2000); Catlos et al. (2018)
				T: 320–420, 514–530, 570–610°C	
6*	XFe> XMg> XCa + Mn	GHC	Mafic granulite, amphibolite, Calc-silicate	P: 5–9, 9–12, 15–17 kbar	Imayama (2014); Walker et al. (2001); Sen et al. (2023); Borghi et al. (2003); Faak et al. (2012); Kang et al. (2020); Zhang et al. (2022); Wang et al. (2024); Catlos et al. (2022)
				T: 600–880°C	
7	XFe, low XMn + Ca + Mg	LHS, Kohistan-Ladakh arc, GHC, HHL	Metasedimentary rocks, migmatite, leucogranite	P: 6.6–10.3, 13.1, 16.1 kbar	Martin et al. (2010); Catlos et al. (2002, 2018); Rai et al. (2004); DiPietro, (1991); Searle and Fryer (1986); Wang et al. (2024)
				T: 525–882°C	
7*	XFe>XMg> XMn+Ca	GHC	Schist; Gneiss	P: 6.8–11.1 kbar	Catlos et al. (2002); Wang et al. (2024)
				T: 692–882°C	

*Abbreviations: Indus–Tsangpo suture zone = ITSZ; MCT = Main Central Thrust; GHC = Greater Himalayan Crystallines; NHG = North Himalayan Granite; HHL = High Himalayan Leucogranite; LHS = Lesser Himalayan Sequence.

isochemical phase diagram suggests that the original Group 2 garnet host rock contained plagioclase + garnet + biotite + muscovite + chlorite + quartz + H O, with titanite or rutile as possible accessory phases (Table 4). We did not incorporate solutions for epidote or spinel, which are present in the North Himalayan granite enclave assemblage. The estimated conditions for the Siwalik Group 2 garnet align with those from the enclaves, suggesting a potential contribution from North Himalayan granites (Fig. 8d). Additional constraints are needed to evaluate alternative sources, such as garnets from blueschists along the Indus Suture Zone in Ladakh, NW Himalaya, that show similarities in terms of zoning (Honegger et al. 1989).

We generated pressure–temperature conditions and paths for three Group 4 garnets from sample SK11 (Fig. 10a–c). Group 4 garnets are almandine-rich, with higher spessartine and grossular contents and low pyrope content. They are found only in samples SK7, SK11 and SK17 (Fig. 9d). These garnets exhibit prograde

zoning with paths that increase pressure over small temperature changes, supporting a burial-driven metamorphic history. Himalayan garnets with similar zoning patterns to those of Group 4 occur in schists from the Bhimphedi Group (central Nepal) and gneisses of the Pangong metamorphic complex (NW India). The origin of Bhimphedi Group garnets remains debated, as they could be associated with GHC or LHS (see discussion in Webb et al. 2011). In contrast, the Pangong metamorphic complex in Ladakh is linked to the Karakoram Fault in the northwestern Himalaya-Karakoram belt (Streule et al. 2009). Peak conditions for garnet-bearing assemblages with zoning patterns similar to Group 4 range from 535–680°C and 8.1–8.5 kbar (Table 5). The core conditions of all Group 4 garnets overlap in temperature with the Bhimphedi Group samples, but their pressures are ~2 kbar lower. The inferred mineral assemblage for all Group 4 garnets (plagioclase + garnet + biotite + muscovite + ilmenite + chlorite + quartz + H O) is broadly consistent with that

of the Bhimphedi Group, increasing confidence in their potential host rock protolith.

Group 5 garnets are almandine-spessartine with low XCa + XMg. These garnets are present in all SK samples but are most dominant at lower stratigraphic levels (Fig. 9d). In the Himalaya, garnets with similar compositions are reported from magmatic rocks, including HHL, that record high temperatures (~700°C) and low emplacement pressures (~3.8 kbar) (LingSen *et al.* 2019; Xie *et al.* 2020; Yan *et al.* 2022). A garnet core composition within a pelitic xenolith inside a north Himalayan granite also yields a similar composition within 0.5 wt% of some of the SK16C-3 analyses and yields a higher P-T condition of 7.5 kbar and 588°C (Thakur & Patel, 2012). Outside the Himalaya, almandine-spessartine garnets are characteristic of evolved melts, where their distinct zoning patterns are associated with granitic differentiation and fractionation (Nabelek *et al.* 1992; Diella *et al.* 2018). Conditions from a Group 5 garnet in sample SK16 show that the core records the lowest pressure of all garnets analysed (3.2–3.6 kbar) at 520–528°C. A pressure–temperature path from this garnet shows isothermal burial over 1 kbar (Fig. 11d). Based on their zoning, Group 5 garnets are likely magmatic and share the low emplacement pressures seen in some HHL outcrop garnets (Table 5). The mineral assemblage suggested by the phase diagram is consistent with what is observed in HHL rocks (Pl + Grt + Bt + Ms + Ilm + Chl + Qz + H₂O) (Table 4).

Group 6 garnets are almandine-rich with low pyrope and exhibit similar XCa and XMn contents. Himalayan outcrop garnets with comparable zoning occur in a variety of lithologies, including garnet blueschists and eclogites from the Indus–Tsangpo suture zone, augen gneiss and schists of the GHC, and graphitic schists from higher structural levels of the LHS near the MCT (Table 5). Two analysed Group 6 garnets record conditions of 505°C at 5.9 and 6.8 kbar, with one exhibiting a slight pressure–temperature increase to 513°C and 6.3 kbar (Fig. 11d, e). These temperatures are comparable to other garnets with Group 6 compositional profiles, and the isochemical phase diagram suggests a felsic protolith (Table 4). A pressure–temperature path from a graphitic schist/pelite in the Kohistan-Ladakh Arc, developed using garnets with compositions similar to Group 6, is shown in Fig. 11d (Thanh *et al.* 2011). This path closely parallels the Siwalik Group 6 garnet but at lower pressures. While the mineral assemblages broadly overlap, the Kohistan-Ladakh garnet likely crystallized in the presence of chloritoid and zoisite, which were not included as solution models for the Siwalik garnets.

Although rooted in several assumptions, the Siwalik garnet conditions and paths are tentative and testable frameworks for linking detrital garnets to potential source lithologies and metamorphic histories. The following section discusses provenance and tectonic implications for all Siwalik garnet groups, using these conditions to interpret sedimentary inputs, exhumation processes and regional metamorphic evolution.

8.c. Provenance and tectonic implications of Siwalik Group Garnets

Although the flat zoning and high-pressure conditions recorded in many Siwalik garnets imply derivation from deep crustal levels, this does not necessarily reflect continuous rapid exhumation of the hinterland. Instead, these garnets may record episodic, short-lived but intense phases of uplift and erosion, interspersed with more extended periods of tectonic quiescence (Thiede *et al.* 2004; Adlakha *et al.* 2013; Thiede & Ehlers, 2013). Such punctuated exhumation

histories may better explain the transport and preservation of high-grade minerals in foreland basin deposits as high-energy transport processes (landslides, debris flows or major flooding events) likely affected their transportation into the Siwalik Group.

Garnet is prone to chemical weathering in outcrop samples (e.g., Baidya *et al.* 2019). The widespread presence of garnet in the Siwalik Group is consistent with efficient sediment routing and minimized exposure to chemical weathering. High-energy mass-wasting events could transport large amounts of previously stored material from uplifted regions into the foreland basin in pulses rather than through steady erosion and exhumation. In the Surai Khola section, this interpretation is consistent with 40Ar/39Ar detrital white mica dates that support lag times of 2–8 Myr.

Siwalik garnets within similar classification groups likely share the bulk rock compositions in which they crystallized, allowing for potential correlation with hinterland rock formations that contain garnets of comparable chemistry. The consistently low XMg contents observed in most Siwalik Group garnets support a derivation from a crustal rather than a mantle source, indicating growth in Fe-, Ca- or Mn-rich and Mg-poor environments, depending on the garnet group. In granulites, lower garnet rim XMg has been linked to proximity to biotite rather than grain size, emphasizing the role of localized chemical equilibrium rather than grain-scale diffusion (O'Brien, 1999). Additionally, XMg is more susceptible to diffusion along sub-grain boundaries than elements like Ca, which diffuses more slowly (Konrad-Schmolke *et al.*, 2007). Most Siwalik garnets that exhibit flat zoning show the trend in all components (XCa, XFe, XMn and XMg) (Fig. 5), indicating that post-growth modification affected all cations to some extent. The near-universal presence of low XMg also suggests that broader environmental controls, rather than localized conditions, likely governed their compositions.

The relatively low MgO contents of the Siwalik garnets observed by us and others (average 1.7 wt% MgO, with most <2.5 wt% MgO; our data; see also Nakajima *et al.* 2020; Rai *et al.* 2021; Yoshida *et al.* 2021) helped narrow the search for potential hinterland sources. Similar low-MgO garnets have also been reported in other Himalayan fluvial deposits (e.g., Jamuna River sands, Rahman *et al.* 2020; Indus Basin, Alizai *et al.* 2016). This disparity further necessitated a broader search that extended beyond the traditionally emphasized GHC and LHS units. Unlike previous studies, our findings suggest additional provenance hypotheses that warrant further investigation.

Garnets with similar zoning as Group 1 have been reported from calc-silicate rocks from the MCT shear zone, GHC and calc-silicate granulites and veins of the CGGC in the Indian Proterozoic mobile belt (Fig. 3, Table 5). The Schönig *et al.* (2021) classification scheme would place the analyses almost evenly divided between MM and MS settings (58% and 42%, respectively), with most (93%) in the CS/MS category and some (7%) in the IF/S setting. Rocks that exhibit Group 1 garnet zoning experienced higher-grade metamorphic conditions (650–890°C, 5.5–12 kbar; see references in Table 5).

As noted in the previous section, conditions estimated for Siwalik Group 2 garnet align with those estimated from enclaves in North Himalayan granites (Fig. 10d). Like the Group 1 garnets, Schönig *et al.* (2021) classification scheme places the majority of Group 2 garnet analyses in the MM (83% setting, followed by MS at 29%). Most analyses are categorized as CS/MS (60%) followed by IF/S settings (40%). In terms of classes, both Group 1 and Group 2

garnets share metamorphic classes with AM, EC/UHP and GR classes represented. Group 2 garnets have the most analyses in the GR setting out of all the analysed garnets (55%).

Spessartine-almandine garnets like those in Group 3 are reported from a high-pressure (14 kbar at <600°C) metagreywacke located in the Indus–Tsangpo suture zone (Laskowski *et al.* 2016) and a magmatic garnet within a highly fractionated rare-metal-bearing aplite from southern Tibet (Xie *et al.* 2020). An igneous origin is also supported by analyses of garnet found in the HHL (640°C, 3.5 kbar, Visonà & Lombardo, 2002) and pegmatite in the Gangdese batholith (~634°C, Yu *et al.* 2021). The Schönig *et al.* (2021) classification scheme places most Group 3 garnet compositions in the IG category (79%) followed by MM (21%).

Groups 1 and 2 garnets with higher XCa contents are only present later in the Surai Khola section, possibly reflecting a shift in sediment sources due to transient changes in erosion patterns or sediment routing. If sourced from the GHC or MCT shear zone (Table 5), the presence of these garnets at upper stratigraphic levels of the Siwalik Group aligns with rapid erosion rates and shorter lag times during the Pliocene (van der Beek *et al.* 2006). A five-fold increase in apparent erosion between 2.5 and 0.9 Ma has been documented in MCT shear zone rocks (Huntington *et al.* 2006). Such rapid erosion is consistent with the exhumation of calcsilicate rocks from the MCT zone, contributing detrital garnets to the foreland basin. However, lag times may be as long as ~8 Myr (SK16) based on 40Ar/39Ar detrital white mica. Based on garnets with similar zoning, Group 1 garnets may originate from mobile belt sources (Table 5). Their presence raises intriguing questions about sediment transport mechanisms and tectonic processes that can deliver this material into the Himalayan foreland basin. Potential transport pathways could include major river systems draining the Indian Proterozoic mobile belt or tectonic processes facilitating the reworking of mobile belt sediments into the basin. Paleohydrological indicators consistent with axial rivers suggest this option should be considered (Burbank *et al.* 1996; Ulak, 2005; Mandal *et al.* 2014).

The core conditions of all almandine Group 4 garnets overlap with the thermal conditions of the Bhimphedi Group samples, which are located closer to the Surai Khola section. Group 4 garnets are only found in samples SK17, SK11 and SK7. The Schönig *et al.* (2021) classification scheme places all Group 4 garnets in the MM setting class. The group has 96% of all analyses in the BS/GS metamorphic class (96%), followed by 4% in the AM class. Most analyses were in the IF/S composition class (99%), with only 1% in the M class.

We have the most confidence in the origin of Group 5 almandine-spessartine garnets as having a magmatic origin, likely crystallized in rocks similar in composition to the HHL. The Schönig *et al.* (2021) classification scheme anticipates that 76% of Group 5 garnets would fall within the IG setting, followed by 25% in the M class. All were in the IF/S compositional category. Group 5 garnet compositions are consistent with those formed in highly fractionated, felsic magmas. Today, the HHL are located at the highest elevations of the Himalayan range (Figs. 1 and 2). These granites are thought to have crystallized over a prolonged period between 7 and 46 Ma reflecting a dynamic interplay of crustal melting, tectonic exhumation, and episodic magmatism associated with the ongoing Indo–Asia collision (see review in Wu *et al.* 2020). Group 5 garnets are present in all Siwalik samples (Fig. 8d), highlighting their widespread distribution and persistence within the foreland basin sediments. These garnets,

now buried as deep as 4 km in the Siwalik strata (e.g., SK7 depth, 9.5 Ma, Fig. 9d), provide evidence of significant erosion and sediment transport from the Himalayan crystalline core. Their preservation across the Siwalik stratigraphy suggests that detritus derived from HHL exposures contributed consistently to sedimentary deposition over time.

Group 6 garnets are almandine with low pyrope contents but have XCa and XMn at roughly similar levels. Himalayan outcrop samples with similar zoning as those seen in Group 6 are found in a variety of lithologies, from garnet blueschists and eclogites of the Indus–Tsangpo suture zone, augen gneiss and schists within the GHC and graphitic schist collected from higher structural levels of the LHS, near the MCT (Table 5).

Group 6* garnets with similar XCa and higher XMg as those in Group 6 are exclusively found in various lithologies associated with the GHC (Table 5). These garnets show a wide range of metamorphic conditions. Group 6 garnets are present in all samples except SK8, but only one Group 6* garnet was found in sample SK17. The Schönig *et al.* (2021) classification scheme places the majority of Group 6 and 6* garnets into the MM class (90% and 100%), except a few Group 6 analyses in the IG class (10%). Most analyses are IF/S, with a few exceptions in Group 6 that are in the M compositional setting (11%).

We classified almost 1/3 of all samples analysed in this study in the Group 7 category, which are almandine-rich and have lower XCa + XMg + XMn. Group 7* is similar to those in Group 7 but has slightly higher XMg contents. Group 7 garnets are found in all samples, and Group 7* garnets are found in all samples except SK11 (Fig. 9d). Like Group 6 garnets, outcrop Group 7 garnets are found in a range of lithologies but are dominated by LHS and GHC rocks. Outcrop garnets in the Group 7* category are found in the LHS and GHC (Table 5). The Schönig *et al.* (2021) classification scheme would place all Group 7 and 7* garnets into the IF/S composition class and MM settings, except 2% in the IG category for Group 7.

The Schönig *et al.* (2021) metamorphic category identifies garnets with BS/GS-sourced garnets as present in all samples, and an EC/UHP origin is present in all samples except SK7. The EC/ UHP classified garnets are the same as four of those we placed in Group 1 (SK17_5, SK17_9, SK16B_scattered and SK16_24) and two in Group 2 (SK11_15 and SK24), and one in Group 7* (SK8_9).

We examined the comparison of Surai Khola garnet compositions with those from stratigraphic sections in Nepal and India. Figure 12 shows analyses reported for Lower Siwalik units along the Karnali River in western Nepal and Tinau Khola in central Nepal, the Muksar Khola in eastern Nepal (Nakajima *et al.* 2020; Rai *et al.* 2021) and pre-Siwalik sedimentary rocks from the Kasauli Formation in NW India (Najman & Garzanti, 2000). Most garnets reported from these sections fall into the Group 7 and 7* categories, except for one garnet resembling Group 2 from the Middle Siwalik of the Muksar Khola section and four analyses from the Tinau Khola, Muksar Khola and Kasauli Formation that resemble Group 6. One garnet from the Lower Siwalik units along the Karnali River exhibits a very high Ca content (35.6 wt% CaO), which was not observed in our studied section (Fig. 12a) but is characteristic of garnets from calc-silicate rocks in the Greater Himalayan Crystallines (GHC) or the CGGC (Neogi *et al.* 1998; Dey *et al.* 2019). Using the Schönig *et al.* (2021) classification scheme, garnet would be classified as having a granulite origin. This scheme also suggests that most garnet compositions reported by others are
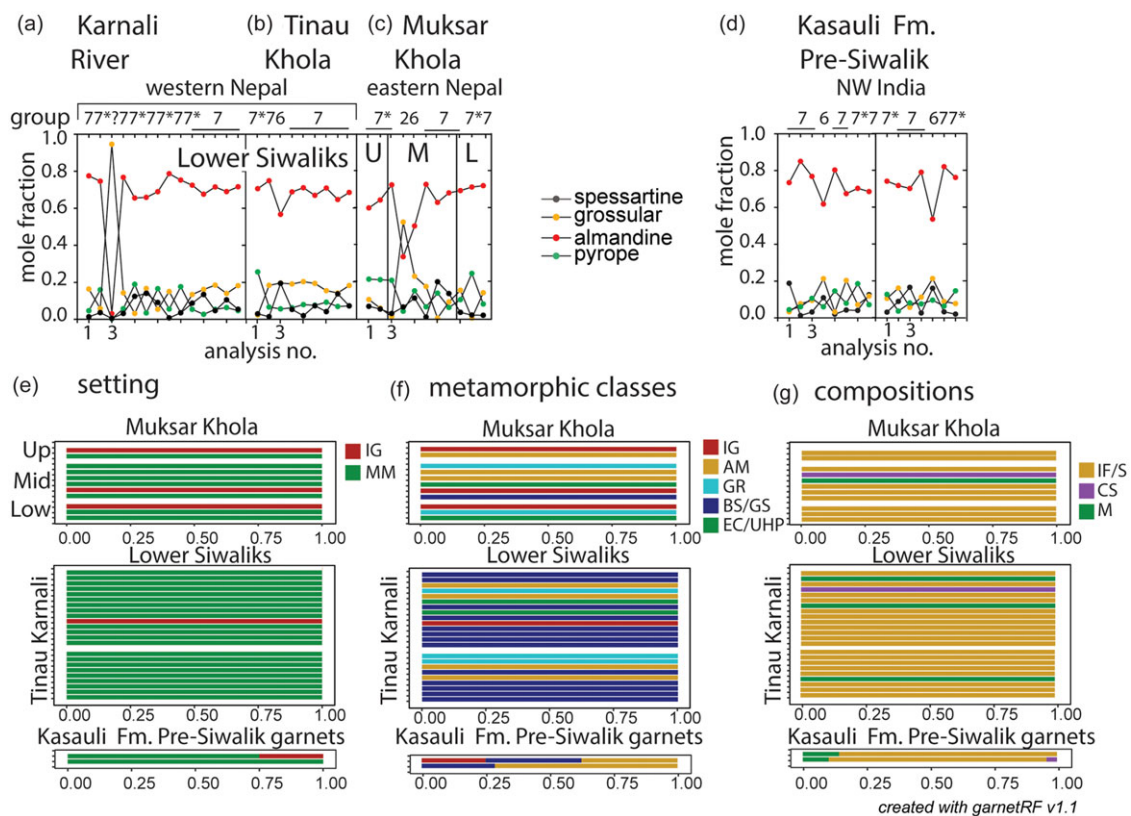
Figure 12. Garnet compositions from Siwalik Group samples are shown for (a) the Karnali River section (Lower Siwalik, 15.8–9.6 Ma), (b) Tinau Khola (Lower Siwalik, 13.2–9.2 Ma) and (c) Muksar Khola, including Upper (<3.5), Middle (10.0–3.5 Ma) and Lower (>10 Ma) Siwalik intervals (Nakajima *et al.* 2020; Rai & Yoshida, 2020; Rai *et al.* 2021). Panel (d) presents garnet compositions from the Kasauli Formation, a pre-Siwalik (Oligocene–Miocene) sedimentary unit (Najman & Garzanti, 2000). Garnet group classifications are noted above each analysis. See Fig. 1 for sample locations. Panel (e) shows garnet classification by tectonic setting, (f) by metamorphic class and (g) by compositional fields after Schönig *et al.* (2021).

metamorphic in origin with minor igneous input. Fig. 12f shows the presence of GR and EC/UHP garnets in both the Middle and Lower Siwalik sedimentary rocks along the Muksar and Karnali Khola transects. However, the figure likely does not reflect any critical heterogeneity that may be present. Our analysis is based solely on selected garnet compositions reported in published datasets and available data repositories.

Baral *et al.* (2016) identified the Tethyan Himalayan Sequence and the upper LHS as primary sources for the Surai Khola section, with minor input from GHC zircon. However, 40Ar/39Ar white mica dates indicate a significant contribution from the GHC (Szulc *et al.* 2006). The oldest sample in our study is 9.5 Ma, placing it well within the timeframe when GHC exhumation was likely underway. The presence of Groups 4–7 garnets supports the interpretation that GHC-derived garnets were actively supplied to the basin by 9.5 Ma, consistent with ongoing hinterland exhumation. The presence of Group 6 and 7 garnets, consistent with LHS sources, also supports previous findings that LHS material contributed significantly to Siwalik deposition in this region (Baral *et al.* 2016). While our study does not provide direct exhumation rate estimates, our findings are consistent with a model of progressive and rapid exhumation of the GHC exhumation (Szulc *et al.* 2006; van der Beek *et al.* 2006).

Tourmaline in the Siwalik Group has been linked to HHL provenance in central Nepal (Rai, 2003), while geochemical and petrological studies of the Middle and Upper Siwalik sedimentary rocks in NW India indicate increased contributions from

plutonic rocks and granitoids (Ranjan & Banerjee, 2009). The presence of sediment sourced from leucogranites in the Siwalik Group and Bengal Fan has been discounted due to the absence of zircon dates linked to the HHL (Bernet *et al.* 2006; Blum *et al.* 2018). However, many HHL zircon dates contain inherited cores that may be mistaken for GHC, THS or LHS affinity (Fig. 8d) (Schärer *et al.* 1986; Fan *et al.* 2021; Liu *et al.* 2022). These inherited cores from older magmatic episodes may obscure the recognition of HHL contributions in detrital zircon datasets. The rims that typically record Cenozoic crystallization could be selectively removed through abrasion or omitted in provenance studies due to analytical approaches that target core analysis. The HHL represents a significant Himalayan lithotectonic component, but its exposures account for only ~2% of the belt (Scaillet *et al.* 1996; Searle, 1999; Searle *et al.* 2003). Group 5 garnet compositions can only be linked to a magmatic environment, underscoring the critical role of the HHL as a sediment source for the Siwalik Group.

8.d. Limitations and cautions

Detrital garnets can survive recycling (Morton & Hallsworth, 2007; Baldwin *et al.* 2021). However, we might anticipate that garnets more susceptible to weathering and erosion would disappear from the section, and recycled grains would appear smaller. For example, grossular garnets are considered less stable than their almandine counterparts (Morton & Hallsworth, 2007; Tolosana-Delgado *et al.* 2018), and in this study, we only identified grossular

compositions in samples from higher stratigraphic levels (Fig. 9d). While low sampling density (ca. n = 20 grains per sample) may have contributed to the absence of grossular-rich garnet, similar trends have been observed in other studies (Yoshida *et al.* 2015; Nakajima *et al.* 2020; Yoshida *et al.* 2021), suggesting that this pattern is consistent and may not be solely an artefact of sample size (Fig. 12).

We correlate Siwalik garnet compositions to those from potentially analogous bedrock samples (Table 5), which requires understanding all possible sources of Himalayan garnet. This approach has been applied elsewhere, including the central Swiss Alps (Stutenbecker *et al.* 2017). We are limited by what is reported in the literature and recognize that other options may exist. We are conservative in our interpretations, including identifying multiple possibilities for each group. Our interpretations are similar to those using ternary diagrams for garnet provenance, which have long been used to relate to lithologies, pressure-temperature conditions and even specific rock units. In addition, it is evidence-based, as we seek to identify options for Siwalik garnet sources based on those found in Himalayan outcrops with similar zoning patterns despite unavoidable limitations. Of the garnet groups identified, we are most confident that Group 5 almandine-spessartine garnets are from an igneous provenance, as these compositions are commonly reported from HHL assemblages in the Himalaya and elsewhere.

We acknowledge that previous studies have highlighted the challenges in generating pressure–temperature conditions and paths from detrital garnets, with some even describing it as 'impossible' (Baldwin *et al.* 2021). Some researchers discard detrital garnet analyses if core and rim compositions differ by more than 5 mol% (Nakajima *et al.* 2020). These grains, however, are precisely those we identified as necessary for thermobarometric analyses. We assume a pelitic lithology, which is reasonable for the Himalayan hinterland, and use specific solution models and effective bulk rock compositions to identify where garnet isopleths intersect. Central section isopleth intersections are also unique solutions. We made what may appear as minor changes in the MA43 bulk rock composition (Table 3), and isopleth intersections only result if these specific changes are made within the context of equilibrium conditions, specific solution models, assumed mineralogy, and garnet composition. Pressure–temperature conditions and paths for central sections of Siwalik detrital garnets were approximated through phase equilibria modelling based on the assumption that a garnet of a specific composition existed within an effective bulk rock composition and underwent metamorphism under closed-system equilibrium conditions.

The fact that garnets from the same groups from which we can generate pressure–temperature results yield similar conditions lends some confidence that the groupings are reasonably meaningful. We acknowledge that only the central regions of the detrital garnets were analysed, and the outer rims, which may have recorded peak metamorphic conditions, are likely absent. As such, the final pressure–temperature estimates from modelling should not be taken as representative of peak metamorphism. In addition, the central sections should not be considered garnet cores. In the pressure–temperature diagrams, intersection regions are slightly off the garnet-in isograd, suggesting that we are not measuring the true garnet core but our best approximation.

9. Conclusions

This study pioneers the use of detrital garnet thermobarometry, deriving pressure-temperature paths from garnet zoning in foreland basin sedimentary rocks to provide new insights into their metamorphic and tectonic histories. The approach is demonstrated through a case study of detrital garnets from Middle and Upper (Late Miocene–Pliocene) Siwalik Group sandstones from the Surai Khola section in central Nepal. Based on the compositions, the detrital garnets are manually grouped into nine specific categories linked to possible provenance options. The combination of manual classification and PCA clustering bridges statistical rigour with geological interpretation, providing a robust framework for interpretation. Detailed analyses of zoning patterns and comparisons to hinterland counterparts reveal links to possible source rock compositions.

While previous studies primarily identified sediment sources from a limited range (GHC, LHS and Tethyan Himalayan Sequence), the data show detrital garnet compositions that align with several additional possible sources through direct comparisons of Siwalik garnets with hinterland compositions and conditions. For example, Group 1 (grossular) garnets exhibit similar zoning patterns to those observed in garnets from the MCT shear zone, the Indian Proterozoic mobile belt or the GHC. Group 2 garnets are unique in that they exhibit similar chemical zoning patterns to those found in Himalayan blueschist garnets or those sourced from magmatic enclaves of the North Himalayan granites. Using the classification scheme by Schönig *et al.* (2021) further highlights the presence of EC/UHP garnets within the Surai Khola Siwalik sedimentary rocks, alongside other potential sources and compositions. Group 3 (spessartine) garnets have been reported from magmatic sources and rocks associated with the Indus–Tsangpo suture zone, whereas Group 5 (almandine-spessartine) garnets are magmatic. Group 6 and 7 garnets have multiple options for provenance, including blueschist and eclogites, GHC, upper LHS or arc rocks. In contrast, higher XMg Group 6* and Group 7* garnets have thus far only been paired with GHC counterparts.

Group 5 and 7 garnets are present in all the Siwalik samples. Our interpretation of the results is that throughout the Late Miocene–Pliocene, the provenance of HHL (Group 5), LHS and GHC (Groups 6 and 7) was continuously eroded. If Group 1 garnets originated in the MCT footwall, calc-silicate rocks are present in the Pliocene-age Siwalik Group rocks, indicating that accelerated erosion occurred during this time. Alternatively, these grossular compositions are also found in lithologies exposed on the Indian Proterozoic mobile belt, suggesting that the erosion of units not associated with Himalayan uplift has occurred.

Using the Siwalik garnet compositions that show higher Mn in central sections and thermodynamic modelling traditionally applied to outcrop samples, pressure–temperature conditions from garnets from Groups 2, 4, 5 and 6 and paths from garnets in Groups 2, 4 and 5 were produced. Other garnets show flat zoning and likely experienced higher temperatures (>600°C) of diffusional modifications; thus, they are not ideal candidates, even in outcrop samples. These conditions are like those suggested by their outcrop counterparts, providing additional confidence in the assigned provenance. Additionally, the mineral assemblages predicted by the isochemical phase diagrams closely match those expected for the corresponding hinterland source rocks. Applying the approach outlined in this study to the Siwalik Group's detrital garnets reveals that multiple provenance sources may be present within the unit. Extending these methods to other geological settings could yield valuable insights into garnet provenance, sedimentary dynamics and tectonic evolution, thereby enhancing our understanding of detrital systems across diverse regions.

References

Abid IA, Abbasi IA, Khan MA and Shah MT (1983) Petrography and geochemistry of the Siwalik sandstone and its relationship to the Himalayan orogeny. *Journal of Himalayan Earth Sciences* **16**, 65–83.

Adlakha V, Patel RC and Lal N (2013) Exhumation and its mechanisms: a review of exhumation studies in the Himalaya. *Journal of the Geological Society of India* **81**, 481–502.

Ague JJ and Carlson WD (2013) Metamorphism as garnet sees it: the kinetics of nucleation and growth, equilibration, and diffusional relaxation. *Elements* **9**, 439–45.

Ali SK, Khan J, Mughal MS, Lashari MR, Sahito AG, Hameed F, Bashir HS, Bilal A and Razzaq SS (2023) Petrotectonic framework of Siwalik Group in Khairi Murat-Kauliar area, Potwar Sub-Basin, Pakistan. *Kuwait Journal of Science* **50**, 1–18.

Alizai A, Clift PD and Still J (2016) Indus Basin sediment provenance constrained using garnet geochemistry. *Journal of Asian Earth Sciences* **126**, 29–57.

Andò S (2020) Gravimetric separation of heavy minerals in sediments and rocks. *Minerals* **10**, 273.

Andò S, Bersani D, Vignola P and Garzanti E (2009) Raman spectroscopy as an effective tool for high-resolution heavy-mineral analysis: Examples from major Himalayan and Alpine fluvio-deltaic systems. *Spectrochimica Acta Part A: Molecular and Biomolecular Spectroscopy* **73**, 450–5.

Andò S, Garzanti E, Padoan M and Limonta M (2012) Corrosion of heavy minerals during weathering and diagenesis: a catalog for optical analysis. *Sedimentary Geology* **280**, 165–78.

Appel E, Rösler W and Corvinus G (1991) Magnetostratigraphy of the Miocene-Pleistocene Surai Khola Siwaliks in West Nepal. *Geophysical Journal International* **105**, 191–8.

Baidya AS, Pal DC and Upadhyay D (2019) Chemical weathering of garnet in Banded Iron Formation: Implications for the mechanism and sequence of secondary mineral formation and mobility of elements. *Geochimica et Cosmochimica Acta* **265**, 198–220.

Baldwin JA, Powell R, Brown M, Moraes R and Fuck RA (2005) Modelling of mineral equilibria in ultrahigh-temperature metamorphic rocks from the Anápolis–Itauçu Complex, central Brazil. *Journal of Metamorphic Geology* **23**, 511–31.

Baldwin SL, Schönig J, Gonzalez JP, Davies H and Von Eynatten H (2021) Garnet sand reveals rock recycling processes in the youngest exhumed high- and ultrahigh-pressure terrane on Earth. *Proceedings of the National Academy of Sciences* **118**, e2017231118.

Baral U, Lin D and Chamlagain D (2016) Detrital zircon U–Pb geochronology of the Siwalik Group of the Nepal Himalaya: implications for provenance analysis. *International Journal of Earth Sciences* **105**, 921–39.

Bernet M, Van Der Beek P, Pik R, Huyghe P, Mugnier J, Labrin E and Szulc A (2006) Miocene to Recent exhumation of the central Himalaya determined from combined detrital zircon fission-track and U/Pb analysis of Siwalik sediments, western Nepal. *Basin Research* **18**, 393–412.

Bhargava ON and Singh BP (2020) Geological evolution of the Tethys Himalaya. *Episodes* **43**, 404–16.

Bhushan B (1973) On the upper Murree-lower Siwalik provenance. *Geological Society of India* **14**, 186–90.

Blum M, Rogers K, Gleason J, Najman Y, Cruz J and Fox L (2018) Allogenic and autogenic signals in the stratigraphic record of the deep-sea Bengal fan. *Scientific Reports* **8**, 7973.

Bora DS and Shukla UK (2005) Petrofacies implication for the lower Siwalik foreland and basin evolution, Kumaun Himalaya, India. *Special Publication of the Palaeontological Society of India* **2**, 163–79.

Borghi A, Castelli D, Lombardo B and Vison D (2003) Thermal and baric evolution of garnet granulites from the Kharta region of S Tibet, E Himalaya. *European Journal of Mineralogy* **15**, 401–18.

Burbank D, Beck R and Mulder T (1996) The Himalayan foreland basin. In *Tectonic evolution of Asia* (eds A Yin & TM Harrison), pp. 149–88. Cambridge, MA: Cambridge University Press.

Burchfiel BC, Zhiliang C, Hodges KV, Yuping L, Royden LH, Changrong D and Jiene X (1992) The South Tibetan Detachment system, Himalayan Orogen: extension contemporaneous with and parallel to shortening in a collisional mountain belt. In *Geological Society of America Special Papers*, pp. 1–41. Boulder, CO: Geological Society of America.

Burgess WP, Yin A, Dubey CS, Shen Z-K and Kelty TK (2012) Holocene shortening across the Main Frontal Thrust zone in the eastern Himalaya. *Earth and Planetary Science Letters* **357–358**, 152–67.

Cai Z and Cao H (2013) The formation mechanism of garnet porphyroblast in quartz schist, Namche Barwa, east Himalaya. *Journal of Nepal Geological Society* **46**, 57–68.

Cao H-W, Pei Q-M, Santosh M, Li G-M, Zhang L-K, Zhang X-F, Zhang Y-H, Zou H, Dai Z-W, Lin B, Tang L and Yu X (2022) Himalayan leucogranites: a review of geochemical and isotopic characteristics, timing of formation, genesis, and rare metal mineralization. *Earth-Science Reviews* **234**, 104229.

Carosi R, Montomoli C and Iaccarino S (2018) 20 years of geological mapping of the metamorphic core across Central and Eastern Himalayas. *Earth-Science Reviews* **177**, 124–38.

Catlos EJ (2000) *Geochronologic and thermobarometric constraints on the evolution of the Main Central Thrust, Himalayan orogen*. PhD Thesis. Los Angeles: University of California, Los Angeles, 393p.

Catlos EJ (2023) Records of Himalayan metamorphism and contractional tectonics in the Central Himalayas (Darondi Khola, Nepal). In *Geophysical Monograph Series* (eds EJ Catlos & İ Çemen), **1 Vol**, pp. 155–201. Hoboken, NJ: Wiley.

Catlos EJ and Çemen İ (2023) When plates collide. In *Geophysical Monograph Series* (eds EJ Catlos & İ Çemen), **1 Vol**, pp. 1–20. Hoboken, NJ: Wiley.

Catlos EJ, Dubey CS and Etzel TM (2022) Imbrication and erosional tectonics recorded by garnets in the Sikkim Himalayas. *Geosciences* **12**, 146.

Catlos EJ, Harrison TM, Kohn MJ, Grove M, Ryerson FJ, Manning CE and Upreti BN (2001) Geochronologic and thermobarometric constraints on the evolution of the Main Central Thrust, central Nepal Himalaya. *Journal of Geophysical Research: Solid Earth* **106**, 16177–204.

Catlos EJ, Harrison TM, Manning CE, Grove M, Rai SM, Hubbard MS and Upreti BN (2002) Records of the evolution of the Himalayan orogen from in situ Th–Pb ion microprobe dating of monazite: Eastern Nepal and western Garhwal. *Journal of Asian Earth Sciences* **20**, 459–79.

Catlos EJ, Lovera OM, Kelly ED, Ashley KT, Harrison TM and Etzel T (2018) Modeling high-resolution pressure-temperature paths across the Himalayan main central thrust (Central Nepal): implications for the dynamics of collision. *Tectonics* **37**, 2363–88.

Catlos EJ, Perez TJ, Lovera OM, Dubey CS, Schmitt AK and Etzel TM (2020) High-resolution P-T-time paths across Himalayan faults exposed along the Bhagirathi transect NW India: implications for the construction of the Himalayan orogen and ongoing deformation. *Geochemistry, Geophysics, Geosystems* **21**, e2020GC009353.

Cenki-Tok B and Chopin C (2006) Coexisting calderite and spessartine garnets in eclogite-facies metacherts of the Western Alps. *Mineralogy and Petrology* **88**, 47–68.

Cerveny PF, Johnson NM, Tahirkheli RAK and Bonis NR (1989) Tectonic and geomorphic implications of Siwalik Group heavy minerals, Potwar Plateau, Pakistan. In *Geological Society of America Special Papers* (eds LL Malinconico Jr & RJ Lillie), pp. 129–36. Boulder, CO: Geological Society of America.

Chakrabarti BK (2016) Chp. 6. Nepal Himalaya. In *Geology of the Himalayan Belt: Deformation, Metamorphism, Stratigraphy* (ed BK Chakrabarti), pp. 89–116. Amsterdam, Netherlands: Elsevier.

Chakraborty T, Taral S, More S and Bera S (2020) Cenozoic Himalayan Foreland basin: an overview and regional perspective of the evolving sedimentary succession. In *Geodynamics of the Indian Plate* (eds N Gupta & SK Tandon), pp. 395–437. Springer Geology, Cham: Springer International Publishing.

Charreau J, Lavé J, France-Lanord C, Puchol N, Blard P, Pik R, Gajurel AP and ASTER Team (2021) A 6 Ma record of palaeodenudation in the central Himalayas from in situ cosmogenic ^{10} Be in the Surai section. *Basin Research* **33**, 1218–39.

Chatterjee N (2017) Constraints from monazite and xenotime growth modelling in the Mn CKFMASH - PYC e system on the *P–T* path of a metapelite from Shillong-Meghalaya Plateau: implications for the Indian shield assembly. *Journal of Metamorphic Geology* **35**, 393–412.

Chatterjee N, Bhattacharya A, Duarah BP and Mazumdar AC (2011) Late Cambrian reworking of Paleo-Mesoproterozoic Granulites in Shillong-Meghalaya Gneissic complex (Northeast India): evidence from *PT* pseudosection analysis and Monazite chronology and implications for East Gondwana assembly. *The Journal of Geology* **119**, 311–30.

Chatterjee N and Ghose NC (2010) Metamorphic evolution of the Naga Hills eclogite and blueschist, Northeast India: implications for early subduction of the Indian plate under the Burma microplate. *Journal of Metamorphic Geology* **28**, 209–25.

Chaudhri RS (1972) Heavy minerals from the Siwalik formations of the northwestern Himalayas. *Sedimentary Geology* **8**, 77–82.

Chaudhri RS and Gill GTS (1981) Heavy mineral assemblage of the Siwalik group of Nepal Himalaya. *Journal Geological Society of India* **22**, 220–6.

Chen X, Schertl H-P, Gu P, Zheng Y, Xu R, Zhang J, Cai P and Lin C (2021) Newly discovered MORB-Type HP garnet amphibolites from the Indus-Yarlung Tsangpo suture zone: implications for the Cenozoic India–Asia collision. *Gondwana Research* **90**, 102–17.

Chernoff CB and Carlson WD (1999) Trace element zoning as a record of chemical disequilibrium during garnet growth. *Geology* **27**, 555.

Choudhury SR, Dey A, Mukherjee S, Sengupta S, Sanyal S, Karmakar S and Sengupta P (2023) Formation of aluminous clinopyroxene-ilmenite-spinel symplectic assemblage in a regionally metamorphosed calc-silicate granulite from the Chotanagpur Granite Gneiss Complex, East Indian shield. *Lithos* **442–443**, 107058.

Clift PD (2020) Asian monsoon dynamics and sediment transport in SE Asia. *Journal of Asian Earth Sciences* **195**, 104352.

Coggon R and Holland TJB (2002) Mixing properties of phengitic micas and revised garnet-phengite thermobarometers. *Journal of Metamorphic Geology* **20**, 683–96.

Corvinus G (1988) The Mio-Plio-Pleistocene litho- and biostratigraphy of the Surai Khola Siwaliks in West-Nepal: first results. *C.R. Academie des Sciences* **306**, 1471–7.

Corvinus G (1993) The Siwalik Group of Sediments at Surai Khola in Western Nepal and its palaeontological record. *Journal of Nepal Geological Society* **9**, 21–35.

Corvinus G and Nanda AC (1994) Stratigraphy and palaeontology of the Siwalik group of Surai Khola and Rato Khola in Nepal. *Neues Jahrbuch für Geologie und Paläontologie* **191**, 25–68.

Corvinus G and Rimal LN (2001) Biostratigraphy and geology of the neogene Siwalik group of the Surai Khola and Rato Khola areas in Nepal. *Palaeogeography, Palaeoclimatology, Palaeoecology* **165**, 251–79.

Critelli S and Ingersoll RV (1994) Sandstone petrology and provenance of the Siwalik group (Northwestern Pakistan and Western-Southeastern Nepal). *SEPM Journal of Sedimentary Research* **64A**, 815–23.

Çubukçu HE, Ersoy O, Aydar E and Çakir U (2008) WDS versus silicon drift detector EDS: a case report for the comparison of quantitative chemical analyses of natural silicate minerals. *Micron* **39**, 88–94.

de Capitani C and Brown TH (1987) The computation of chemical equilibrium in complex systems containing non-ideal solutions. *Geochimica et Cosmochimica Acta* **51**, 2639–52.

de Capitani C and Petrakakis K (2010) The computation of equilibrium assemblage diagrams with Theriak/Domino software. *American Mineralogist* **95**, 1006–16.

Debnath A, Taral S, Mullick S and Chakraborty T (2021) The Neogene Siwalik succession of the Arunachal Himalaya: a revised lithostratigrphic classification and its implications for the regional paleogeography. *Journal of the Geological Society of India* **97**, 339–50.

DeCelles PG, Gehrels GE, Najman Y, Martin AJ, Carter A and Garzanti E (2004) Detrital geochronology and geochemistry of Cretaceous–early Miocene strata of Nepal: implications for timing and diachroneity of initial Himalayan orogenesis. *Earth and Planetary Science Letters* **227**, 313–30.

DeCelles PG, Gehrels GE, Quade J, LaReau B and Spurlin M (2000) Tectonic implications of U–Pb Zircon ages of the Himalayan Orogenic belt in Nepal. *Science* **288**, 497–9.

DeCelles PG, Gehrels GE, Quade J, Ojha TP, Kapp PA and Upreti BN (1998) Neogene foreland basin deposits, erosional unroofing, and the kinematic history of the Himalayan fold-thrust belt, western Nepal. *Geological Society of America Bulletin* **110**, 2–21.

Deer WA, Howie RA and Zussman J (2009) An Introduction to the Rock-Forming Minerals 2. ed., [Nachdr.]. Harlow: Pearson/Prentice Hall, 696p.

Dewey JF (1977) Suture zone complexities: a review. *Tectonophysics* **40**, 53–67.

Dey A, Choudhury SR, Mukherjee S, Sanyal S and Sengupta P (2019) Origin of vesuvianite-garnet veins in calc-silicate rocks from part of the Chotanagpur Granite Gneiss Complex, East Indian Shield: the quantitative P-T-XCO2 topology in parts of the system CaO-MgO-Al2O3-SiO2-H2O-CO2 (+Fe2O3, F). *American Mineralogist* **104**, 744–60.

Dhamodharan S, Rawat G, Kumar S and Bagri DS (2020) Sedimentary thickness of the northern Indo-Gangetic plain inferred from magnetotelluric studies. *Journal of Earth System Science* **129**, 156.

Dhital MR (2015) Siwaliks of Karnali–Bheri region. In *Geology of the Nepal Himalaya: Regional Perspective of the Classic Collided Orogen (ed MR Dhital)*, pp. 391–408. Cham: Springer International Publishing.

Dhital MR, Gajurel AP, Pathak D, Paudel LP and Kizaki K (1995) Geology and structure of the Siwaliks and Lesser Himalaya in the Surai Khola-Baradana area, mid-western Nepal. *Bulletin of Department of Geology, Tribhuvan University, Kathmandu (Nepal)* **4**, 1–70.

Diella V, Bocchio R, Marinoni N, Langone A, Adamo I and Rotiroti N (2018) The spessartine–almandine garnet from Val Codera pegmatite, Central Alps, Italy: a new insight on the crystallochemistry and a 3D image analysis of its inclusions. *Rendiconti Lincei. Scienze Fisiche e Naturali* **29**, 699–707.

Ding H, Zhang Z, Palin RM, Kohn MJ, Niu Z, Chen Y, Qin S, Jiang Y and Li W (2022) Late cretaceous metamorphism and anatexis of the Gangdese Magmatic arc, South Tibet: implications for thickening and differentiation of Juvenile Crust. *Journal of Petrology* **63**, egac017.

DiPietro JA (1991) Metamorphic pressure-temperature conditions of Indian Plate rocks south of the main mantle thrust, lower swat, Pakistan. *Tectonics* **10**, 742–57.

DiPietro JA, Pogue KR, Hussain A and Ahmad I (1999) Geologic map of the Indus syntaxis and surrounding area, northwest Himalaya, Pakistan. In *Himalaya and Tibet: Mountain Roots to Mountain Tops* (eds A Macfarlane, RB Sorkhabi & J Quade), pp. 159–78. Geological Society of America.

Dong P, Weinberg RF, Zhu D-C, Green ECR, Yi J, Cawood PA, Li S-M and Chen S (2024) Anorthosites produced by water-fluxed anatexis of deep arc gabbros, Gangdese batholith, Tibet. *Earth and Planetary Science Letters* **648**, 119093.

Dutta D, Biswas T and Mukherjee S (2019) Arc-parallel compression in the NW Himalaya: evidence from structural and palaeostress studies of brittle deformation from the clasts of the Upper Siwalik, Uttarakhand, India. *Journal of Earth System Science* **128**, 125.

Faak K, Chakraborty S and Dasgupta S (2012) Petrology and tectonic significance of metabasite slivers in the Lesser and Higher Himalayan domains of Sikkim, India. *Journal of Metamorphic Geology* **30**, 599–622.

Fan Y, Zhang J, Lin C, Wang X and Zhang B (2021) Miocene granitic magmatism constrains the early E-W extension in the Himalayan Orogen: a case study of Kung Co leucogranite. *Lithos* **398–399**, 106295.

Flynn LJ, Pilbeam D, Barry JC, Morgan ME and Mahmood Raza S (2016) Siwalik synopsis: a long stratigraphic sequence for the Later Cenozoic of South Asia. *Comptes Rendus Palevol* **15**, 877–87.

Galbraith, R.F. (1990) The radial plot: Graphical assessment of spread in ages. *International Journal of Radiation Applications and Instrumentation. Part D. Nuclear Tracks and Radiation Measurements*, **17**, 207-214.

Gautam P (2008) Magnetic fabric of Siwalik sediments (Nepal): implications to time–space evolution of stress field. *Journal of Nepal Geological Society* **38**, 39–48.

Gautam P and Rösler W (1999) Depositional chronology and fabric of Siwalik group sediments in Central Nepal from magnetostratigraphy and magnetic anisotropy. *Journal of Asian Earth Sciences* **17**, 659–82.

Gautam P, Ulak PD, Paudayal KN, Gyawali BR and Bhandari S (2012) Magnetostratigraphic dating of the prime-time sedimentary record of Himalayan tectonics and climate: new age constraints (13–10 Ma) from the Siwaliks of the Tinau Khola north section, Nepal: magnetic polarity and fabric of Siwaliks, Nepal. *Geophysical Journal International* **190**, 1378–92.

Gehrels G, Kapp P, DeCelles P, Pullen A, Blakey R, Weislogel A, Ding L, Guynn J, Martin A, McQuarrie N and Yin A (2011) Detrital zircon geochronology of pre-Tertiary strata in the Tibetan-Himalayan orogen. *Tectonics* **30**, 2011TC002868.

George FR, Waters DJ, Gough SJ, Searle MP and Forshaw JB (2022) Phase equilibria and microstructural constraints on the high-*T* building of the Kohistan island arc: the Jijal garnet granulites, northern Pakistan. *Journal of Metamorphic Geology* **40**, 145–74.

Goswami PK and Deopa T (2018) Petrotectonic setting of the provenance of Lower Siwalik sandstones of the Himalayan foreland basin, southeastern Kumaun Himalaya, India. *Island Arc* **27**, e12242.

Gradstein FM, Ogg JG, Schmitz MD and Ogg GM (eds) (2020) *Geologic Time Scale 2020*. Amsterdam: Elsevier.

Groppo C, Rolfo F, Castelli D and Connolly JAD (2013) Metamorphic CO2 production from calc-silicate rocks via garnet-forming reactions in the CFAS–H2O–CO2 system. *Contributions to Mineralogy and Petrology* **166**, 1655–75.

Guilmette C, Hébert R, Dostal J, Indares A, Ullrich T, Bédard É and Wang C (2012) Discovery of a dismembered metamorphic sole in the Saga ophiolitic mélange, South Tibet: assessing an Early Cretaceous disruption of the Neo-Tethyan supra-subduction zone and consequences on basin closing. *Gondwana Research* **22**, 398–414.

Guilmette C, Hébert R, Dupuis C, Wang C and Li Z (2008) Metamorphic history and geodynamic significance of high-grade metabasites from the ophiolitic mélange beneath the Yarlung Zangbo ophiolites, Xigaze area, Tibet. *Journal of Asian Earth Sciences* **32**, 423–37.

Guilmette C, Hébert R, Wang C and Villeneuve M (2009) Geochemistry and geochronology of the metamorphic sole underlying the Xigaze Ophiolite, Yarlung Zangbo Suture Zone, South Tibet. *Lithos* **112**, 149–62.

Harangi SZ, Downes H, Kósa L, Szabó CS, Thirlwall MF, Mason PRD and Mattey D (2001) Almandine Garnet in Calc-alkaline Volcanic rocks of the Northern Pannonian Basin (Eastern–Central Europe): geochemistry, petrogenesis and geodynamic implications. *Journal of Petrology* **42**, 1813–43.

Hodges KV, Hubbard MS and Silverberg DS (1988) Metamorphic constraints on the thermal evolution of the central Himalayan Orogen. *Philosophical Transactions of the Royal Society of London. Series A, Mathematical and Physical Sciences* **326**, 257–80.

Hodges KV, Parrish RR, Housh TB, Lux DR, Burchfiel BC, Royden LH and Chen Z (1992) Simultaneous Miocene extension and shortening in the Himalayan orogen. *Science* **258**, 1466–70.

Holland T, Baker J and Powell R (1998) Mixing properties and activity-composition relationships of chlorites in the system MgO-FeO-Al2O3-SiO2-H2O. *European Journal of Mineralogy* **10**, 395–406.

Holland T and Powell R (2003) Activity? Composition relations for phases in petrological calculations: an asymmetric multicomponent formulation. *Contributions to Mineralogy and Petrology* **145**, 492–501.

Holland TJB and Powell R (1998) An internally consistent thermodynamic data set for phases of petrological interest. *Journal of Metamorphic Geology* **16**, 309–43.

Honegger K, Le Fort P, Mascle G and Zimmermann J-L (1989) The blueschists along the Indus Suture Zone in Ladakh, NW Himalaya. *Journal of Metamorphic Geology* **7**, 57–72.

Hong D, Jian X, Fu L and Zhang W (2020) Garnet trace element geochemistry as a sediment provenance indicator: an example from the Qaidam basin, northern Tibet. *Marine and Petroleum Geology* **116**, 104316.

Hoorn C, Ohja T and Quade J (2000) Palynological evidence for vegetation development and climatic change in the Sub-Himalayan Zone (Neogene, Central Nepal). *Palaeogeography, Palaeoclimatology, Palaeoecology* **163**, 133–61.

Hu X, Garzanti E, Wang J, Huang W, An W and Webb A (2016) The timing of India-Asia collision onset – facts, theories, controversies. *Earth-Science Reviews* **160**, 264–99.

Hubbard MS (1989) Thermobarometric constraints on the thermal history of the Main Central Thrust Zone and Tibetan Slab, eastern Nepal Himalaya. *Journal of Metamorphic Geology* **7**, 19–30.

Huntington KW, Blythe AE and Hodges KV (2006) Climate change and Late Pliocene acceleration of erosion in the Himalaya. *Earth and Planetary Science Letters* **252**, 107–18.

Huyghe P, Galy A, Mugnier J-L and France-Lanord C (2001) Propagation of the thrust system and erosion in the Lesser Himalaya: geochemical and sedimentological evidence. *Geology* **29**, 1007.

Imayama T (2014) P–T conditions of metabasites within regional metapelites in far-eastern Nepal Himalaya and its tectonic meaning. *Swiss Journal of Geosciences* **107**, 81–99.

Jadoul F, Berra F and Garzanti E (1998) The Tethys Himalayan passive margin from Late Triassic to Early Cretaceous (South Tibet). *Journal of Asian Earth Sciences* **16**, 173–94.

Jagoutz O, Bouilhol P, Schaltegger U and Müntener O (2019) The isotopic evolution of the Kohistan Ladakh arc from subduction initiation to continent arc collision. *Geological Society, London, Special Publications* **483**, 165–82.

Jain V and Sinha R (2003) River systems in the Gangetic plains and their comparison with the Siwaliks: a review. *Current Science* **84**, 1025–33.

Jalal P, Ghosh SK and Sundriyal YP (2011) Detrital modes of Late Neogene Siwalik Sandstone of the Ramganga Sub basin, Kumaun Sub- Himalaya: implication for the source area tectonic history. *Himalayan Geology* **32**, 123–35.

Jamaludin NFA, Muthusamy K, Isa NN, Md Jaafar MF and Ghazali N (2022) Use of spent garnet in industry: a review. *Materials Today: Proceedings* **48**, 728–33.

Jassal HS, Sidhu PS, Sharma BD and Mukhopadhyay SS (2000) Mineralogy and geochemistry of some soils of Siwalik Hills. *Journal of the Indian Society of Soil Science* **48**, 163–72.

Jayabun Sk, Pathak S and Sengupta A (2021) Characterization & categorization of garnet samples for major and minor constituents by energy dispersive X-ray fluorescence spectroscopy. *Nuclear Instruments and Methods in Physics Research Section A: Accelerators, Spectrometers, Detectors and Associated Equipment* **1019**, 165854.

Johnson TA, Cottle JM and Larson KP (2021) Delineation of multiple metamorphic events in the Himalayan Kathmandu Complex, central Nepal. *Journal of Metamorphic Geology* **39**, 443–72.

Jonnalagadda MK, Karmalkar NR and Duraiswami RA (2019) Geochemistry of eclogites of the Tso Morari complex, Ladakh, NW Himalayas: insights into trace element behavior during subduction and exhumation. *Geoscience Frontiers* **10**, 811–26.

Kang D, Zhang Z, Palin RM, Tian Z and Dong X (2020) Prolonged partial melting of Garnet Amphibolite from the Eastern Himalayan Syntaxis: implications for the tectonic evolution of large hot orogens. *Journal of Geophysical Research: Solid Earth* **125**, e2019JB019119.

Kaul R, Umamaheswar K, Chandrasekaran S, Deshmukh RD and Swarnkar BM (1983) Uranium mineralization in the Siwaliks of Northwestern Himalaya, India. *Journal Geological Society of India* **41**, 243–58.

Kawabata R, Imayama T, Bose N, Yi K and Kouketsu Y (2021) Tectonic discontinuity, partial melting and exhumation in the Garhwal Himalaya (Northwest India): constrains from spatial and temporal pressure–temperature conditions along the Bhagirathi valley. *Lithos* **404–405**, 106488.

Kellett DA, Cottle JM and Larson KP (2019) The South Tibetan Detachment system: history, advances, definition and future directions. *Geological Society, London, Special Publications* **483**, 377–400.

Kelly S, Beaumont C and Jamieson RA (2022) Eohimalayan metamorphism and subsequent tectonic quiescence explained. *Earth and Planetary Science Letters* **584**, 117350.

Khan MA, Bera M, Spicer RA, Spicer TEV and Bera S (2019) Palaeoclimatic estimates for a latest Miocene-Pliocene flora from the Siwalik Group of Bhutan: evidence for the development of the South Asian Monsoon in the eastern Himalaya. *Palaeogeography, Palaeoclimatology, Palaeoecology* **514**, 326–35.

Khan MA, Mahato S, Spicer RA, Spicer TEV, Ali A, Hazra T and Bera S (2023) Siwalik plant megafossil diversity in the Eastern Himalayas: a review. *Plant Diversity* **45**, 243–64.

Khan ZA and Tewari RC (2015) Paleocurrents, Paleohydraulics, and Palaegeography of Miocene-Pliocene Siwalik Foreland Basin of India. *Advances in Geology* **2015**, 1–14.

Knierzinger W, Wagreich M, Kiraly F, Lee EY and Ntaflos T (2019) TETGAR_C: a novel three-dimensional (3D) provenance plot and calculation tool for detrital garnets. *Journal of Geosciences* **64**, 127–48.

Kohn MJ (2014) Himalayan metamorphism and its tectonic implications. *Annual Review of Earth and Planetary Sciences* **42**, 381–419.

Kohn MJ, Catlos EJ, Ryerson FJ and Harrison TM (2001) Pressure–temperature-time path discontinuity in the Main Central thrust zone, central Nepal. *Geology* **29**, 571.

Konrad-Schmolke, M., O'Brien, P.J., Heidelbach, F. (2007) Compositional re-equilibration of garnet: the importance of sub-grain boundaries. *European Journal of Mineralogy*, **19**, 431–38.

Kontak DJ and Corey M (1988) Metasomatic origin of spessartine-rich garnet in the South Mountain Batholith, Nova Scotia. *Canadian Mineralogist* **26**, 315–34.

Kopylova MG, Russell JK, Stanley C and Cookenboo H (2000) Garnet from Cr- and Ca-saturated mantle: implications for diamond exploration. *Journal of Geochemical Exploration* **68**, 183–99.

Krippner A, Meinhold G, Morton AC, Russell E and Von Eynatten H (2015) Grain-size dependence of garnet composition revealed by provenance signatures of modern stream sediments from the western Hohe Tauern (Austria). *Sedimentary Geology* **321**, 25–38.

Krippner A, Meinhold G, Morton AC and Von Eynatten H (2014) Evaluation of garnet discrimination diagrams using geochemical data of garnets derived from various host rocks. *Sedimentary Geology* **306**, 36–52.

Kundu A, Matin A and Eriksson PG (2016) Petrography and geochemistry of the Middle Siwalik sandstones (tertiary) in understanding the provenance of sub-Himalayan sediments in the Lish River Valley, West Bengal, India. *Arabian Journal of Geosciences* **9**, 1–18.

Labotka TC (1995) Evidence for immiscibility in Ti-rich garnet in a calc-silicate hornfels from northeastern Minnesota. *American Mineralogist* **80**, 1026–30.

Larson KP, Kellett DA, Cottle JM, King J, Lederer G and Rai SM (2016) Anatexis, cooling, and kinematics during orogenesis: miocene development of the Himalayan metamorphic core, east-central Nepal. *Geosphere* **12**, 1575–93.

Laskowski AK, Kapp P, Vervoort JD and Ding L (2016) High-pressure Tethyan Himalaya rocks along the India-Asia suture zone in southern Tibet. *Lithosphere* **8**, 574–82.

Laurs BM and Knox K (2001) Spessartine garnet from Ramona, San Diego County, California. *Gems & Gemology* **37**, 278–295.

Lavé J and Avouac JP (2000) Active folding of fluvial terraces across the Siwaliks Hills, Himalayas of central Nepal. *Journal of Geophysical Research: Solid Earth* **105**, 5735–70.

Le Fort P (1996) Evolution of the Himalaya. In *The Tectonic Evolution of Asia.* (eds A Yin & TM Harrison), pp. 95–109. Cambridge: Cambridge University Press.

Lee J, Hacker BR, Dinklage WS, Wang Y, Gans P, Calvert A, Wan J, Chen W, Blythe AE and McClelland W (2000) Evolution of the Kangmar Dome, southern Tibet: structural, petrologic, and thermochronologic constraints. *Tectonics* **19**, 872–95.

Li W, Yin C, Yakymchuk C, Ding L, Li S, Qian J, Gao P and Zhang Y (2024) High-pressure, low-temperature metamorphism preserved in the Indus-Yarlung suture zone of the eastern Himalaya: overprinting at amphibolite facies and comparison with occurrences in the western Himalaya. *Geological Society of America Bulletin* **137.** 116–36.

LingSen Z, LingHao Z, LiE G, KeJun H., Qian W and MNR Key Laboratory of Deep-Earth Dynamics, Institute of Geology, Chinese Academy of Geological Sciences, Beijing 100037, China (2019) Magmatic garnet from Mid-Miocene co-genetic high Sr/Y granite and leucogranite from the Himalayan orogenic belt, southern Tibet. *Acta Petrologica Sinica* **35**, 1599–626.

Liu L, Zhu D, Wang Q, Cawood PA, Stockli DF, Stockli LD, Lin C, Zhang J, Zhang L and Zhao Z (2022) Leucogranite records multiple collisional orogenies. *Geophysical Research Letters* **49**, e2021GL096817.

Liu X, Ju Y, Wei L and Li G (2010) An alternative tectonic model for the Yarlung Zangbo suture zone. *Science in China Series D: Earth Sciences* **53**, 27–41.

Locock AJ (2008) An excel spreadsheet to recast analyses of garnet into end-member components, and a synopsis of the crystal chemistry of natural silicate garnets. *Computers & Geosciences* **34**, 1769–80.

Ma L, Wang Q, Kerr AC, Yang J-H, Xia X-P, Ou Q, Yang Z-Y and Sun P (2017) Paleocene (c. 62 Ma) Leucogranites in Southern Lhasa, Tibet: products of Syn-collisional Crustal anatexis during Slab Roll-back? *Journal of Petrology* **58**, 2089–114.

Mahar EM, Baker JM, Powell R, Holland TJB and Howell N (1997) The effect of Mn on mineral stability in metapelites. *Journal of Metamorphic Geology* **15**, 223–38.

Mandal S, Sarkar S, Chakraborty N, Bose PK, Liu M and Wang Y (2014) Palaeogeography, palaeohydraulics and palaeoclimate of the Mio–Pliocene Siwalik Group, eastern India. *Journal of Palaeogeography* **3**, 270–96.

Mange MA and Maurer HFW (1992) 7 Heavy mineral descriptions and colour plates. In *Heavy Minerals in Colour (eds MA Mange & HFW Maurer)*, pp. 45–6. Hong Kong, China: Chapman and Hall.

Mark, C, O'Sullivan, G, Glorie, S, Simpson, A, Andò, S, Barbarano, M, Stutenbecker, L , Daly, JS, Gilbert, S. (2023). Detrital garnet geochronology by in situ U-Pb and Lu-Hf analysis: A case study from the European Alps. *Journal of Geophysical Research: Earth Surface*, **128**, e2023JF007244.

Martin AJ (2017) A review of definitions of the Himalayan main central thrust. *International Journal of Earth Sciences* **106**, 2131–45.

Martin AJ, Ganguly J and DeCelles PG (2010) Metamorphism of greater and lesser Himalayan rocks exposed in the Modi Khola valley, central Nepal. *Contributions to Mineralogy and Petrology* **159**, 203–23.

Meigs AJ, Burbank DW and Beck RA (1995) Middle-late Miocene (>10 Ma) formation of the Main Boundary thrust in the western Himalaya. *Geology* **23**, 423.

Miller C, Klötzli U, Frank W, Thöni M and Grasemann B (2000) Proterozoic crustal evolution in the NW Himalaya (India) as recorded by circa 1.80 Ga mafic and 1.84 Ga granitic magmatism. *Precambrian Research* **103**, 191–206.

Mishra S, Singh VK, Slabunov AI, Nainwal HC, Singh PK, Chaudhary N and Nainwal DC (2019) Geochemistry and geodynamic setting of Paleoproterozoic granites of Lesser Garhwal Himalaya, India. *Journal of Geoscience, Engineering, Environment, and Technology* **42**, 28–38.

Morton A, Hallsworth C and Chalton B (2004) Garnet compositions in Scottish and Norwegian basement terrains: a framework for interpretation of North Sea sandstone provenance. *Marine and Petroleum Geology* **21**, 393–410.

Morton AC (1985) A new approach to provenance studies: electron microprobe analysis of detrital garnets from Middle Jurassic sandstones of the northern North Sea. *Sedimentology* **32**, 553–66.

Morton AC (1987) Influences of provenance and diagenesis on Detrital Garnet suites in the Paleocene Forties Sandstone, Central North Sea. *Journal of Sedimentary Research* **57**, 1027–32.

Morton AC and Hallsworth C (2007) Chapter 7 stability of detrital heavy minerals during Burial diagenesis. In *Developments in Sedimentology (eds MA Mange & DT Wright)*, **58 Vols**, pp. 215–45. Elsevier.

Morton AC and Hallsworth CR (1999) Processes controlling the composition of heavy mineral assemblages in sandstones. *Sedimentary Geology* **124**, 3–29.

Mugnier J-L, Huyghe P, Chalaron E and Mascle G (1994) Recent movements along the Main Boundary Thrust of the Himalayas: normal faulting in an over-critical thrust wedge? *Tectonophysics* **238**, 199–215.

Mukherjee S, Dey A, Sanyal S, Ibanez-Mejia M and Sengupta P (2019) Bulk rock and zircon geochemistry of granitoids from the Chotanagpur Granite Gneissic Complex (CGGC): implications for the late Paleoproterozoic continental arc magmatism in the East Indian Shield. *Contributions to Mineralogy and Petrology* **174**, 67.

Mukhopadhyay DK, Bhadra BK, Ghosh TK and Srivastava DC (1996) Evidence for the thrust emplacement of the 'Lesser Himalaya' Chur granite, Himachal Pradesh. *Journal of Earth System Science* **105**, 157–71.

Nabelek PI, Russ-Nabelek C and Denison JR (1992) The generation and crystallization conditions of the Proterozoic Harney Peak Leucogranite, Black Hills, South Dakota, USA: petrologic and geochemical constraints. *Contributions to Mineralogy and Petrology* **110**, 173–91.

Nag R, Hrushikesh H, Cogné N and Prabhakar N (2024) Late Neoproterozoic to early Cambrian high-grade metamorphism from Mikir Hills (Assam-Meghalaya gneissic Complex, northeast India): Implications for eastern Gondwana assembly. *Geoscience Frontiers* **15**, 101850.

Najman Y and Garzanti E (2000) Reconstructing early Himalayan tectonic evolution and paleogeography from Tertiary foreland basin sedimentary rocks, northern India. *Geological Society of America Bulletin* **112**, 435–49.

Najman Y, Jenks D, Godin L, Boudagher-Fadel M, Millar I, Garzanti E, Horstwood M and Bracciali L (2017) The Tethyan Himalayan detrital record shows that India–Asia terminal collision occurred by 54 Ma in the Western Himalaya. *Earth and Planetary Science Letters* **459**, 301–10.

Nakajima T, Matsumoto Y, Rai LK and Yoshida K (2020) Middle Miocene denudation of the Higher Himalayan Crystallines revealed by chemical composition of detrital garnets from the Siwalik foreland basin sediments, western and central Nepal. *Journal of Asian Earth Sciences* **200**, 104473.

Nakayama K and Ulak PD (1999) Evolution of fluvial style in the Siwalik Group in the foothills of the Nepal Himalaya. *Sedimentary Geology* **125**, 205–24.

Neogi S, Dasgupta S and Fukuoka M (1998) High P-T Polymetamorphism, dehydration melting, and generation of migmatites and granites in the higher Himalayan crystalline complex, Sikkim, India. *Journal of Petrology* **39**, 61–99.

Nyame F (2001) Petrological significance of manganese carbonate inclusions in spessartine garnet and relation to the stability of spessartine in metamorphosed manganese-rich rocks. *Contributions to Mineralogy and Petrology* **141**, 733–46.

O'Brien, P.J. (1999) Asymmetric zoning profiles in garnet from HP-HT granulite and implications for volume and grain-boundary diffusion. *Mineralogical Magazine*, **63**, 227-238.

O'Brien PJ (2001) Subduction followed by collision: Alpine and Himalayan examples. *Physics of the Earth and Planetary Interiors* **127**, 277–91.

O'Brien PJ, Zotov N, Law R, Khan MA and Jan MQ (2001) Coesite in Himalayan eclogite and implications for models of India-Asia collision. *Geology* **29**, 435.

Ojha TP, Butler RF, DeCelles PG and Quade J (2009) Magnetic polarity stratigraphy of the Neogene foreland basin deposits of Nepal. *Basin Research* **21**, 61–90.

Olen SM, Bookhagen B, Hoffmann B, Sachse D, Adhikari DP and Strecker MR (2015) Understanding erosion rates in the Himalayan orogen: a case study from the Arun Valley. *Journal of Geophysical Research: Earth Surface* **120**, 2080–102.

Owen LA (2010) Landscape development of the Himalayan–Tibetan orogen: a review. *Geological Society, London, Special Publications* **338**, 389–407.

Pant CC and Sharma AK (1993) Quaternary sedimentation in the Indo-Gangetic basin: a review. *Current Science* **64**, 855–62.

Pant NC, Singh P and Jain AK (2020) A re-look at the Himalayan metamorphism. *Episodes* **43**, 369–80.

Parkash B, Sharma RP and Roy AK (1980) The Siwalik group (Molasse) — sediments shed by collision of continental plates. *Sedimentary Geology* **25**, 127–59.

Parsons AJ, Hosseini K, Palin RM and Sigloch K (2020) Geological, geophysical and plate kinematic constraints for models of the India-Asia collision and the post-Triassic central Tethys oceans. *Earth-Science Reviews* **208**, 103084.

Pathak PS, Dagar JC, Kaushal R and Chaturvedi OP (2014) Agroforestry Inroads from the Traditional Two-Crop Systems in Heartlands of the Indo-Gangetic Plains. In *Agroforestry Systems in India: Livelihood Security & Ecosystem Services* (eds JC Dagar, AK Singh & A Arunachalam), pp. 87–116. Advances in Agroforestry, New Delhi: Springer India.

Patnaik R (2013) Chapter 17. Indian Neogene Siwalik Mammalian Biostratigraphy an overview. In *Fossil Mammals of Asia* (eds X Wang, LJ Flynn & M Fortelius), pp. 423–44. New York Chichester, West Sussex: Columbia University Press.

Petrakakis K, Schuster-Bourgin N, Habler G and Abart R (2018) Ca-rich garnets and associated symplectites in mafic peraluminous granulites from the Gföhl Nappe System, Austria. *Solid Earth* **9**, 797–819.

Petterson MG (2010) A review of the geology and tectonics of the Kohistan island arc, north Pakistan. *Geological Society, London, Special Publications* **338**, 287–327.

Petterson MG (2019) The plutonic crust of Kohistan and volcanic crust of Kohistan–Ladakh, north Pakistan/India: lessons learned for deep and shallow arc processes. *Geological Society, London, Special Publications* **483**, 123–64.

Pilgrim GE (1910) Preliminary note on a revised classification of the Tertiary freshwater deposits of India. *Records of the Geological Survey of India* **40**, 185–205.

Pilgrim GE (1913) The correlation of the Siwalik with mammal horizons of Europe. *Records of the Geological Survey of India* **43**, 264–325.

Poon J, Madden DC, Wood MH, Van Tol R, Sonke H and Clarke SM (2020) Surface chemistry of Almandine Garnet. *The Journal of Physical Chemistry C* **124**, 5099–117.

Powell R and Holland T (1999) Relating formulations of the thermodynamics of mineral solid solutions; activity modeling of pyroxenes, amphiboles, and micas. *American Mineralogist* **84**, 1–14.

Prakash A, Saha L, Petrik I, Janak M and Bhattacharya A (2018) Metamorphic evolution of Palaeoproterozoic anatectic migmatites in the eastern part of the Aravalli–Delhi Fold Belt, India: constraints from thermodynamic modelling and monazite dating. *Geological Magazine* **155**, 955–78.

Preston J, Hartley A, Mange-Rajetzky M, Hole M, May G, Buck S and Vaughan L (2002) The Provenance of Triassic Continental Sandstones from the Beryl Field, Northern North Sea: mineralogical, geochemical, and sedimentological constraints. *Journal of Sedimentary Research* **72**, 18–29.

Price JR, Bryan-Ricketts DS, Anderson D and Velbel MA (2013) Weathering of Almandine Garnet: influence of secondary minerals on the rate-determining step, and implications for Regolith-Scale Al mobilization. *Clays and Clay Minerals* **61**, 34–56.

Quade J, Cater JML, Ojha TP, Adam J and Mark Harrison T (1995) Late Miocene environmental change in Nepal and the northern Indian subcontinent: stable isotopic evidence from paleosols. *Geological Society of America Bulletin* **107**, 1381–97.

Rahman MJJ, Pownceby MI and Rana MS (2020) Occurrence and distribution of valuable heavy minerals in sand deposits of the Jamuna River, Bangladesh. *Ore Geology Reviews* **116**, 103273.

Rai LK (2003) *The Provenance and the Paleo-Environment of the Siwalik Group along the Muksar Khola Section, Eastern Nepal Himalaya*. Japan: Shinshu University, 170p.

Rai LK and Yoshida K (2020) Lithostratigraphy of the Siwalik Group along the Muksar Khola section, Siraha-Udayapur districts, eastern Nepal Himalaya. *Journal of Nepal Geological Society* **60**, 207–24.

Rai LK and Yoshida K (2021) Sedimentary facies analysis of the fluvial environment in the Siwalik Group of eastern Nepal: deciphering its relation to contemporary Himalayan tectonics, climate and sea-level change. *Progress in Earth and Planetary Science* **8**, 49.

Rai LK, Yoshida K and Kuritani T (2021) Reconstruction of the exhumation history of the eastern Nepal Himalaya based on provenance changes. *Sedimentary Geology* **420**, 105920.

Rai SM, Guillot S, Upreti BN, Pecher A and Fort PL (2004) Mineral chemistry (biotite, muscovite, garnet, and plagioclase) in the Kathmandu and Gosainkund regions, central Nepal Himalaya. *Journal of Nepal Geological Society* **30**, 55–66.

Raimondo T, Payne J, Wade B, Lanari P, Clark C and Hand M (2017) Trace element mapping by LA-ICP-MS: assessing geochemical mobility in garnet. *Contributions to Mineralogy and Petrology* **172**, 17.

Ranjan N and Banerjee DM (2009) Central Himalayan crystallines as the primary source for the sandstone–mudstone suites of the Siwalik Group: new geochemical evidence. *Gondwana Research* **16**, 687–96.

Rao DR and Rai H (2006) Signatures of rift environment in the production of garnet-amphibolites and eclogites from Tso-Morari region, Ladakh, India: a geochemical study. *Gondwana Research* **9**, 512–23.

Raz U and Honegger K (1989) Magmatic and tectonic evolution of the Ladakh Block from field studies. *Tectonophysics* **161**, 107–18.

Reichardt H, Weinberg RF, Andersson UB and Fanning CM (2010) Hybridization of granitic magmas in the source: the origin of the Karakoram Batholith, Ladakh, NW India. *Lithos* **116**, 249–72.

Rickwood PC (1968) On recasting analyses of garnet into end-member molecules. *Contributions to Mineralogy and Petrology* **18**, 175–98.

Robinson DM, DeCelles PG, Patchett PJ and Garzione CN (2001) The kinematic evolution of the Nepalese Himalaya interpreted from Nd isotopes. *Earth and Planetary Science Letters* **192**, 507–21.

Robinson DM and Martin AJ (2014) Reconstructing the Greater Indian margin: a balanced cross section in central Nepal focusing on the Lesser Himalayan duplex: Lesser Himalayan Duplex, Central Nepal. *Tectonics* **33**, 2143–68.

Robinson DM and Martin AJ (2023) Genesis of Himalayan stratigraphy and the tectonic development of the thrust belt. In *Geophysical Monograph Series* (eds EJ Catlos & İ Çemen), **1** Vol, pp. 119–53. Hoboken, NJ: Wiley.

Rösler W and Appel E (1998) Fidelity and time resolution of the magneto-stratigraphic record in Siwalik sediments: high-resolution study of a complete polarity transition and evidence for cryptochrons in a Miocene fluviatile section. *Geophysical Journal International* **135**, 861–75.

Rösler W, Metzler W and Appel E (1997) Neogene magnetic polarity stratigraphy of some fluviatile Siwalik sections, Nepal. *Geophysical Journal International* **130**, 89–111.

Rowley DB (1996) Age of initiation of collision between India and Asia: a review of stratigraphic data. *Earth and Planetary Science Letters* **145**, 1–13.

Roy B, Ghosh S and Sanyal P (2020) Morpho-tectonic control on the distribution of C3-C4 plants in the central Himalayan Siwaliks during Late Plio-Pleistocene. *Earth and Planetary Science Letters* **535**, 116119.

Rubatto D, Burger M, Lanari P, Hattendorf B, Schwarz G, Neff C, Keresztes Schmidt P, Hermann J, Vho A and Günther D (2020) Identification of growth mechanisms in metamorphic garnet by high-resolution trace element mapping with LA-ICP-TOFMS. *Contributions to Mineralogy and Petrology* **175**, 61.

Sabeen HM, Ramanujam N and Morton AC (2002) The provenance of garnet: constraints provided by studies of coastal sediments from southern India. *Sedimentary Geology* **152**, 279–87.

Sami M, Ntaflos T, Mohamed HA, Farahat ES, Hauzenberger C, Mahdy NM, Abdelfadil KM and Fathy D (2020) Origin and petrogenetic implications of Spessartine Garnet in highly-fractionated granite from the Central Eastern Desert of Egypt. *Acta Geologica Sinica – English Edition* **94**, 763–76.

Sanyal P, Bhattacharya SK and Prasad M (2005) Chemical diagenesis of Siwalik sandstone: isotopic and mineralogical proxies from Surai Khola section, Nepal. *Sedimentary Geology* **180**, 57–74.

Sanyal P and Sinha R (2010) Evolution of the Indian summer monsoon: synthesis of continental records. *Geological Society, London, Special Publications* **342**, 153–83.

Sanyal S and Sengupta P (2012) Metamorphic evolution of the Chotanagpur Granite Gneiss Complex of the East Indian Shield: current status. *Geological Society, London, Special Publications* **365**, 117–45.

Sayab M, Shah SZ and Aerden D (2016) Metamorphic record of the NW Himalayan orogeny between the Indian plate-Kohistan Ladakh Arc and Asia: revelations from foliation intersection axis (FIA) controlled P–T–t–d paths. *Tectonophysics* **671**, 110–26.

Scaillet B, Holtz F, Pichavant M and Schmidt M (1996) Viscosity of Himalayan leucogranites: implications for mechanisms of granitic magma ascent. *Journal of Geophysical Research: Solid Earth* **101**, 27691–9.

Schärer U, Xu R-H and Allègre CJ (1986) U(Th)Pb systematics and ages of Himalayan leucogranites, South Tibet. *Earth and Planetary Science Letters* **77**, 35–48.

Scheibner B, Wörner G, Civetta L, Stosch H-G, Simon K and Kronz A (2007) Rare earth element fractionation in magmatic Ca-rich garnets. *Contributions to Mineralogy and Petrology* **154**, 55–74.

Schönig J, Meinhold G, Von Eynatten H and Lünsdorf NK (2018) Provenance information recorded by mineral inclusions in detrital garnet. *Sedimentary Geology* **376**, 32–49.

Schönig J, Von Eynatten H, Tolosana-Delgado R and Meinhold G (2021) Garnet major-element composition as an indicator of host-rock type: a machine learning approach using the random forest classifier. *Contributions to Mineralogy and Petrology* **176**, 98.

Searle MP (1999) Emplacement of Himalayan leucogranites by magma injection along giant sill complexes: examples from the Cho Oyu, Gyachung Kang and Everest leucogranites (Nepal Himalaya). *Journal of Asian Earth Sciences* **17**, 773–83.

Searle MP and Fryer BJ (1986) Garnet, tourmaline and muscovite-bearing leucogranites, gneisses and migmatites of the Higher Himalayas from Zanskar, Kulu, Lahoul and Kashmir. *Geological Society, London, Special Publications* **19**, 185–201.

Searle MP, Metcalfe RP, Rex AJ and Norry MJ (1993) Field relations, petrogenesis and emplacement of the Bhagirathi leucogranite, Garhwal Himalaya. *Geological Society, London, Special Publications* **74**, 429–44.

Searle MP, Simpson RL, Law RD, Parrish RR and Waters DJ (2003) The structural geometry, metamorphic and magmatic evolution of the Everest massif, High Himalaya of Nepal–South Tibet. *Journal of the Geological Society* **160**, 345–66.

Sen A, Dey A and Sen K (2023) Age, petrogenesis, and metamorphic modelling of high-pressure garnet-amphibolite from the Tethyan Himalayan Sequence of Bhagirathi Valley, Western Garhwal Himalaya. *Geological Journal* **58**, 981–97.

Shah SZ, Sayab M, Aerden D and Khan MA (2011) Foliation intersection axes preserved in garnet porphyroblasts from the Swat area, NW Himalaya: a record of successive crustal shortening directions between the Indian plate and Kohistan–Ladakh Island Arc. *Tectonophysics* **509**, 14–32.

Shi Q, He Y, Zhao Z, Liu D, Harris N and Zhu D (2021) Petrogenesis of Himalayan Leucogranites: perspective from a combined elemental and Fe-Sr-Nd isotope study. *Journal of Geophysical Research: Solid Earth* **126**, e2021JB021839.

Singh BP, Pawar JS and Karlupia SK (2004) Dense mineral data from the northwestern Himalayan foreland sedimentary rocks and recent river sediments: evaluation of the hinterland. *Journal of Asian Earth Sciences* **23**, 25–35.

Singh M (2012) Heavy mineral assemblage of the Pinjor formation of the Northwestern Himalaya and its significance in deciphering the provenance of the sediments. *Geosciences* **2**, 157–63.

Singh M, Singh IB and Müller G (2007) Sediment characteristics and transportation dynamics of the Ganga River. *Geomorphology* **86**, 144–75.

Singh S, De Waele B, Shukla A, Umasankar BH and Biswal TK (2021) Tectonic fabric, geochemistry, and zircon-monazite geochronology as proxies to date an orogeny: example of South Delhi Orogeny, NW India, and implications for East Gondwana Tectonics. *Frontiers in Earth Science* **8**, 594355.

Sinha RN (1970) Heavy mineral investigations in the Siwaliks of Mohand, district Saharanpur, Uttar Pradesh, India. *Journal of the Geoological Society of India* **11**, 163–77.

Smit MA, Hacker BR and Lee J (2014) Tibetan garnet records early Eocene initiation of thickening in the Himalaya. *Geology* **42**, 591–4.

Sorkhabi R (2010) Geologic formation of the Himalaya. *Himalayan Journal* **66**, 87–102.

Spear FS (1995) *Metamorphic Phase Equilibria and Pressure–Temperature-Time Paths* 2nd print. corr. Washington, DC: Mineralogical Society of America, 799p.

Srivastava V, Mukul M and Barnes JB (2016) Main Frontal thrust deformation and topographic growth of the Mohand Range, northwest Himalaya. *Journal of Structural Geology* **93**, 87–102.

St-Onge MR, Rayner N and Searle MP (2010) Zircon age determinations for the Ladakh batholith at Chumathang (Northwest India): implications for the age of the India–Asia collision in the Ladakh Himalaya. *Tectonophysics* **495**, 171–83.

Steck A, Epard J-L, Vannay J-C, Hunziker J, Girard M, Morard A and Robyr M (1998) Geological transects acress the Tso Morari and Spiti areas: the nappe structures of the Tethys Himalaya. *Eclogae Geologicae Helvetiae* **91**, 103–21.

Stone M (1988) The significance of Almandine Garnets in the Lundy and Dartmoor Granites. *Mineralogical Magazine* **52**, 651–8.

Streule MJ, Phillips RJ, Searle MP, Waters DJ and Horstwood MSA (2009) Evolution and chronology of the Pangong Metamorphic Complex adjacent to the Karakoram Fault, Ladakh: constraints from thermobarometry, metamorphic modelling and U–Pb geochronology. *Journal of the Geological Society* **166**, 919–32.

Stuart FM (2002) The exhumation history of orogenic belts from 40Ar/39Ar ages of detrital micas. *Mineralogical Magazine* **66**, 121–35.

Stutenbecker L, Berger A and Schlunegger F (2017) The potential of detrital garnet as a provenance proxy in the Central Swiss Alps. *Sedimentary Geology* **351**, 11–20.

Stutenbecker L, Hinderer M, Berndt J, Glotzbach C, Schlunegger F and Schwenk M (2024) Pliocene to modern sediment routing in the Aare valley: implications for sediment recycling. *Swiss Journal of Geosciences* **117**, 21.

Suggate SM and Hall R (2014) Using detrital garnet compositions to determine provenance: a new compositional database and procedure. *Geological Society, London, Special Publications* **386**, 373–93.

Szulc AG, Najman Y, Sinclair HD, Pringle M, Bickle M, Chapman H, Garzanti E, Andò S, Huyghe P, Mugnier J, Ojha T and DeCelles P (2006) Tectonic evolution of the Himalaya constrained by detrital [40]Ar–[39]Ar, Sm–Nd and petrographic data from the Siwalik foreland basin succession, SW Nepal. *Basin Research* **18**, 375–91.

Tamrakar NK and Yokota S (2008) Types and processes of slope movements along East-West Highway, Surai Khola area, Mid-Western Nepal Sub-Himalaya. *Bulletin of the Department of Geology* **11**, 1–4.

Taral S and Chakraborty T (2018) Deltaic coastline of the Siwalik (Neogene) foreland basin: evidences from the Gish River section, Darjeeling Himalaya. *Geological Journal* **53**, 203–29.

Taral S, Chakraborty T, Huyghe P, Van Der Beek P, Vögeli N and Dupont-Nivet G (2019) Shallow marine to fluvial transition in the Siwalik succession of the Kameng River section, Arunachal Himalaya and its implication for foreland basin evolution. *Journal of Asian Earth Sciences* **184**, 103980.

Taral S, Kar N and Chakraborty T (2017) Wave-generated structures in the Siwalik rocks of Tista valley, eastern Himalaya: implication for regional palaeogeography. *Current Science* **113**, 889–901.

Teraoka Y, Suzuki M, Hayashi T and Kawakami K (1997) Detrital garnets from Paleozoic and Mesozoic sandstones in the Onogawa area, East Kyushu, Southwest Japan. *Bulletin of the Faculty of School Education, Hiroshima University* **II**, 87–101.

Teraoka Y, Suzuki M and Kawakami K (1998) Provenance of Cretaceous and Paleogene sediments in the Median Zone of Southwest Japan. *Bulletin of the Geological Survey of Japan* **49**, 395–411.

Thakur SS and Patel SC (2012) Mafic and pelitic xenoliths in the Kinnaur Kailash Granite, Baspa river valley, NW Himalaya: evidence of pre-Himalayan granulite metamorphism followed by cooling event. *Journal of Asian Earth Sciences* **56**, 105–17.

Thakur SS, Singh AK, Rao DR, Sharma R, Pandey S and Ao A (2018) Garnetiferous metamorphic rocks in Jaspa granite, Himachal Pradesh, India: implication of Tethyan Himalayan metamorphism and tectonics. *Current Science* **115**, 1576–83.

Thakur VC (1981) Regional framework and geodynamic evolution of the Indus–Tsangpo suture zone in the Ladakh Himalayas. *Transactions of the Royal Society of Edinburgh: Earth Sciences* **72**, 89–97.

Thanh NX, Sajeev K, Itaya T and Windley BF (2011) Multiple garnet growth in garnet–kyanite–staurolite gneiss, Pangong metamorphic complex, Ladakh Himalaya: new constraints on tectonic setting. *Lithos* **127**, 552–63.

Thiede RC, Bookhagen B, Arrowsmith JR, Sobel ER and Strecker MR (2004) Climatic control on rapid exhumation along the Southern Himalayan Front. *Earth and Planetary Science Letters* **222**, 791–806.

Thiede RC and Ehlers TA (2013) Large spatial and temporal variations in Himalayan denudation. *Earth and Planetary Science Letters* **371–372**, 278–93.

Thiede RC, Ehlers TA, Bookhagen B and Strecker MR (2009) Erosional variability along the northwest Himalaya. *Journal of Geophysical Research: Earth Surface* **114**, 2008JF001010.

Tolosana-Delgado R, Von Eynatten H, Krippner A and Meinhold G (2018) A multivariate discrimination scheme of detrital garnet chemistry for use in sedimentary provenance analysis. *Sedimentary Geology* **375**, 14–26.

Ulak PD (2005) Palaeohydrological reconstruction of Siwalik Group in Surai Khola section of west Nepal Himalaya. *Journal of Nepal Geological Society* **31**, 33–42.

Ullah K, Arif M and Shah MT (2015) Geochemistry and provenance of the Lower Siwaliks from southwestern Kohat, western Himalayan Foreland Basin, NW Pakistan. *Geologica Acta* **13**, 45–61.

Upreti BN (1999) An overview of the stratigraphy and tectonics of the Nepal Himalaya. *Journal of Asian Earth Sciences* **17**, 577–606.

Valdiya KS (2016) Himalayan Foreland Basin. In *The Making of India: Geodynamic Evolution (ed. KS Valdiya)*, pp. 621–74. Society of Earth Scientists Series, Cham: Springer International Publishing.

Van Der Beek P, Robert X, Mugnier J, Bernet M, Huyghe P and Labrin E (2006) Late Miocene – Recent exhumation of the central Himalaya and recycling in the foreland basin assessed by apatite fission-track thermochronology of Siwalik sediments, Nepal. *Basin Research* **18**, 413–34.

Vance D, Bickle M, Ivy-Ochs S and Kubik PW (2003) Erosion and exhumation in the Himalaya from cosmogenic isotope inventories of river sediments. *Earth and Planetary Science Letters* **206**, 273–88.

Velbel MA (1984) Natural weathering mechanisms of almandine garnet. *Geology* **12**, 631.

Vermeesch, P. (2009). RadialPlotter: A Java application for fission track, luminescence and other radial plots. *Radiation Measurements*, **44**, 409-410.

Visonà D and Lombardo B (2002) Two-mica and tourmaline leucogranites from the Everest–Makalu region (Nepal–Tibet). Himalayan leucogranite genesis by isobaric heating? *Lithos* **62**, 125–50.

Walker CB, Searle MP and Waters DJ (2001) An integrated tectonothermal model for the evolution of the High Himalaya in western Zanskar with constraints from thermobarometry and metamorphic modeling. *Tectonics* **20**, 810–33.

Wang J, Wu F, Zhang J, Khanal G and Yang L (2022b) The Himalayan Collisional Orogeny: a metamorphic perspective. *Acta Geologica Sinica – English Edition* **96**, 1842–66.

Wang J-M, Larson KP, Zhang J-J, Zhao L and Wu F-Y (2024) Buchan-type metamorphic decarbonation during the upward expansion of the South Tibetan Detachment system: a new carbon source in the Himalaya. *Lithos* **464–465**, 107428.

Wang Y, Zeng L, Gao L-E, Chen Z and Li S (2022a) Eocene thickening without extra heat in a collisional orogenic belt: A record from Eocene metamorphism in mafic dike swarms within the Tethyan Himalaya, southern Tibet. *GSA Bulletin* **134**, 1217–30.

Webb AAG, Schmitt AK, He D and Weigand EL (2011) Structural and geochronological evidence for the leading edge of the Greater Himalayan Crystalline complex in the central Nepal Himalaya. *Earth and Planetary Science Letters* **304**, 483–95.

Weinberg RF (2016) Himalayan leucogranites and migmatites: nature, timing and duration of anatexis. *Journal of Metamorphic Geology* **34**, 821–43.

White, Powell, Holland and Worley (2000) The effect of TiO_2 and Fe_2O_3 on metapelitic assemblages at greenschist and amphibolite facies conditions: mineral equilibria calculations in the system $K_2O–FeO–MgO–Al_2O_3 –SiO_2 –H_2O–TiO_2 –Fe_2O_3$. *Journal of Metamorphic Geology* **18**(5), 497–511.

White RW, Pomroy NE and Powell R (2005) An *in situ* metatexite–diatexite transition in upper amphibolite facies rocks from Broken Hill, Australia. *Journal of Metamorphic Geology* **23**, 579–602.

Whitney DL, Broz M and Cook RF (2007) Hardness, toughness, and modulus of some common metamorphic minerals. *American Mineralogist* **92**, 281–8.

Whitney DL and Evans BW (2010) Abbreviations for names of rock-forming minerals. *American Mineralogist* **95**, 185–7.

Wilke FDH, O'Brien PJ, Schmidt A and Ziemann MA (2015) Subduction, peak and multi-stage exhumation metamorphism: Traces from one coesite-bearing eclogite, Tso Morari, western Himalaya. *Lithos* **231**, 77–91.

Wright WI (1938) The composition and occurrence of garnets. *American Mineralogist* **23**, 436–49.

Wu F-Y, Liu X-C, Liu Z-C, Wang R-C, Xie L, Wang J-M, Ji W-Q, Yang L, Liu C, Khanal GP and He S-X (2020) Highly fractionated Himalayan leucogranites and associated rare-metal mineralization. *Lithos* **352–353**, 105319.

Xie L, Tao X, Wang R, Wu F, Liu C, Liu X, Li X and Zhang R (2020) Highly fractionated leucogranites in the eastern Himalayan Cuonadong dome and related magmatic Be–Nb–Ta and hydrothermal Be–W–Sn mineralization. *Lithos* **354–355**, 105286.

Yan H, Yu D, Wang S and Ma C (2022) Magmatic garnet and magma evolution in Cuonadong Leucogranites: constraints from petrology and mineral geochemistry. *Minerals* **12**, 1275.

Yin A (2006) Cenozoic tectonic evolution of the Himalayan orogen as constrained by along-strike variation of structural geometry, exhumation history, and foreland sedimentation. *Earth-Science Reviews* **76**, 1–131.

Yin A and Harrison TM (2000) Geologic Evolution of the Himalayan-Tibetan Orogen. *Annual Review of Earth and Planetary Sciences* **28**, 211–80.

Yoshida K, Matsumoto Y and Sakai H (2015) Sandstone composition and geochemistry of the detrital garnets in the Middle-Upper Miocene sandstones in Siwalik Group, central Nepal. In *122nd Annual Conference* (Nagano, 2015), p. 1. Shinshu University Nagano (Engineering) Campus: Geological Society of Japan.

Yoshida K, Nakajima T, Matsumoto Y, Osaki A, Rai LK, Cruz JW and Sakai H (2021) Miocene provenance change in Himalayan foreland basin and Bengal Fan sediments, with special reference to detrital garnet chemistry. *Island Arc* **30**, e12408.

Yu M, Xia Q-X, Zheng Y-F, Zhao Z-F, Chen Y-X, Chen R-X, Luo X, Li W-C and Xu H (2021) The composition of garnet in granite and pegmatite from the Gangdese orogen in southeastern Tibet: Constraints on pegmatite petrogenesis. *American Mineralogist* **106**, 265–81.

Zaheenullah SMT, Khattak N and Ahmed HA (2017) Morphological and geochemical studies of heavy minerals in the Siwalik sandstone of Karak anticline, Khyber Pakhtunkhwa Pakistan. In *Proceedings of XXXIV International Conference*, pp. 313–15. Magmatism of the Earth and related strategic metal deposits, Miass, Russia: Vernadsky Institute of Geochemistry and Anlytical Chemistry of Russian Academy of Sciences.

Zech R, Zech M, Kubik PW, Kharki K and Zech W (2009) Deglaciation and landscape history around Annapurna, Nepal, based on 10Be surface exposure dating. *Quaternary Science Reviews* **28**, 1106–18.

Zeh A and Holness MB (2003) The effect of reaction overstep on garnet microtextures in metapelitic rocks of the Ilesha Schist Belt, SW Nigeria. *Journal of Petrology* **44**, 967–94.

Zhang H, Harris N, Parrish R, Kelley S, Zhang L, Rogers N, Argles T and King J (2004) Causes and consequences of protracted melting of the mid-crust exposed in the North Himalayan antiform. *Earth and Planetary Science Letters* **228**, 195–212.

Zhang S (2024) Review of the Himalayan leucogranites: comparison between the North and South belts, from geochemistry, petrogenesis, and rare-metal mineralization. *International Geology Review* **66**, 1560–89.

Zhang Z, Ding H, Palin RM, Dong X, Tian Z, Kang D, Jiang Y, Qin S and Li W (2022) On the origin of high-pressure mafic granulite in the Eastern Himalayan Syntaxis: implications for the tectonic evolution of the Himalayan orogen. *Gondwana Research* **104**, 4–22.